Modelling the manufacturing and installation costs of offshore wind farm substructures for a micro siting model

Max Verhaegh - May 26, 2014

University of Technology Delft

TU Delft Delft University of Technology

Challenge the future

Master of Science Thesis
Delft University of Technology
Faculty of Aerospace Engineering
Program: Sustainable Energy Technology

Modelling the manufacturing and installation costs of offshore wind farm substructures for a micro siting model

Max Verhaegh
May 26, 2014

Committee:

Prof. dr. G.J.W. van Bussel	TU Delft
Dr. ir. M.B. Zaaijer	TU Delft
Dr. ir. M. Voskuijl	TU Delft
Ir. P. van der Male	TU Delft
Ir. J. Blokland	Ballast Nedam

Acknowledgements

This thesis marks the end of my master Sustainable Energy Technology in Delft. I would like to thank my supervisors ir. M.B. Zaaijer and ir. P. van der Male for their guidance and help. In addition I would like to thank my supporting company Ballast Nedam and in particular J. Blokland and the work preparation department for the Butendiek offshore wind farm.

Furthermore, thanks to all my family and friends for their support throughout my entire study in Delft. Also I would like to thank Linda for her support throughout the graduation process. Finally, I would like to thank my brother Bob for showing me the true meaning of perseverance.

Delft, May 2014
Max Verhaegh

Summary

Offshore wind energy is expected to generate a large part of Europe's sustainable electrical energy by the year 2020. In the design of an offshore wind farm a large number of components interact with each other, resulting in a certain cost of electricity. In order to reduce these costs of electricity the design of an offshore wind farm can be optimized by a micro siting model. A micro siting model uses a description of both the expenses and revenues of all offshore wind farm components in order to find the optimal offshore wind farm. It is found that current literature does not describe the estimation of substructure manufacturing- and installation cost for the purpose of a micro siting model. Therefore, the objective of this thesis is to:

" *Develop a model that provides data to a micro siting model, concerning the manufacturing and installation costs of offshore wind farm substructures. The model should be able to analyze different combinations of substructure types and installation vessel types.*"

The developed model is divided in two separate models, one called the installation process model and one called the structural design model. The goal of installation process model is to calculate the total installation time of all substructures. The purpose of the structural design model is to find the design option resulting in the lowest amount of costs or structural mass.

The structural design model uses a combination of knowledge based engineering rules, assumptions, constraint based variables and two optimization variables to generate the support structure dimensions. After the dimensions of a support structure are generated the structure is evaluated based on a number of design requirements. Two types of substructures are implemented in the model. These are the monopile and the gravity base substructure types. Both substructure types use natural frequency and local buckling requirements. The monopile based support structure uses lateral pile stability as additional requirement. The gravity base structure uses the soil bearing capacity as additional design requirement. A genetic optimization solver is used to find the optimal design option by iteratively changing the values of the two optimization variables.

The installation process model uses two computation methods, called the workability percentage method and the time series method. The time series method is not described in current literature as far as the author is aware of. Both methods have, among others, the capability of using offshore wind farm site specific environmental data, different installation vessels, installation strategies, substructure types, harbors, different installation start dates and a grouting process.

Individual sub-models of the structural design model have been evaluated using preliminary monopile designs of the Butendiek and Baltic I offshore wind farm. Based on these evaluations a number of empirical corrections are implemented to account for inaccuracies. Using these

empirical factors and a specified set of independent variables the structural design model is able to recreate the dimensions of the preliminary monopile reference design with a high degree of accuracy. Less data is available for a gravity base structure design. A copy of the Thorntonbank gravity base structure dimensions resulted in a support structure that complied with all the aforementioned design requirements. The genetic solver is able to find the optimal design solution with an higher degree of accuracy and lower amount of iterations than using a brute force computation method, which evaluates all combinations of optimization variables within a grid of 0.005m by 0.005m. A sensitivity analysis revealed the importance of incorporating the water depth, wave height, soil properties, hub height and wind turbine type for the purpose of substructure mass estimation.

A sensitivity analysis is performed to compare the workability method and time series method using hind cast data sets of two offshore wind farm locations. The workability method underpredicts the required substructures installation time. This underprediction error increases for activities with a low workability. The time series method provides a more realistic description of the installation process, resulting in a more accurate estimation of the substructures installation time.

In conclusion a model has been successfully developed that provides the necessary data concerning the estimation of the manufacturing- and installation cost of offshore wind farm substructures. The developed model is able to select the optimal combination of substructure type and installation vessel. The developed model shows the potential of improving the cost estimations currently described in literature. Nevertheless, further adjustments are required to improve the developed model and implement it in a micro siting model. Especially the structural design model requires more reference designs and a fatigue analysis to accurately generate the correct support structure dimensions. Finally, the implementation of more substructure types can contribute to making the model applicable for a larger range of offshore wind farm locations.

List of Symbols

ΔD_{TP}	change in transition piece wall thickness
δp	difference in pressure
ΔWL	increased wave height
δy	difference in displacement
$\dot{U}$	acceleration of water particles
λ	Weibull scale parameter
ν	Poisson's ratio (soil)
ω	angular frequency
ω_{clamp}	first natural angular frequency of structure clamped at mud-line
ω_{lat}	first natural angular frequency of system translation at mud-line
ω_{rot}	first natural angular frequency of system rotation at mud-line
ω_n	angular wave frequency
ω_t	first natural angular frequency
$\phi(x)$	mode shape
ρ	density
$\mathbf{F}$	force and bending moment vector
$\mathbf{K}$	soil stiffness matrix
$\mathbf{u}$	displacement and rotation vector
$\zeta_{a,n}$	wave amplitude
C_D	drag coefficient
C_M	inertia coefficient
cc_{main}	carrying capacity of the main installation vessel
cc_{sup}	carrying capacity of a supply vessel
$D_{GBS,bs}$	diameter of base slab GBS
$D_{GBS,con}$	diameter of bottom concical section GBS
$D_{GBS,cyl}$	diameter of cylindrical section GBS
d_{harbor}	distance to from harbor to center offshore wind farm
$D_{MP,low}$	diameter of lower part of the monopile
$D_{MP,up}$	diameter of upper part of the monopile
$D_{TP,low}$	diameter of lower part of the transition piece
$D_{TP,up}$	diameter of upper part of the transition piece
d_0	water depth
dL	element length
dS	frontal area
E_{loc}	location specific environmental conditions
E_{max}	allowable environmental conditions for an installation step

EI	flexural rigidity
F_{e50}	change for recurrence period of 50 years
F_{tot}	total force
F_d	force induced by drag term Morison
F_d	tower drag force
F_i	force induced by inertia term Morison
g	gravitation acceleration on Earth
G	soil shear modulus
H	height sand layer
h_{month}	number of hours within a month
$H_{s,e50}$	significant wave height with a recurrence period of 50 years
$h_{w,50years}$	highest wave with a recurrence period of 50 years
H_D	design wave height
H_s	significant wave height
h_w	wave height
hw_{crest}	height of wave crest
I_{lat}	structure's translation inertia
I_{rot}	structure's rotational inertia
k	Weibull shape parameter
K_{lat}	lateral spring stiffness
K_{rot}	rotational spring stiffness
k_{soil}	stiffness soil layer
k_{spring}	spring stiffness
$L_{GBS,con}$	length of conical section of a GBS
$L_{GBS,cyl}$	length of cylinder section of a GBS
L_{GBS}	gravity base structure length
L_{grout}	length of grouted connection
$L_{MP,con}$	length of the conical section of the monopile
$L_{MP,top}$	length of the upper cylindrical part of the monopile
L_{MP}	monopile length
$L_{nacelle}$	nacelle length
L_{tow}	tower length
$L_{TP,con}$	length of the conical section of the transition piece
L_{TP}	transition piece length
L_p	pile penetration depth
$m(x)$	mass distribution function
$m_{water,in}$	water mass within MP
$m_{water,out}$	water mass outside MP
N_{50y}	number of data samples in 50 year period
n_{act}	number of installation activities
$n_{sub,month}$	number of substructure to be installed within a month
n_{sup}	number of supply vessels
q	non-dimension Wheeler stretching parameter
R_{bs}	radius base slab of GBS
t	time
T	period
$t_{g,act}$	gross installation activity time
$t_{g,cycle}$	gross installation cycle time

$t_{g,load}$	gross loading time at harbor per substructure onto the main installation vessel
$t_{g,step}$	gross time of an installation step
$t_{g,sub}$	gross installation time per substructure
$t_{g,trav}$	gross traveling time of main installation vessel
t_{grout}	grout thickness
t_{ho}	time until last component is handed over from supply vessel to main installation vessel with respect to start of first installation cycle of batch
$t_{load,batch}$	onshore loading time of a batch of substructures
$t_{load,sub}$	onshore loading time of one single substructure
$t_{main,cycle}$	net installation cycle time at main installation vessel
T_{max}	maximal kinetic energy
$t_{MP,low}$	lower monopile wall thickness
$t_{MP,mud}$	MP wall thickness at mud-line
$t_{MP,up}$	upper monopile wall thickness
$t_{n,act}$	net installation activity time
$t_{n,cycle}$	net installation cycle time
$t_{n,load}$	net loading time at harbor per substructure onto the main installation vessel
$t_{n,step}$	net time of an installation step
$t_{n,step}$	net time of an installation step
$t_{n,trav}$	net traveling time of main installation vessel
T_{ref}	reference time / number of seconds in data sample
$t_{sup,cycle}$	net cycle time of a supply vessel
$t_{tow,low}$	lower tower wall thickness
$t_{tow,up}$	upper tower wall thickness
$t_{TP,low}$	lower transition piece wall thickness
$t_{TP,up}$	upper transition piece wall thickness
$t_{trav,main}$	traveling time of main installation vessel
$t_{trav,sup}$	net traveling time of supply vessel
T_D	design wave period
t_g	gross time
t_n	net time
T_p	wave period
u	hourly mean wind speed at 10m height
U	velocity of water particles
$U_{c,sub}$	subsurface current velocity
$U_{c,wind}$	wind induced current
$v(x)$	vibration shape
V_{hub}	wind speed at hub height
v_{main}	speed of main installation vessel
V_{max}	maximal potential energy
V_{ref}	reference wind speed
V_w	wind speed
V_z	wind speed specific altitude
W	workability
W_{act}	workability of an installation activity
W_{load}	workability for loading of a substructure onto main installation vessel
W_{trav}	workability for traveling of main installation vessel
z	altitude with respect to LAT

z_{air}	air gap
z_{bs}	distance from mud line to bottom of GBS base slab
$z_{con,top}$	distance from LAT level to the top of the conical section of a GBS
z_{hub}	distance from LAT to the hub / hub height
z_{LAT}	distance mud line to lowest astronomical tide water level
$z_{MP,top}$	distance from LAT level to the top of the monopile
z_{plat}	distance from LAT level to the top of the transition piece
z_{ref}	reference altitude w.r.t. LAT
z_{surge}	water level increment as a result of storm surge
z_{tide}	water level increment as a result of maximum tidal difference
$z_{WL,mean}$	distance structural element to mean water level
Z_0	amplitude of mode shape

List of Abbreviations

API	American petroleum institute
BN	Ballast Nedam
CAPEX	Capital expenses
DNV	Det Norske Veritas
GBS	gravity base structure
GL	Germanischer Lloyd
HAT	Highest Astronomical Tide
LAT	Lowest Astronomical Tide
LCOE	levelized cost of electricity
OPEX	operational expenses
OWECOP	offshore wind energy cost and potential
OWF	offshore wind farm
OWFLO	offshore wind farm layout optimization
MP	monopile
MPV	multi purpose installation vessel
RNA	rotor nacelle assembly
TP	transition piece
TS	time series
WIV	wind farm installation vessel
WP	workability percentage
1P	operating frequency range of a wind turbine

Contents

Chapter 1

Introduction

European countries have set a target to generate 20% of Europe‘s electrical demand with sustainable energy sources by the year 2020 [56]. Ambitious projections predict the deployment of 80 GW worldwide by the end of 2020 [10]. In order to achieve this target new sustainable power plants have to be constructed at a high rate. Offshore wind energy is considered as one of the main technologies in achieving this target. Despite the harsh economic climate, the offshore wind market keeps on growing with the help of governmental energy policies.

1.1 Offshore wind energy

In this section a brief overview is given of the components required for offshore wind energy and which are relevant for this thesis.

1.1.1 Offshore wind farms

Wind turbines located offshore are commonly placed in a cluster, also called an Offshore Wind Farm (OWF), to reduce the cost of maintenance and electrical cable costs. The main components of an OWF are the wind turbines, the support structures, the internal and external power cables and an offshore substation. The construction process of an entire OWF usually takes one to three years and is divided in two stages. First the substructures for all turbines are installed and then the tower and turbines are placed. After an OWF is completed it starts to generate electricity, without any required fuel costs. Still regular preventive and corrective maintenance will be necessary throughout the OWF's life time of 20-25 years.

1.1.2 Micro siting

An well designed OWF generates electricity for the lowest possible price for a given offshore location. This will be vital in making electricity generated by offshore wind turbines competi-

tive with fossil fuel based electricity generating technologies. In order to design such an OWF both the revenues and expenses need to be modeled accurately. Modeling and optimizing the configuration of a wind farm is called micro siting [38]. In section 2.1 an elaborate overview of current micro siting models is presented.

1.1.3 Substructures

The support structure of an offshore wind turbine is defined as the entire structure below the Rotor Nacelle Assembly (RNA). The objective of the support structure is to provide a stable platform throughout the wind turbine's lifetime. The support structure can be divided into two components called the tower and the substructure, see figure 1.1. In this thesis two substructure design options are considered. These two substructure design options are a Monopile (MP) with a Transition Piece (TP) and a Gravity Base Structure (GBS). More information about the properties of these two substructures can be found in section 2.3. Reasons for including only these two substructure types are given in section 1.3.

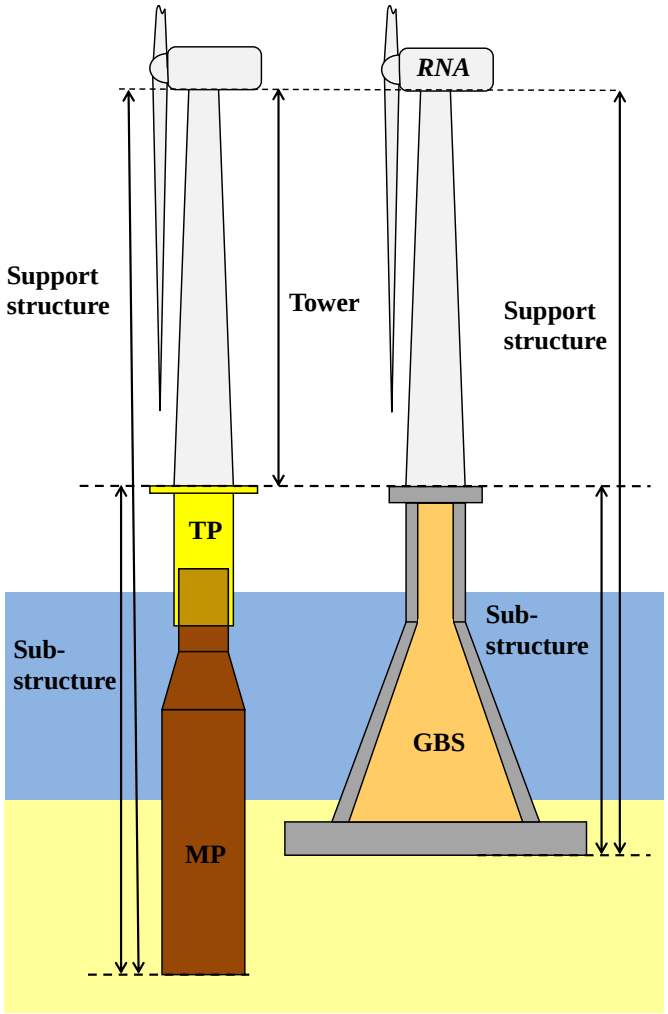

Figure 1.1: Overview of offshore support structure terminology

1.2 Problem description

Previous research on offshore wind farm micro siting models has not included comprehensive modeling of the substructure manufacturing and installation costs. However, these components account for a significant part of an offshore wind farm's total lifetime expenses. Commonly either simple empirical relations or a simplified design process is used to assess the costs of these components. Furthermore, no interaction exists between the chosen substructure type and the choice of installation vessel.

1.3 Thesis objectives and scope

Objective: Micro siting models use submodels to describe OWF components in order to optimize the OWF layout. The objective of this thesis is as follows:

Develop a model that provides data to a micro siting model, concerning the manufacturing and installation costs of offshore wind farm substructures. The model should be able to analyze different combinations of substructure types and installation vessel types.

Research questions: Concerning the developed model two research question are formulated.

1. Can the developed model provide a contribution to current micro siting models concerning the estimation of the substructure's manufacturing- and installation cost?

2. Is it useful to integrate the estimation of the substructure's manufacturing- and installation process cost into one model?

Scope: The challenge in designing an OWF is combining the large amount of design variables into one optimum design. In the description of the objectives it is stated that the model should be able to analyze different design options. Each design option consists of a substructure type and specific installation vessel. Only MP and GBS substructure types are considered during this research. This decision is based on the large difference in installation process and the structural working principle, which is explained in chapter 2. This large difference will help to see the structural design and installation process as an integrated whole. Furthermore, all installation vessels in the offshore market are incorporated within the scope of this research, provided that the user himself inserts the necessary input data describing the properties of an installation vessel. The logistics of manufacturing and transporting the substructures is limited to the offshore transport from the harbor to the location of the OWF. Finally, the goal of the model is to provide the necessary data to a micro siting model. With this the substructure installation- and manufacturing costs can be estimated.

1.4 Methodology and report structure

The objective of this research is to describe the substructure's structural design and installation process by means of a numerical model. In Chapter 2 current micro siting models, substructure installation vessels and two types of substructures are analyzed. Chapter 3 contains a set-up of the model. A description of the installation process and structural design is presented in Chapters 5 and 4. Chapter 6 and 7 provide the verification and validation of the entire model and several individual components. Finally, conclusions and recommendations are given in Chapter 8. An overview of the methodology and corresponding report structure is presented in figure 1.2.

Chapter	Content
1	Introduction: • problem description • objectives, research questions and scope
2	Background information on: • current micro siting models • different types of substructure installation vessels
3	Description of model set-up: • required input and output • required components and their interaction with the input data and other components
4	Structural design model • dimensions and design requirements • optimization solver
5	Installation process model • included and excluded variables • two different computation methods
6	Verification of individual model components • structural design model • installation model
7	Validation • theoretical case study • evaluation thesis objective
8	Conclusions and recommendations

Figure 1.2: Overview of the methodology applied for this research

Chapter 2

Background

The goal of this chapter is to provide some background information concerning current micro siting models, the substructure installation process and the MP and GBS substructure types.

2.1 Implementation of support structure and installation cost calculations in current Micro Siting Models

A micro siting model simulates and evaluates different OWF configurations in order to find the "optimal" OWF lay-out. The "optimal" OWF lay-out is the configuration that leads to the lowest Levelized Cost of Electricity (LCOE). Calculating the LCOE is a method to assess the cost of electricity over an entire project's lifetime, see equation 2.1 [25].

$$LCOE = \frac{\sum_{t=1}^{n} \frac{CAPEX_t + OPEX_t}{(1+r)^t}}{\sum_{t=1}^{n} \frac{E_t}{(1+r)^t}} \tag{2.1}$$

Here, a summation over the project's lifetime of the energy yield, E, corrected by a discount factor is divided by a summation of the capital expenses (CAPEX) and operational expenses (OPEX), also corrected by the same discount factor. The discount factor depends on the discount rate, r, and the moment in time in which the revenues and expenses are created, t. Other economic calculations can also be performed, such as a Fisher correction for inflation, as stated by Gonzalez et al. [36]. However, this does not change the principle behind finding the optimal OWF lay-out, meaning describing and evaluating different OWF configurations.

The combination of OWF substructure, logistics and installation life cycle costs vary between 12% and 40%, with an average of 22% [55]. Different turbine types, substructure types, distances to shore, environmental conditions, water depths and governmental policies all contribute to this difference. Nevertheless, no matter what specific properties a new OWF project has, a significant part of the CAPEX always is reserved for the manufacturing and installation of

substructures [6]. Therefore, a micro siting optimization could benefit from a more precise description of these components.

An overview of the current micro siting models and their interface with the cost estimation of the support structures or installation process is presented in table 2.1. Most OWF micro siting research is devoted to either modeling the wake losses or improving the optimization algorithms, [54] [37] [16] [61] [64] [38] [60] [63]. In these papers no calculations concerning the manufacturing and installation process of substructures are performed. Gonzalez et al., [36], estimate the support structure cost with a cost function based on empirical data. The offshore wind energy cost and potential (OWECOP) research, [23], assesses the potential of an offshore site by analyzing, among others, the substructure and installation costs. Here, a macro siting model is used, which assesses the economic potential of a different offshore wind farm locations. However, neither models include the variations of soil properties within an OWF site. Elkinton et al.,[14] [15], use soil properties in order to calculate the substructure costs, though, the reference data used to validate their model is limited. In conclusion, at best the substructure manufacturing- and installation cost calculations are only partly incorporated within a micro siting model, despite the fact that they significantly contribute to the total CAPEX. None of the researches specifically describe an interaction between the choice of substructure type and installation vessel type.

Table 2.1: Overview of literature study concerning micro siting models

OWF micro siting research	**Integration of substructure manufacturing- and installation cost calculations**	**Limitations / Not included**
[54], [37], [16], [61], [64], [38], [60], [63]	None	Support structures and installation costs
[36]	Support structure and installation cost are calculated via a function based on empirical data	Variations in soil properties are not included
[23][1]	MP and Tripod design and installation are included	Variations in soil properties are not included
[14] [15]	GBS and MP cost are calculated	- Limited amount of reference designs - Wave height calculations not included

[1] *macro siting model*

2.2 Substructure installation process

2.2.1 Installation vessels

Two types of vessels, required for the installation of an OWF, can be identified. First there is the main installation vessel, which is responsible for the installation of all heavy components or

components situated at a large altitude. Second there are support vessels, which are responsible for transporting crew, components and/or equipment. At the moment a large amount of different installation vessels is available on the international market [1]. For installation substructure purposes the following two main categories are identified, the Multi Purpose Vessel (MPV) and the Wind farm Installation Vessel (WIV) [4] [44].

Multi-Purpose Vessels: MPVs are originally not constructed for the offshore wind farm industry. Some of them are converted to match the requirements of the offshore wind industry. Consequently, these vessels are not optimized to perform an OWF installation process, but have been and remain crucial in today's OWF industry. The MPV category can be divided in four sub-categories; jack-up barges, jack-up vessels, crane vessels and other MPVs.

- **Jack-up barges**
  These vessels use legs to elevate themselves above the water level, see figure 2.1(a). The advantage of this method is that a stable platform is created from which the installation procedure can be performed even during rough weather conditions. Disadvantages of this type of vessel are the large amount of time required to jack-up the entire vessel, their limited crane capacity, finding suitable soil conditions to insert legs and their maximum operable water depth. A jack-up barge is a non-self-propelled vessel and relies on support vessels to tow it into position.

- **Jack-up vessel**
  Jack-up vessels are essentially the same as the jack-up barges except for the fact that they are self-propelled. This makes them independent from support vessels, see figure 2.1(b).

- **Crane ships**
  Unlike most offshore installation vessels crane ships do not rely on a jack-up system, see figure 2.1(c). They remain floating throughout the entire installation procedure. This increases the limitations set by the maximum allowable wave height, but saves time since elevating the entire vessel is not required. Crane ships use a large shear leg of pedestal mounted cranes and are capable of lifting heavy loads. Most crane ships have no deck space available and rely on support vessels to supply substructure components.

- **Other MPVs**
  All MPVs that do not comply with one of the aforementioned categories belongs to this category. Generally these are vessels with a good stability, large deck space and heavy lifting capacity. Their downside is their reduced agility and high operating costs. An example of this is a semi-submersible platform, see figure 2.1(d).

(a) Jack up barge - Buzzard

(b) Jack up vessel - Seajacks Kraken

(c) Crane ship - HLV Svanen

(d) Other MPV: semi-submersible - Thialf

Figure 2.1: Overview of four different types of MPVs [4] [1]

Wind farm installation vessels: WIV are specially designed for the installation and transportation of all OWF components, see figure 2.2. This includes (partly) onshore assembled turbines, loose wind turbines components, towers and different types of substructures. Their working principle is practically the same as for jack-up vessels. However, WIV are equipped with optimized onboard structures, more deck space, higher transit speeds, higher deck loads and more lifting capabilities.

2.2.2 Installation strategies

According to Orecca [5] two types of installation strategies exist. These are the feeding and the transiting method. The choice of main installation vessel determines for a large part the installation strategy. Conversely, it also be stated that the choice of installation strategy determines the choice of installation vessel.

Feeding method: The main installation vessel remains at the offshore site throughout the entire installation procedure of all OWF substructures, unless severe weather conditions force it to

Figure 2.2: Example of a WIV - MPI resolution [4] [1]

retreat to the harbor. Supply vessels are used to feed the main installation vessel with substructure components. It is possible to transport these components directly from a manufacturing port or use a feeder port to store the components first. Either way the goal is to keep the utilization factor of the main installation vessel as high as possible. Substructure components are supplied one at a time or by means of a set of components. For the latter method the set of components is first lifted on board of the main installation vessel after which they are installed. This provides the supply vessel with more time to supply the next set of components, resulting in a lower amount of required supply vessels.

The feeding method is usually applied to jack-up barges and crane ships, due to their low speed and small carrying capacity. The advantage of this method is that no precious time is lost commuting between the offshore site and the harbor. On the other hand a small fleet of supply vessels is required to feed the main installation vessel. Substructure components are commonly supplied by transporting them on barges. Another method is to create a floating substructure component, which can be towed to the main installation vessel [18].

Transiting method: The main installation vessel commutes between the offshore site and the harbor. In the harbor components are loaded on the main installation vessel. Then the vessel sails to the offshore site to install all components after which it sails back to the harbor in order to repeat the whole process. Requirements for this method are a main installation vessel with a high sailing speed and large carrying capacity. The maximum amount of components that can be transported in one trip mainly depends on the deck space and maximum deck loading capacity [70]. The advantage of this method is the fact that one single vessel can perform the entire OWF substructure installation, without the need for support vessels. The disadvantage of the transiting method is the reduced utilization factor of the ability to install substructures.

2.2.3 Substructure installation methods

Monopile and transition piece: The procedure to install a MP is relatively simple compared to other support structure types. In sandy soils it is commonly possible to drive a monopile into the soil using a hydraulic hammer. Typically 40 to 50% of the pile length is driven into the soil [42], more specific calculations concerning the pile penetration depth will be given in Chapter

4. If pile driving is not possible due to rocky soil conditions, the MP is drilled into the soil. However, due to the higher cost involved this should be avoided if possible.

The TP transfers the loads from the tower to the MP. The outside of the TP contains boat fenders, access ladders, access deck and handrails. The inside contains electrical components [43]. Therefore, the TP has to be installed offshore, because it cannot withstand the forces caused by pile driving. After installation the TP is situated partly below and partly above the water line. The MP and TP are connected to each other by a grouting connection. Here a special type of cement is pumped in the void between the MP and the TP. Before the grout is inserted there is the possibility to adjust the angle of the TP in such a way that any vertical misalignment of the MP can be corrected, which could be induced by the pile driving [71]. A sea surface temperature of 5^oC is required for the grout to cure properly [52].

Gravity base structure: The installation procedure of a GBS is quite intensive. The two main reasons for this are the need for dredging and subsurface preparation, and the use of heavy-lift vessels [43]. After the sea surface is prepared properly the GBS can be installed. This requires heavy lifting cranes that can lift the entire GBS. Once the GBS is placed onto the sea bed it is filled with ballast sand. Another method is to design a floating structure. At the specified location this structure is first filled with water in order to sink and position it onto the sea bed. Then the water is replaced with ballast sand.

2.2.4 Other installation considerations

Scour protection: In sandy soils a special type of erosion, called scour, can occur around a support structure. Due to the presence of an obstruction the flow accelerates taking with it particles of sand. As a result a scour hole emerges, which can reach a depth of 1.5 times the pile diameter [84]. As a result this can negatively impact the stability and natural frequency of the entire structure. To prevent scour a scour protection layer will have to be applied on the sea floor. This is done by placing a filter layer, consisting of small rocks, on the sea floor. Its purpose is to prevent the sandy soil from eroding. Then, after the MP is installed, a layer of larger rocks, called the armor layer, is put on top of the filter layer in order to prevent it from being washed away. During the rest of this research it is assumed that the scour protection has already been installed. The design and installation of the scour protection is not included in the scope of this research.

Installation noise: Under water marine life can be threatened by underwater noise produced by the installation of OWF substructures. Most countries have legislations concerning the production of underwater noise during the installation process. In the Netherlands for example pile driving is only allowed from July through December [2]. In Germany a maximum of 160 dB is allowed [2]. The latter case requires noise reducing measures, which increase the total installation complexity, time and costs. GBS structures can be installed throughout the year, since no harmful noise is produced during their installation. This means that the choice of substructure type influences the installation costs. Consequently, this is considered as one of the major difference in the installation of both substructure types. The GBS structure is not limited by the

production of underwater noise. Hence, extra cost in the prevention of underwater noise and / or time delays can be prevented during the installation process.

Installation time constraints: The installation time of all OWF substructures should be kept as short as possible in order to reduce the total installation costs, see section 2.2.5. However, it is possible to deviate from the ideal (smallest) installation time due to some constraints concerning the start and/or end of installation. These constraints are determined by governmental legislation and the combined planning of contracting companies. Noise production limitations could limit the installation start and/or end date. Since multiple companies are involved in the construction of an OWF the start and/or end date of substructure installation can be limited by overall OWF project planning.

2.2.5 Installation costs

According to Kaiser et al. [44] the installation costs, C_I, are determined by the total amount of installation time, t_I, multiplied by the cost per day, $C_{tot,day}$, added on top of the mobilization costs, C_{mob}, see equation 2.2. The costs per day are determined by the cost of the main installation vessel, $C_{main,day}$, plus the costs of all other support vessels and equipment, $C_{sup,day}$, see equation 2.3. This is a simplification since Kaiser et al. [44] also state that the main installation vessel day rates changes throughout the year. González et all. [36] also identify different installation and transporting vessel rates.

$$C_I = t_I \cdot C_{tot,day} + C_{mob} \tag{2.2}$$

$$C_{tot,day} = C_{main,day} + N_{sup} \cdot C_{sup,day} \tag{2.3}$$

In conclusion, to calculate the total substructure installation cost only the total installation time and the number of support vessels needs to be computed. Also data concerning the day rates and mobilization costs of the all vessels is required.

2.3 Substructures

2.3.1 Monopile and transition piece

The MP is the most simple and applied substructure type. It consists of a cylindrical tube, which is drilled or driven in the sea bed, see figure 2.3(a). Vertical and horizontal stability is provided by choosing the appropriate pile depth. By varying the pile diameter and length the appropriate stiffness and desired natural frequency can be obtained. A larger diameter is more sensitive to higher wave loading, which gives the MP a maximum operational water depth of approximately 30 m [24].

On top of the MP a TP is required. This component is commonly equipped with a boat landing platform, an interface platform and other components. Furthermore, it is possible to correct the structure's alignment with the TP in case of the MP being installed under a small angle. The TP is connected to the MP by means of a grouted overlap area. Here, grout, a special kind of concrete, acts a bonding material between both substructure components.

2.3.2 Gravity base structure

The GBS uses a large base together with a low center of gravity to prevent the entire structure from overturning. A GBS requires a high amount of substructure mass to obtain this low center of gravity. Here, almost always a steel reinforced concrete body filled with ballast sand is used for its low material price, compared to a steel structure. The structure does not penetrate the soil. Therefore, no pile driving or drilling process is required, but instead an intensive soil preparation process is required. The GBS structure can consist of one single part, reaching from slightly below the sea bed up to the interface level above the water line, see figure 2.3(b).

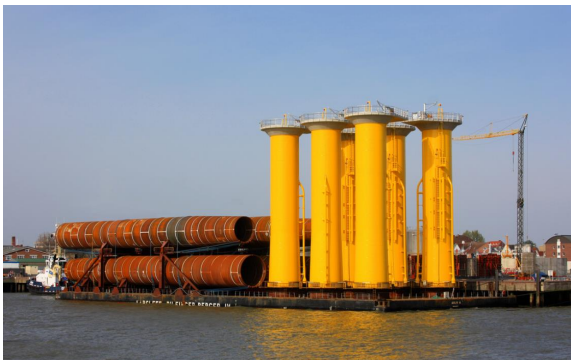

(a) MPs and TPs delivered on barges for OWF London Array [69]

(b) Construction of GBS substructures for Thornton Bank OWF [17]

Figure 2.3: Examples of MP and GBS substructures

2.3.3 Substructure costs

The cost of the substructures mainly depends on the required amount of materials and labor and the use of specialized manufacturing facilities. For simplicity it is assumed that a linear relation exists between the substructure mass and manufacturing costs. For both the MP and GBS substructures the costs are calculated by multiplying the mass, m, with the cost per kilogram of material, P, see equations 2.4 and 2.5. Within the cost per kilogram price all cost components, such as labor and the use of manufacturing facilities, are also included.

$$C_{MP} = (m_{MP} + m_{TP}) \cdot P_{MP} \tag{2.4}$$

$$C_{GBS} = m_{GBS} \cdot P_{GBS} \tag{2.5}$$

Chapter 3

Model Set-Up

An overview of the developed model is provided in the first section of this chapter. Then the model's required input and desired output are discussed. Finally, a number of design interaction between the substructure design and installation process model are presented.

3.1 Model overview

The model developed in this research uses a data set from a micro siting model as input. This data set should describe the conditions in which the OWF is placed and the properties of each individual wind turbine location. This input data will be processed by the model and an output is given to the micro siting model. The output contains information, which enables the micro siting model to calculate the cost of manufacturing and installing all OWF substructures. This process is repeated due to the iterative design process as defined by the micro siting model, see figure 3.1.

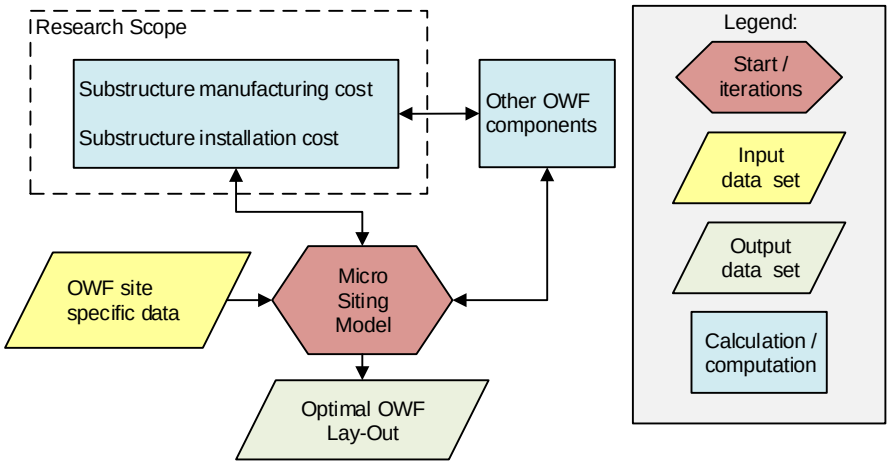

Figure 3.1: Substructure manufacturing and installation cost interaction with micro siting model

The numerical computation software application Matlab is chosen to be used to develop the model. The advantage of using Matlab is that it can be easily used in an iterative process. Furthermore, a link between the installation and structural design can be established. This would not be possible if for example a finite element based software (for example Ansys) is used.

3.2 Model input

The main model developed by this research is considered as a submodel for micro siting model. Nevertheless, during this thesis the developed model will be called the "main model". The input data for the model can be summarized by two sets of independent variables; set by the developed model and set by a micro siting model.

3.2.1 Independent variables set by the developed model

Independent variables as design options: The main model described in this research uses multiple design options to describe possible substructure types and installation process options. Each design option is described by a set of two independent variables, see table 3.1.

Table 3.1: Independent variables used by the model

Category	**Independent variables**
Substructure type	MP and TP GBS
Main installation vessel	Vessel 1 Vessel 2 Vessel 3 ..... Vessel N

Independent variables defined by the user: The user of the micro siting model has the ability to insert and change a set of independent variables. One can add, remove or change properties concerning a specific installation vessel. In such a way main installation vessels can be added resulting in a more comprehensive search for the ideal installation vessel. Still, knowledge and insight is required by the user to assign the right properties to each main installation vessel in order to describe the installation process. The required set of independent variables is presented in table 5.1 of chapter 5.

3.2.2 Independent variables set by micro siting model

Variables used within the micro siting model are considered to be independent variables for the main model of this research. These independent variables can be divided into three categories, see table 3.2:

• **Site specific data:** This set of independent variables is defined by the location of the OWF. It is used for both the calculations of the installation process and the structural design.
• **Wind turbine data:** Wind turbine properties are used to calculate the wind loads the turbine experience, which is required for the structural design.
• **Wind turbine location data:** The location of wind turbine within the OWF determines the water depth and soil conditions. These properties are both required for the structural design.

Table 3.2: Independent variables defined by micro siting model

Category	**Independent variable**
Site specific data	Water level differences: • Maximal tidal difference • Maximal storm surge Environmental conditions: • Extreme wind speed • Extreme wave height • Extreme water current Weather conditions: • Measurement or Hind cast data • Persistence data Other site specific data: • Distance to port • Start date of installation[1] • Number of foundations
Wind turbine data	Rotor diameter Rated wind speed[2] Hub height 1P operation range RNA mass: • blade mass • hub mass • nacelle mass
Wind Turbine location data	Soil data: [3,4] • Sand layer: - submerged unit weight - soil friction angle • Clay layer: - submerged unit weight - undrained shear strength - stress at 50% strain Water depth:[3] • LAT

[1] *start date could depend on foundation type*
[2] *only required when wind turbine thrust force is calculated*
[3] *required for each foundation within OWF*
[4] *required per soil layer*

3.3 Model output

In the previous chapter the assumption has been made that there exists a linear relation between the substructure's mass and the cost to produce it, see section 2.3. Furthermore, it has been stated that the total installation cost depends on the total installation time and the number of required vessels, see section 2.2.5. A simple cost function is used to translate the structural mass and installation time into manufacturing and installation costs. As a result, a design option consisting of one substructure type and one specific installation vessel, will produce the following two output values:

1. The total installation time and number of support vessels.
2. Mass of all support structures.

The output of the developed model is summarized in two data sets, see table 3.3. One set describes the main cost component of the installation process, which is the number of days the main installation vessel is required and the number of supply vessels. The other set describes the main cost components of the structural design, which are the required amount of steel and/or concrete. An elaborate description of the calculations involved to produce this output for installation process and for structural design can be found respectively in chapters 5 and 4.

Table 3.3: Output parameters of the main model

Modeling of the	**Output data**
Structural design	Dimensions: • Diameter and wall thickness per structural segment • Mass per support structure component
Installation process	Total installation time Number of supply vessels Ideal start date of installation

3.4 Design interactions

Numerous design interactions exist between the substructure design and the installation process. However, the amount of interactions existing on a preliminary design level is limited compared to the detailed design phase. For the purpose of this research only the most important interactions are stated. Also a consideration is made whether or not to include a particular design interaction in the model and how to include it. The choice of substructure type and substructure design affects the installation process and vice versa, this is summarized in table 3.4 and table 3.5.

The effect of the substructure design on the installation process is described in table 3.4. Here, the location of the substructure manufacturing yard is not used as a variable within the model, because the onshore or offshore transportation of substructures to the installation harbor is not incorporated in the scope of this research. Furthermore, the dimensions of the substructure are not considered to be a limiting factor for the handling and installation processes. It is assumed that a vessel capable of lifting a substructure, is not limited by the substructure's size.

The effect of the installation process on the substructure design is presented in table 3.5. Pile driving fatigue loads are not considered in the structural design model, because no fatigue analysis will be performed, see section 4.3. Furthermore, it is assumed that the designed substructures are able to float when this is required by the installation strategy. Finally, the transportation loads are assumed to be negligible compared to the loads experience during the substructures operation life time.

Table 3.4: Effect of substructure design on the installation process

Effect of substructure design on the installation process	**Included in research**	**Required information**
Main installation vessel crane should be able to lift heaviest substructure component	Yes	Crane capacity
Installation start and end date constraints due to noise production limits caused by pile driving legislations	Yes	Start / end date of installation
Installation start and end date constraints due to water temperature stated by grouting requirements	Yes	Start / end date of installation
Longer weather windows required for grout curing time (definition of "weather window" is given in Chapter 5)	Yes	Grout curing time and allowable environmental conditions
Installation net cycle time differs per vessel and substructure type	Yes	Installation cycle times
Substructure component mass determines the amount of components on board of the main installation vessel	Yes	Number of components on main installation vessel
Substructure component mass and size determines the type of barge required or the amount of components on a barge	Yes	Number of components on barge
Location of the substructure manufacturing yard	No	
Maximal dimensions of substructure	No	

Table 3.5: Effect of installation process on substructure design

Effect of the installation process on the substructure design	**Included in research**
Fatigue loads due to pile driving	No
Design of floating substructure	No
Transportation loads	No

In conclusion only the effects of the substructure design on the installation process are incorporated within the develop model. Therefore, the substructure design and the installation process model can be performed in series. An example of evaluating the two substructure types and seven different installation vessels is shown in figure 3.2. Here, it is assumed that vessel 1-4 can only install MP substructures and vessel 5-7 can only perform the installation of a GBS substructure. The number of installation vessels can be increased, provide that substructure type specific information concerning the installation process is present. Note that vessel 1 could be the exact same vessel as vessel 5. Still two sets of data describing two different installation processes are required. It could also be that vessel 1 and 2 are the same vessels using a different MP installation process. This results in a total of seven design options. The goal of the model is to assign the substructure manufacturing and installation cost to each of these design options.

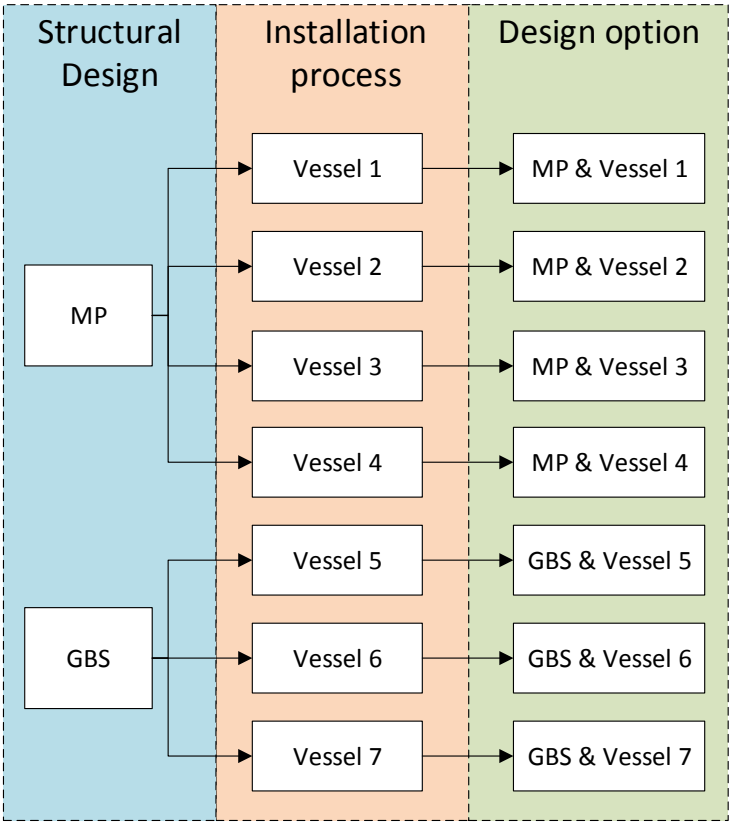

Figure 3.2: In series computation of design options

Chapter 4

Structural Design Model

The structural design module consists of a number of components, which are all described in this chapter. The goal of the structural design module is to find the optimal design option, which results into the lowest structural mass. This is done by creating and evaluating a large number of different support structures. Firstly, section 4.1 describes the creation of the support structure dimensions based on two optimization variables. Secondly, the environmental loads corresponding to the created structure and site specific conditions, are calculated in section 4.2. Then, the design requirements are chosen and described in section 4.3. Finally, the implementation of these three components into an optimization module is specified in section 4.4.

4.1 Structural dimensioning

4.1.1 Introduction

In this section the MP and GBS structural dimensions are defined. A dimensioning model will be able to create support structure dimensions for each design option. Each design options is initiated by the optimization algorithm, which chooses the values for two independent optimization variables. Then a combination of design rules is used to determine the values of all dependent variables.

The dependent variables are determined by knowledge based engineering (KBE) rules, calculated by constraints or defined by the optimization algorithm [83]. KBE rules are commonly found in literature (design standards) or are based on empirical data. The independent variables set by the optimization algorithm are changed iteratively until an optimal design is found. Variables set by constraints are used to scale a variable using a single design requirement. In that case no conflict exists between the design variable and other design checks or the objective function. This reduces the amount of opitmization variables, which saves computing time. In this chapter the location of the lowest astronomical tide (LAT) is chosen as reference height. An overview of the MP and GBS dimensions are showed in 4.1.

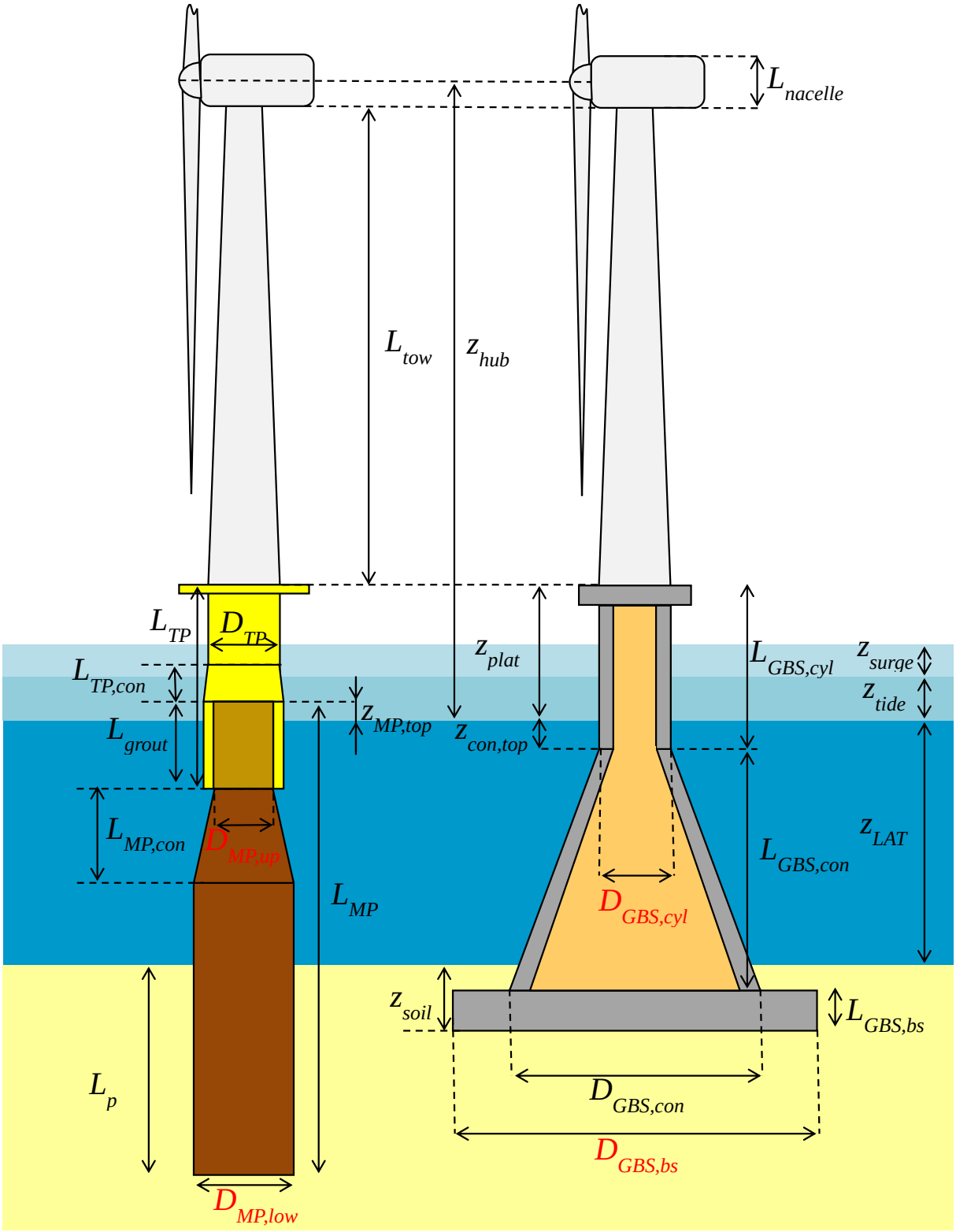

Figure 4.1: Schematic overview of the MP and GBS support structure dimensions

4.1.2 Independent variables for structural dimensioning

The independent variables, which are only used for the structural dimensioning of both substructure types, are presented in table 4.1. No large scale research has been performed to find the best or most commonly applied values for these variables. Instead the values presented in table 4.1 are based on one or two sources.

Material properties are presented in table 4.2. Only one kind of steel and concrete is assumed to be applied.

Table 4.1: Independent variables used for structural dimensioning

Independent variable	**Default value**	**Required for:**	**Source**
Length conical section MP	5.0 m		[21] [20]
Length conical section TP	4.0 m		[21] [20]
Difference in wall thickness MP pile toe	0.035 m		[21] [20]
Difference in wall thickness MP top part	0.020 m	MP	[21] [20]
Difference in wall thickness TP top part	0.020 m	and	[21] [20]
Difference in outer pile diameter TP top part	0.50 m	TP	[21] [20]
Wall thickness of pile toe	0.090 m		[21] [20]
Distance LAT to to top part of MP	3.0 m		[21] [20]
Grout thickness	0.075 m		[21] [20]
Maximum wave height for boat landing	2.5 m	GBS	assumption
GBS wall thickness	0.5 m		[13]
Air gap	1.5 m	Both	

Table 4.2: Material properties

Independent variable	**Default value**	**Source**
Material density		
- steel	7850 kg/m^3	[26]
- concrete	2400 kg/m^3	
- sea water	1025 kg/m^3	[27]
- sand	2000 kg/m^3	
- ballast material	2000 kg/m^3	
- air at sea level	1.225 kg/m^3	[27]
Young's modulus		
- steel	210 GPa	[28]
- concrete	17 GPa	[68]
Yield stress (tensile)		
- steel	355 MPa	[26]
- concrete	45 MPa	[13]

4.1.3 Monopile and transition piece dimensions

The structural optimization module uses four design variables together with a set of KBE rules to scale the MP and TP dimensions. In this section a short description of the MP and TP scaling variables is given, an overview of all dependent variables is presented in table 4.3.

Table 4.3: Design variables concerning MP and TP

Design variable	Design rule
MP length	Constraint & KBE
MP diameter	Optimization & KBE
MP wall thickness	Constraint & KBE
TP length	KBE
TP diameter	KBE
TP wall thickness	Constraint & KBE

Monopile length: The MP length is calculated by the summation of the pile penetration depth, L_p, the water depth, $zLAT$, and the location of the top side of the MP with respect to the lowest astronomical tide, $z_{MP,top}$. The latter one is an independent design variable, which can be found in table 4.1.

$$L_{MP} = L_p + z_{LAT} + z_{MP,top} \tag{4.1}$$

Appropriate lateral soil stability can be obtained by choosing the correct pile penetration depth. Increasing the pile penetration depth beyond the minimum requirements for soil stability will have virtually no effect on the structures natural frequencies. The shortest pile penetration, which complies with the lateral soil stability requirements, will therefore be the cheapest design option.

Monopile diameter: Most MP designs have a conical section in order to reduce the mass of the overall structure and the wave loading. The conical section is assumed to end at the bottom of the TP. The length of the conical section is inserted as an independent design variable based on data obtained from OWFs Butendiek and Baltic I. The length of the cylindrical part on top of the conical section of the MP, $L_{MP,top}$, is assumed to be equal to the grout length, equation 4.3.

The overlap length between the MP and TP equals the grout length, L_{grout}. The Germanischer Lloyd (GL) [29] states that the total grout length should be analyzed using a finite element model. In case no finite element analysis is performed, a length of at least 1.5 times the diameter of the MP is recommended.

$$L_{grout} = 1.5 D_{MP,up} \tag{4.2}$$

$$L_{MP,top} = L_{grout} \tag{4.3}$$

Monopile wall thickness: The mud line wall thickness is scaled to the lowest value, while complying to the local buckling requirement, see section 4.3.4. The rest of the segments wall thickness is scaled according to a set of KBE rules. The highest lateral forces and bending moments occur below the sea bed. Therefore, it is assumed that from the mud line to the top of the MP the wall thickness decreases linearly. From the mud line to half the pile penetration depth the wall thickness remains constants. Then it decreases linearly until the pile toe. At the pile toe (bottom 2.0 meters of the pile) again the maximum wall thickness is assumed to account for pile driving loads, see figure 4.2. The pile thickness at the top and bottom of the MP chosen to be a factor $\Delta t_{MP,up}$ and $\Delta t_{MP,low}$ lower than the mud line wall thickness, see table 4.1.

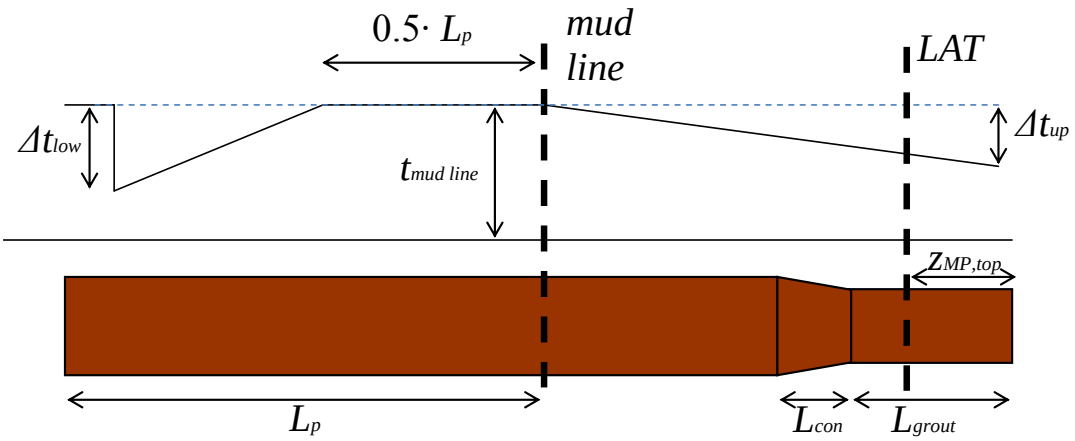

Figure 4.2: Overview MP dimensions and wall thickness distribution

Transition piece length: Under no circumstances a wave crest is allowed to reach the top of the platform, [71]. The location of the platform with respect to LAT, z_{plat}, is calculated by the addition of the maximum tidal difference, the water level increase due to storm surge, $3/4$ of the highest 50 year wave, $h_{w,50years}$, and an air gap, z_{air}, see equation 4.4. The total TP length, L_{TP}, can be found by adding the platform height to the grout length and subtracting the part of the MP above the LAT water level, $z_{MP,top}$, see equation 4.5.

$$z_{plat} = z_{tide} + z_{surge} + 0.75 \cdot h_{w,50years} + z_{air} \tag{4.4}$$

$$L_{TP} = z_{plat} - L_{grout} + z_{MP,top} \tag{4.5}$$

Transition piece diameter: The TP bottom outer diameter results from the addition of the MP upper outer diameter, twice the grout thickness, t_{grout}, and twice the TP bottom wall thickness, $t_{TP,low}$, see equation 4.6. The grout thickness should be calculated together with the grout length, but for simplicity it is considered as a constant.

$$D_{TP,low} = D_{MP,up} + 2 \cdot (t_{grout} + t_{TP,low}) \tag{4.6}$$

The TP also has a conical section starting immediately on top of the overlap length between the MP and TP. The TP upper outer diameter is calculated by subtracting a constant, ΔD_{TP}, from the lower TP diameter, see equation 4.7. The TP diameter difference, ΔD_{TP}, and the length of the conical section, $L_{TP,con}$, are both considered as independent variables, see table 4.1.

$$D_{TP,up} = D_{TP,low} - \Delta D_{TP} \tag{4.7}$$

Transition piece wall thickness: The TP bottom wall thickness is scaled to the lowest value, while complying with the local buckling requirement, see section 4.3.4. It is constant over the entire overlap length and conical section. After that it linearly decreases to up to the upper part of the TP, see figure 4.3.

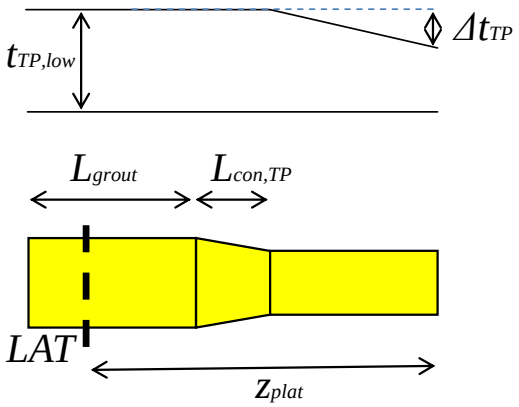

Figure 4.3: Overview TP dimensions and wall thickness distribution

4.1.4 Gravity base structure dimensions

Two design variables in combination with a set of KBE rules are used to scale the GBS, see table 4.4. The GBS wall thickness is not calculated but assumed to be constant.

Table 4.4: Design variables concerning GBS design

Design variable	Design rule
GBS length	KBE
Base slab diameter	Optimization
Conical section lower diameter	KBE
Cylindrical section diameter	Optimization
Wall thickness	KBE
Base slab height	KBE

Gravity base structure length: The distance of the bottom part of the base slab with respect to the mud line is defined by the independent variable, z_{bs}. The platform level is located at the top part of the cylindrical part of the GBS, see equation 4.4. The length of the GBS, L_{GBS}, is equal to the distance between these levels, see equation 4.8.

$$L_{GBS} = z_{plat} + z_{LAT} + z_{bs} \tag{4.8}$$

Gravity base structure diameter: The diameter of the base slab and diameter of the cylindrical section are all defined by the structural optimization module. The bottom diameter of the conical section results from the multiplication of the base slab diameter with an independent reduction factor, $c_{GBS,con}$, see equation 4.9. The diameter of the upper part of the conical section is equal to the diameter of the cylindrical section. The diameter of the conical section varies linear from the bottom to the top.

$$D_{GBS,con} = c_{GBS,con} \cdot D_{GBS,bs} \tag{4.9}$$

Gravity base structure wall thickness: The wall thickness of the conical and cylindrical section, t_{GBS}, is assumed to be constant. The base slab is considered to be a solid block of reinforced concrete.

4.1.5 Tower dimensions

The structural optimization module uses two design variables together with a set of KBE rules to scale the tower dimensions. In this section a short description of the tower scaling variables is given, an overview of all dependent variables is presented in table 4.5.

Table 4.5: Design variables concerning tower design

Design variable	Design rule
Tower length	KBE
Tower diameter	KBE
Tower lower wall thickness	Constraint
Tower upper wall thickness	Constraint

Tower length: The tower length, L_{tow}, is equal to the distance from the platform to the bottom of the nacelle. This can be calculated by substractinng the distance from LAT to the platform and half of the nacelle height, $L_{nacelle}$, from the distance from LAT to hub, z_{hub}, (assumed to be the center of the nacelle), see equation 4.10. The hub height is defined by the micro siting algorithm.

$$L_{tow} = z_{hub} - z_{plat} - 0.5 \cdot L_{nacelle} \tag{4.10}$$

Tower diameter: The lower tower diameter is set equal to the upper diameter of the TP or the cylindrical part of the GBS. The upper tower diameter is set by the yaw bearing and therefore defined by the type of WT.

Tower wall thickness: The tower wall thickness is assumed to be thickest at the tower base and smallest at the tower top. Both the upper and lower tower wall thicknesses are defined by the local buckling design check. Over the length of the tower the wall thickness varies linearly.

Note: It is known from a confidential report from Vestas that the wall thickness distribution does not represent the proposed distribution. Implementing the actual distribution would reveal to much information behind the tower dimensions scaling rules. Because this project focuses on the substructure design and corresponding installation process, the tower dimensions are only of minor importance. The tower dimensions are mainly required for an appropriate natural frequency assessment. In section 6.2.5, it is shown that the difference between implementing the reference tower of Vestas and the tower dimensions according to the scaling laws, used in this project, result in a change in natural frequency of 4.5%.

4.2 Environmental loads

The environmental loads consist of a combination of wind and wave loads. This chapter describes the load cases to which the support structure is subjected and the procedures to obtain the wind and wave loads.

4.2.1 Load cases

A support structure is subjected to a set of load cases to evaluate its structural integrity. Design standards commonly give an elaborate description of these load cases required for obtaining a detailed design, for example see page 4-36 of the Gemanischer Loyd [30] or table E1 of DNV [74]. However, the goal of this research is to obtain the preliminary design of a support structure. Therefore, only one load case will be included in the structural design model. The single load case used, is based on table F1 of DNV [74] and consists of a combination of the 50 year highest wave loads and a wind turbine operating at rated wind speed, that experiences a sudden increase in wind speed (gust). DNV states that for these load cases the obtained loads from wind, waves and currents can be calculated independently from one another and linearly summarized to obtain the total structural loads. Differences in the direction of wind, wave and current loads are not taken into account. As a result the wind, wave and current loads are assumed to act in a two-dimensional plane.

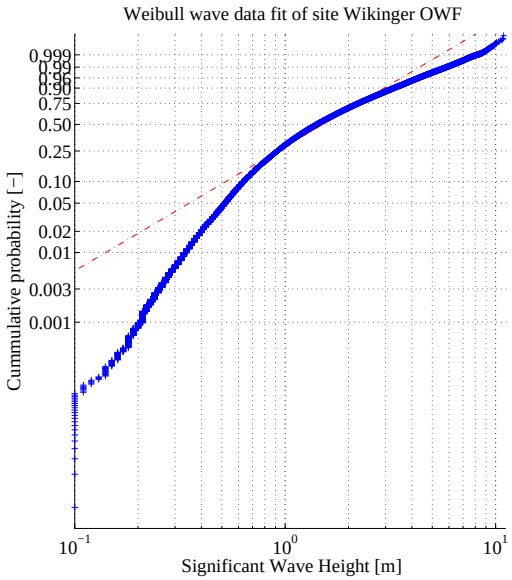

Figure 4.4: Weibull fit to hourly hind cast data of OWF Wikinger

Weibull fit to environmental data: A fit of the environmental conditions data on to a Weibull probability distribution is used to determine the highest significant wave height and wind speed in a certain number of years. This is or could be the same environmental data which has been used to calculate the installation time according to the TS method, see section 5.2. This is done according to the Matlab function *wblfit* [50]. From this the Weibull's shape parameter, k, and scale parameter, λ, are obtained. Now the cumulative Weibull distribution can be used to find the 50 year highest wave height, see equation 4.11. Here, x corresponds to either the wave height or wind speed and F to the probability that the value for x is not exceeded. An example of significant wave height data fit to a cumulative Weibull distribution is showed in figure 4.4.

$$F(x) = 1 - e^{-(x/\lambda)^k} \tag{4.11}$$

Now let's consider the following example to calculate the 50 year highest value, x_{e50}. Note that the time length of a data sample is required to calculate the probability that the 50 year highest value, F_{e50}, is exceeded, see equation 4.12 [31]. Further equation 4.11 can be rewritten to find x_{e50}, see equation 4.13.

$$F_{e50} = F(H_s < H_{s,e50}) = 1 - 1/N_{50y} \tag{4.12}$$

$$x_{e50} = \lambda \left[-\ln(1 - F_{e50}) \right]^{1/k} \tag{4.13}$$

The 50 year highest value can now be found since the probability and the Weibull shape and scale parameter are all known.

Wave height: The significant wave height needs to be converted to the highest wave within a data sample. The significant wave height of the spectrum is defined as the mean of the $1/3$ highest waves in a data set [72]. Calculating the design wave height, H_D, is described by the Germanischer Lyod [31], see equations 4.14 and 4.15.

$$H_D = H_{s50}\sqrt{0.5 \cdot ln\left(\frac{T_{ref}}{T_D}\right)} \tag{4.14}$$

With:

$$11.1\sqrt{\frac{H_{s50}}{g}} \leq T_D \leq 14.3\sqrt{\frac{H_{s50}}{g}} \tag{4.15}$$

$$T_{ref} = 10800\ s \tag{4.16}$$

The highest design wave corresponds with the lowest wave period.

Current: Sea currents can be divided in the two main categories: wind induced currents, $U_{c,wind}$, and sub-surface currents, $U_{c,sub}$. Both are a function of the distance from the water level. The total sea current is obtained by adding both components to each other. Wind induced current is created by wind blowing along the sea surface. It will only affect the top 20 meters of water. For those first 20 meters, $d_0 = 20m$, the wind induced current is linear dependent on distance from the water level, z, see equation 4.17 and 4.19 [32].

$$U_{c,wind}(z) = U_{c,wind}\left(\frac{d_0+z}{d_0}\right) \quad \text{for} \quad -d_0 \leq z \leq 0 \tag{4.17}$$

$$U_{c,wind}(z) = 0 \quad \text{for} \quad z \leq -d_0 \tag{4.18}$$

$$U_{c,wind} = 0.015 \cdot u \tag{4.19}$$

Here, u, is the hourly mean wind speed at 10m height. The wind speed obtained by hind cast or manual input applies to a 10 minute average wind speed at hub height. This can be converted to the desired form by two steps described the GL [33]. The conversion from a 10 minute to an hourly average can be obtained by multiplying by a factor 0.91, see table B.1. A conversion of wind speed from hub height to 10 meters above sea level can be obtained by using the power law, equation B.1, with $\alpha = 0.14$ and $z = 10m$. The combined result can be observed in equation 4.20.

$$u = (0.91) \cdot \left(\frac{10}{z_{hub}}\right)^{0.14} \cdot V_{hub} \tag{4.20}$$

Sub-surface currents, $U_{c,sub}$, mainly emerge from tidal motions combined with topological boundaries, see equation 4.21. The value for the sub surface current at the water level, $U_{c,sub_{wl}}$, will have to be provided by site specific data, which needs to be manually imported into the model.

$$U_{c,sub}(z) = U_{c,sub_{wl}}\left(\frac{d+z}{d}\right)^{1/7} \tag{4.21}$$

4.2.2 Wave loads

The forces and resulting bending moments exerted by waves and currents on the substructure need to be computed in order to properly design the dimensions of the substructure. In order to accurately determine the wave loads, both a wave kinematics model and a wave load calculation method are required. The wave kinematics describe the properties of a wave in terms of water particles speed and acceleration as function of the water depth and direction. The wave load calculation method converts the wave properties, described by the wave kinematics, into a wave load as a function of the water depth.

Henderson describes ten different wave kinematics models and four different wave load calculation methods [40]. The two most commonly used wave kinematics models are the Airy wave theory, also called Linear wave theory, and Dean's Stream function. Airy wave theory is suitable for low wave heights in deep waters and its simple theory results in fast computation time. Dean's Stream Function uses a velocity potential function to obtain an accurate and widely applicable wave kinematics model. This results in a more accurate description of the wave kinematics at the expense of an increase in computation time. Therefore, the Airy wave theory is used in this research for its simplicity and short computation time. The downside of this Linear wave theory is the lack of accuracy compared to the Dean Stream Function. For computing the wave loads the Morison's method is chosen also for its simplicity and computation speed. This method is applied to both the MP and GBS substructure type.

Airy wave theory and Morison's method: A simple expression for the normal force on a fixed pile in shallow water has been derived by Morison [53]. This expression consist of a drag, F_d, and a inertia force term, F_i, see equation 4.22.

$$F_{tot} = F_i + F_d \tag{4.22}$$

The drag term is a function of the water density, ρ, the drag coefficient, C_D, the frontal surface of a pile segment, dS, and the velocity of the water particles, U. The inertia term is a function of an element volume, dV, the inertia coefficient, C_M, and the acceleration of the water particles, $\dot{U}$, equation 4.23. Both the velocity and acceleration of the water particles can be positive and negative, which means that the direction of the drag and inertia force can change.

$$F_{tot} = C_M \cdot \rho \cdot dV \cdot \dot{U} + \frac{1}{2} \cdot C_D \cdot \rho \cdot dS \cdot |U| \cdot U \tag{4.23}$$

The velocity, u_n, and acceleration, $\dot{u}_n$, of the water particles at the center of a structural segment are described by the Airy wave Theory [3], see equations 4.24 and 4.25. Required are the wave amplitude, $\zeta_{a,n}$, angular frequency, ω_n, location of the segment, z, water depth, d, angular wave number, k_n, and moment in time, t.

$$u_n(z,t) = \zeta_{a,n} \cdot \omega_n \frac{\cosh k_n(z+d)}{\sinh k_n d} \sin(\omega_n \cdot t) \tag{4.24}$$

$$\dot{u}_n(z,t) = \zeta_{a,n} \cdot {\omega_n}^2 \frac{\cosh k_n(z+d)}{\sinh k_n d} \cos(\omega_n \cdot t) \tag{4.25}$$

With:

$$k_n = \frac{{\omega_n}^2}{g \cdot \tanh k_n d} \tag{4.26}$$

$$\omega_n = \frac{2\pi}{T} \tag{4.27}$$

Wheeler stretching: The linear wave theory calculates the velocity and acceleration of the water particles up to the mean water level. In order to be able to calculate the wave force in the wave crest, Wheeler stretching is applied in addition to the linear wave theory. Here, the velocity and acceleration profile from the mud line to the mean water level is extended to the wave top. This is done by changing the values of the z-coordinate, [12] referring to [80]. Without Wheeler stretching the z-coordinate represented the distance from a structural segment to the mean water level (always negative), this value is now called, $z_{WL,mean}$. The new z coordinate is taken with respect to the wave top, which changes as a function of time, $^{hw(t)}/_2$. The new z-coordinate can be calculated by combining equation 4.28 with 4.29. Here, q, is a non-dimensional variable that is used to stretch the water level to the top of the wave.

$$q = \frac{d}{d + {}^{hw(t)}/_2} \tag{4.28}$$

$$z = z_{WL,mean} \cdot q + d \cdot (q - 1) \tag{4.29}$$

Water level: The water level used for the wave force calculation is the 50 year highest water level. During the verification of the wave loads computation it is showed that the reference design uses a 9th order Stokes wave, see section 6.2.3. This wave has a higher wave crest than wave trough. The linear wave theory uses a symmetric wave. As a result, the top of the linear wave is located lower than the Stokes wave. Therefore, the water level is increased with a factor, ΔWL, see figure 4.5. The increase in water level is calculated by subtracting the wave crest height, hw_{crest}, from the wave amplitude of the linear wave theory, $^{hw}/_2$, see equation 4.30.

$$\Delta WL = hw_{crest} - {}^{hw}/_2 \tag{4.30}$$

4.2.3 Wind loads

The wind loads should be obtained via the micro siting model. For the purpose of this research they are manually inserted for the Ultimate Limit State (ULS) scenario. It is also possible to calculate the wind loads using a set of some simple equations. These equations are presented in appendix B, but are less accurate than the manually inserted wind loads values.

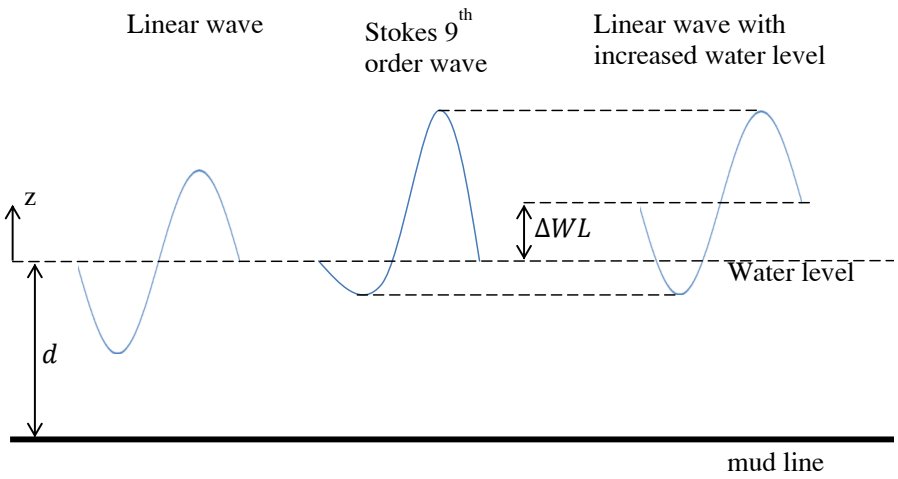

Figure 4.5: Wave shapes for Linear wave, Stokes 9th order wave and linear wave with increased water level

4.2.4 Load factors

A load factor is applied on top of the calculated loads. These load factors are chosen according to table A1 of the DNV design standards [74]. For the Ultimate Limit State (ULS) this results in a load factor of 1.35. The Service Limit State (SLS) is used to calculate the natural frequency. In this case a load factor of 1.00 is applied, also according the DNV design standards.

4.3 Structural design requirements

Each structural design is subjected to a number of design checks. These design checks are implemented as a set of constraints within the constraint function. If a structural design satisfies all applicable constraints, it is considered a viable design. Still further optimization could be required to reduce the structure's weight. In this section a description is given of all design checks used within the model. A summary of all included design checks for the MP substructure is given in table 4.6 and for the GBS substructure it is given in table 4.7. Further an overview of the most important design checks that were not included within the model can be found in table 4.8.

Table 4.6: Design checks used for MP, TP and tower design

Design check	**Applies to**	**Limit State**	**Main design variable**	**Goal**
Natural frequency	Support structure[1]	SLS	MP bottom diameter	First natural frequency should be between the 1P and 3P WT operating range
Local buckling	MP[2], TP and tower	ULS	D/t ratio	Segments compressive stress should not exceed maximum local buckling strength
Lateral Soil Stability	MP	ULS	Pile penetration length	− Pile toe displacement < 0.02 m − Pile tip (at mudline) rotation < 0.25 deg − Pile tip (at mudline) deflection $< 3D/100$

[1] *including non-structural masses*
[2] *except MP part embedded in soil*

Table 4.7: Design checks used for GBS and tower design

Design check	**Applies to**	**Limit State**	**Main design variable**	**Goal**
Natural frequency	Support structure[1]	SLS	Tower wall thickness	First natural frequency should exceed the 3P WT operating range[2]
Local buckling	Tower	ULS	D/t ratio	Segments compressive stress should not exceed maximum local buckling strength
Soil Bearing Capacity	Base slab	ULS	Base slab diameter	

[1] *including non-structural masses*
[2] *a soft-stiff design will probably not be possible*

Table 4.8: Design checks that were not included within the model

Design check	**Would apply to**	**Reason for not including**	**Effect on final design**
Fatigue	MP GBS	Too complex	Model obtains a lower mass, due to underestimation of wall thicknesses
Sliding Resistance	GBS	Design is limited by soil bearing capacity	None
Global Buckling	MP GBS	Design is limited by local buckling	None
Bouyancy	GBS	Design is limited by soil bearing capacity	None
Axial bearing capacity	MP	Design is limited by lateral bearing capacity	None

4.3.1 Lateral soil stability

The soil, in which a MP substructure is installed, must provide sufficient stability in the vertical and horizontal direction during the structures lifetime. The soil properties together with the defined load cases are the design drivers for the pile penetration depth. During ULS wind and wave loading a maximal pile toe deflection of 0.02 m is allowed [66]. Other criteria have also been suggested, such as a deflection and rotation at the mud line of respectively 3D/100 and 0.25 degree [66], but these lead to much longer pile lengths than those of the reference design presented in section 6.2.4.

In order to assess these requirements a lateral bearing capacity calculation model is used. The model only consists of the part of the MP that is embedded in the soil, reaching from the mud line down to the pile toe. This part of the structure is still divided in segments with a length of 1 m. Each of these segments is connected to a non-linear spring, see figure 4.6. The spring stiffness depends on the properties of the local soil layer and the elongation of the spring. Now the model uses the applied lateral force and bending moment at the mud line as a vector input, **F**, for a matrix representing the combined structural stiffness and soil stiffness, **K**. The output vector contains the deflection and rotation per segment, **u**, see equation 4.32.

$$\mathbf{F} = \mathbf{K}\mathbf{u} \tag{4.31}$$

$$\mathbf{u} = \mathbf{K}^{-1}\mathbf{F} \tag{4.32}$$

The matrix, **K**, is based on a finite element method. As input it requires the stiffness of each segment and the corresponding spring stiffness. An example of equation 4.31 fully written out for a pile of two elements is showed in appendix C.1. The spring stiffness of a soil layer can be found using a p-y curve. Such curve contains data on the lateral compression of the soil, y, and the corresponding reaction force, p. The slope of this curve reflects the stiffness of a soil layer, see equation 4.33. This soil stiffness is represented within the model as a spring. The corresponding spring stiffness, k_{spring}, is equal to the soil stiffness multiplied with the length of a segment, dL, see equation 4.34. Each spring is attached at the bottom of a pile segment. Soil properties are described by the American Petroleum Institute (API) for sand and clay soil layers [41]. The calculations required to transform some basic soil properties into p-y data is showed in appendix C.2. The required input for these calculations is the effective unit weight of the soil, γ. A sandy soil also requires the soil friction angle, ϕ, where clay layers require the undrained shear strength, Cu, and the amount of the stress at 50% strain, e_{50}, as input, see figure 4.6. However, it is also possible to manually insert p-y data in the model.

$$k_{soil} = \frac{\Delta p}{\Delta y} \tag{4.33}$$

$$k_{spring} = k_{soil} \cdot dL \tag{4.34}$$

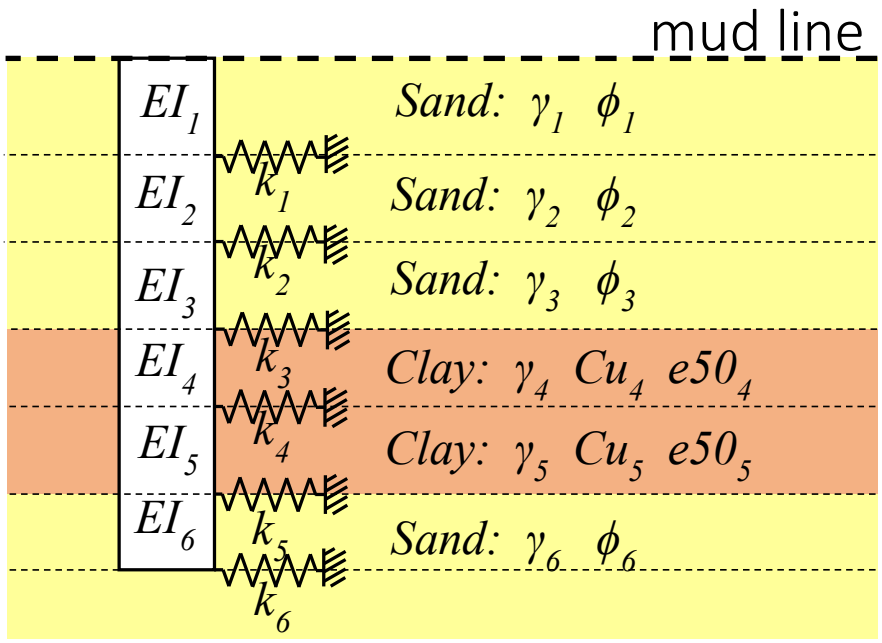

Figure 4.6: Example of soil model for six soil layers of sand and clay

4.3.2 Natural frequency

An offshore wind turbine constantly experiences structural vibrations throughout its lifetime. These vibrations are mainly induced by harmonic excitations from a blade passing the tower and waves hitting the substructure. When the frequency of these excitations coincides with one of the structure's natural frequencies resonance can occur. This can be prevented by designing the structure in such a way that its natural frequencies does not coincide with the wind turbine's operating range or the wave spectrum frequency range. The wind turbines operation range is called the 1P range. A structure with its first natural frequency below the 1P operating range is called a soft-soft design. When the first natural frequency lies between the 1P and 3P (three times the 1P range) operating range it is called a soft-stiff design. Also a stiff-stiff design is possible, this happens when the structure's first natural frequency lies above the 3P operating range.

A soft-soft design results in the lowest structural mass, but the wave spectrum frequency range commonly lies in the soft-soft region [73]. Furthermore, it is difficult to obtain a sufficiently strong, stiff and stable design within the soft-soft region. Hence, this is usually not a viable design option. A stiff-stiff design will result in a high structural mass, which should be avoided for economic reasons. Therefore, the majority of offshore wind structures have a first natural frequency within the soft-stiff region. The lightest design can be obtained when the first natural frequency lies at the lower limit of the soft-stiff region.

One can tune the structure's natural frequency by changing distribution of mass and stiffness. Multiple methods to calculate the first natural frequency of a clamped structure are described by Chopra [8] and Clough and Penzien [9]. The representation of the effect of the soil on the

clamped structure's natural frequency has been described by Zaaijer [81]. The model used in this research is based on the combination of the uncoupled spring method from Zaaijer and the improved Rayleigh method from Clough and Penzien.

Structure clamped at mud line The natural frequency is determined by the mass and stiffness distribution of a structure [8] [9]. When the structure is vibrating at its natural frequency no vibrational energy is lost to the environment. In that case conservation of energy applies and the maximum potential energy, V_{max}, is converted to the maximum kinetic energy, T_{max}, and vice versa. The vibration shape needs to be known to assess the amount of vibrational energy. For now the vibration shape, v, is assumed to be a function of a known shape function, $\phi(x)$, and a corresponding maximal amplitude, Z_0, see equation 4.35.

$$v(x) = Z_0 \cdot \phi(x) \tag{4.35}$$

The potential and kinetic energy can now be expressed as a function of the mode shape, amplitude, mass distribution, $m(x)$, stiffness distribution, $EI(x)$ and the angular frequency, ω. To obtain the potential energy the stiffness distribution is multiplied with the squared of a second derivative of the mode shape, $\phi''(x)$, and integrated over the structure's length, L, see equation 4.36. The kinetic energy is obtained by the integration over the structure's length of the multiplication of mass distribution with the square of a segments velocity, see equation 4.37. Here, the velocity term is expressed as the angular frequency times the mode shape.

$$V_{max} = {}^1\!/_2 \, Z_0 \int_0^L EI(x)[\phi''(x)]^2 \, dx \tag{4.36}$$

$$T_{max} = {}^1\!/_2 \, Z_0^2 \, \omega^2 \int_0^L m(x)[\phi(x)]^2 \, dx \tag{4.37}$$

Combining equations 4.36 and 4.37 results in Rayleigh's method describing the angular frequency as function of the structure's mass and stiffens distribution, see equation 4.38.

$$\omega^2 = \frac{\int_0^L EI(x)[\phi''(x)]^2 \, dx}{\int_0^L m(x)[\phi(x)]^2 \, dx} \tag{4.38}$$

The accuracy of Rayleigh's method depends on the chosen mode shape. If the chosen mode shape does not represent the actual vibration shape, then this will result in an overestimation of the natural frequency. Therefore, the improved Rayleigh method is used. This method uses an iterative process to obtain the exact natural frequency independent of the initially chosen mode shape. The implementation of this method into the model is described in Appendix D.

Addition of non-structural mass: Non-structural masses also play a role in the determination of the natural frequency. Examples are the mass of the RNA assembly, electrical unit, the grouted connection, water inside and outside the MP, ice and marine growth. In table 4.9 an overview is provided how these masses are added to the structure's structural mass.

Table 4.9: Overview of non structural masses

Non-structural mass	**Location**	**Point mass** [kg]	**Density** $[kg/m^3]$
RNA assembly	Tower top	Wind turbine specific	
Electrical unit	Platform	$50 \cdot 10^3$	
Marine growth	Mud line to LAT		1400
Grouted connection	Overlap MP and TP		2500
Water [1]	Mud line to water level		1050
Ice [2]	not included		900

[1] *see equation 4.39 and 4.40*

[2] *in the verification of the natural frequency computation ice mass has been included to improve to comparison with Butendiek reference data*

The inner water mass, $m_{water,in}$, is only added to the mass of the MP design, see equation 4.39. Here, dV represent the volume of one segment. The outer water mass depends on the inertia coefficient, C_M, required by the Morison inertia term, see equation 4.40.

$$m_{water,in} = \rho_{water} \cdot dV \tag{4.39}$$

$$m_{water,out} = (C_M - 1) \cdot \rho_{water} dV \tag{4.40}$$

Soil Interaction: The soil interaction is represented by angular frequency of three parallel systems. The first system is described by the clamped structure. The second and third systems corresponds to the soil interaction of the structure. The total system is described by putting the three systems in parallel. Here the squared angular frequency of the total system is equal to summation of one divided by the squared angular frequency of each system, see equation 4.41 [39] [45].

$$\frac{1}{\omega_t^2} = \frac{1}{\omega_{clamp}^2} + \frac{1}{\omega_{lat}^2} + \frac{1}{\omega_{rot}^2} \tag{4.41}$$

Here, the lateral angular frequency, ω_{lat}, and rotational angular frequency, ω_{rot} , are derived from a lateral and rotational spring that represent the soil interaction, see figure 4.7 [81].

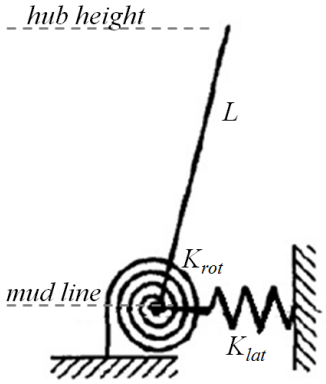

Figure 4.7: Uncoupled spring representing soil interaction

Soil interaction monopile: The MP soil interaction is represented by one lateral translation and one rotational spring. The lateral soil deflection model, described in section 4.3.1, is used to obtain the stiffness of both springs. This is done by loading the springs linearly, hence representing a SLS load case. To find the stiffness of the lateral translation spring a force is applied at the mud line, $F_{mud\ line}$. As a result a deflection, du, is induced. The lateral translation spring stiffness, K_{lat}, can be found by dividing the applied force by the obtained lateral deflection, see equation 4.42. The same method results in the rotational spring stiffness, K_{rot}, but now only a bending moment, M, is applied, see equation 4.43. A schematic overview of this process can be seen in figure 4.8(a). Because all springs behave linear, the deflection or rotation at the mud line also varies linearly with the force of bending moment. Hence, the obtained spring stiffness values are independent of the applied force or bending moment.

$$K_{lat} = \frac{F_{mud\ line}}{du} \tag{4.42}$$

$$K_{rot} = \frac{M_{mud\ line}}{\phi} \tag{4.43}$$

Now the angular frequency can be found by using equation 4.44 and 4.45.

$$\omega_{rot}^2 = \frac{K_{rot}}{I_{rot}} \tag{4.44}$$

$$\omega_{lat}^2 = \frac{K_{rot}}{I_{lat}} \tag{4.45}$$

The structure's rotational inertia, I_{rot}, is equal to mass multiplied with the distance to the mudline integrated over the length, x, see equation 4.46. The inertia term corresponding to the lateral system, I_{lat}, is equal to the mass of the structures mass, see equation 4.47. For both cases the

mass of the pile embedded in the soil is not used.

$$I_{rot} = \int_0^L m(x) \cdot x^2 dx \tag{4.46}$$

$$I_{lat} = \int_0^L m(x) dx \tag{4.47}$$

Soil interaction gravity base structure: For a GBS substructure the lateral and rotation spring stiffness are described by the DNV [74]. In both cases the spring stiffness is a function to the soil shear modulus, G, the Poisson's ratio, ν, the base slab radius, R_{bs}, the depth at the bottom of the base slab with respect to the mud line, z_{bs}, and the total length of the sand layers (before a rock bottom is reached), H, see equation 4.48, equation 4.49 and figure 4.8(b).

$$K_{lat} = \frac{8GR}{2-\nu}\left(1+\frac{R_{bs}}{2H}\right)\left(1+\frac{2z_{bs}}{3R_{bs}}\right)\left(1+\frac{5z_{bs}}{4H}\right) \tag{4.48}$$

$$K_{rot} = \frac{8GR^3}{3(1-\nu)}\left(1+\frac{R_{bs}}{6H}\right)\left(1+2\frac{z_{bs}}{R_{bs}}\right)\left(1+0.7\frac{z_{bs}}{H}\right) \tag{4.49}$$

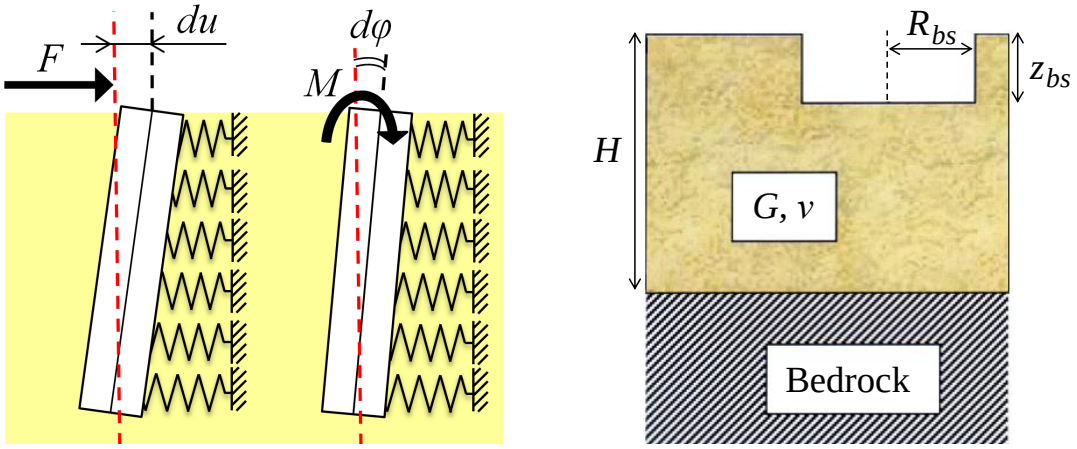

(a) Force method used to obtain soil stiffness properties for MP substructure [81]

(b) Method described to obtain soil stiffness properties for GBS substructure type [74]

Figure 4.8: Methods to obtain soil stiffness properties for the natural frequency calculations

4.3.3 Soil bearing capacity

According to Zaaijer [82] sufficient bearing capacity is the most important stability requirement for a GBS structure. Other stability requirements such as resistance against sliding, tilting and lifting of the GBS structure are therefore not considered. Sufficient soil bearing capacity means that the maximum vertical soil pressure, acting at the bottom of the base slab, can support the

combination of the total vertical force, horizontal force and bending moment acting on the structure. These forces and moments are generated by a passing wave and the statistically assumed wind loads of the tower and RNA. Hence, the soil bearing capacity requirements needs to be fulfilled for all moments of a passing wave during the lowest and highest water level. Buoyancy and heave forces also change during a passing wave as a result of a change in water level. For simplicity it is assumed that there is no difference in water level with respect to the center of the structure. The area over which the soil pressure reaction force acts is not equal to the base slab area, but depends on the ratio between the vertical force and the bending moment, see figure 4.9. The procedure to test whether or not the soil bearing capacity required is fulfilled, is described by DNV-OS-J101 [75]. A overview of the implementation of this procedure can be found in Appendix E.

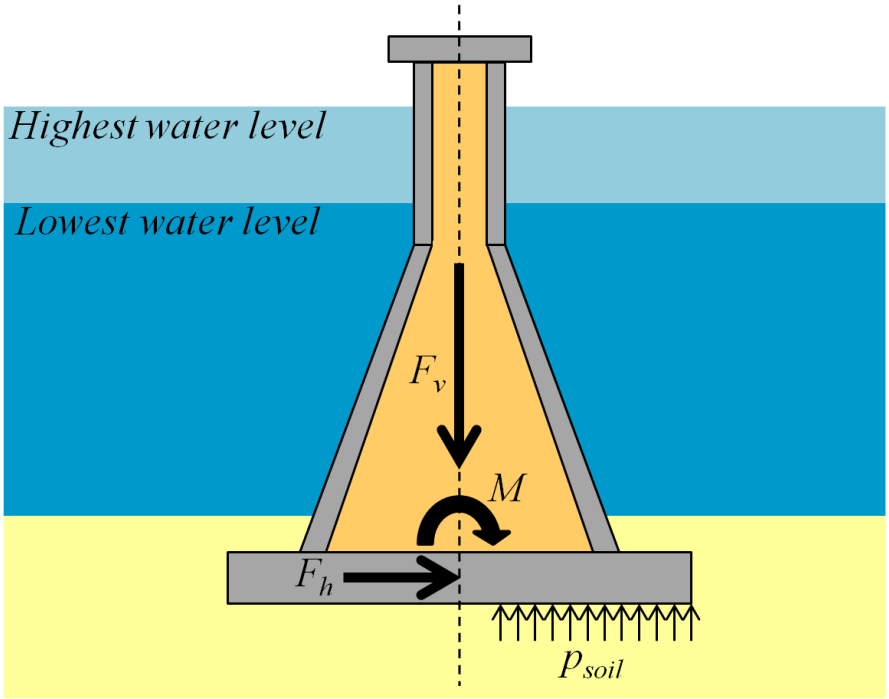

Figure 4.9: Soil pressure at bottom of the base slab as a reacting to forces and moments acting on the GBS structure

4.3.4 Local buckling

Buckling is a phenomena caused due to instability under compressive loading. Local buckling is a form of buckling where a structure starts to wrinkle locally. The structural design module evaluates the local buckling criteria at the bottom of each segment. In this research the local buckling criteria have been established according the GL [34]. In this section only a summary of these criteria are stated. Appendix F contains the entire procedure including an example calculation.

The local buckling calculations are performed for each segment of the steel construction from the mud line up to the tower top. Here, the ratio of a segments diameter over the thickness de-

termines the maximal allowable local buckling stress, see table 4.10. This is always a reduction compared to the material's yield strength.

Within the structural design model the local buckling criteria is used to scale the wall thickness of the MP, TP and tower. Here, an iterative process ensures that the MP, TP and tower all have a minimum of one element to have at least a 99.9% utilization factor for local buckling.

Table 4.10: Local buckling strength in relation to a segments outer diameter and wall thickness, generated using the method described in Appendix F

		Outer diameter [m]									
		3.0		4.0		5.0		6.0		7.0	
		[MPa] [1]	[-] [2]	[MPa] [1]	[-] [2]	[MPa] [1]	[-] [2]	[MPa] [1]	[-] [2]	[MPa] [1]	[-] [2]
	10	184	55%	156	47%	132	39%	110	33%	91	27%
	20	241	72%	220	66%	201	60%	184	55%	170	51%
	30	267	80%	249	74%	233	70%	220	66%	207	62%
Wall	40	284	85%	267	80%	254	76%	241	72%	230	69%
thick-	50	295	88%	280	84%	267	80%	256	76%	246	73%
ness	60	303	90%	290	86%	278	83%	267	80%	258	77%
[mm]	70	305	91%	297	89%	286	85%	276	82%	267	80%
	80	305	91%	303	90%	293	87%	284	85%	275	82%
	90	305	91%	305	91%	298	89%	290	86%	282	84%
	100	305	91%	305	91%	303	90%	295	88%	287	86%

[1] *Local buckling material strength with original material yield strength of 335 MPa*
[2] *Relative difference with material yield strength*

Finally, note that stress concentration factors, as a result of transitions in wall thickness or conical sections, have not been included in the calculation of a segment's stress. Also the strength of welds are not included in this research.

4.4 Optimization module

In previous sections the evaluation of a single design options is discussed. The goal of this section is to describe the procedure of finding the optimal design solution. The optimal design solution is the one that results in the lowest structural mass or costs. Furthermore, it is preferable to find this optimal solution using a low amount of computations to reduce the overall computation time. Therefore, an optimization algorithm is used.

4.4.1 Selection optimization algorithm

The implementation of optimization algorithms is a science on itself. In section 2.1 it is shown that a large amount of the studies performed on micro siting models for OWF applications is dedicated to finding a suitable optimization algorithm. Within this research only two different types of algorithms have been considered; a gradient based algorithm and a genetic algorithm. However, the gradient based algorithm results proved to be insufficiently accurate. Therefore,

the rest of this section is dedicated to describe the working principles and implementation of the genetic algorithm. Documentation of the working principles and implementation of the gradient base algorithm is provided is Appendix G.1.

4.4.2 Genetic algorithm

The chosen optimization algorithm is based on the principle of evolution and is therefore called a "genetic algorithm" [47]. The specific settings for performing this optimization process are described in Appendix G.2. The genetic algorithm uses the following steps to find the optimal design option:

1. **Creation of initial population**
   The algorithm commences by creating a number of design options, called individuals, within the boundary conditions, representing an initial population [49]. Here, each individual is composed of a value for each optimization variable, called a gene. The algorithm starts by creating a set of individuals according to a uniform distribution within the boundary conditions. Increasing the number of individuals increases the change of finding the optimal solutions, but increases the amount of computations.

2. **Evaluation of all individuals**
   A matrix containing the dimension of a support structure is created, using the values for the two optimization variables describing an individual. Each support structure is given a score based on the objective function, called the fitness value. Support structures that exceed one of the constraints receive an infinite high score [48]. The specific execution of the evaluation process is described in the next subsection.

3. **Selection of best scoring individuals**
   The support structures with the lowest scores are selected to become parents for a new population.

4. **Creation of new population**
   A population of new individuals is created using the selected parents from the previous population. Three types of new individuals exist, these are called children [49]. A crossover child is created by combining the genes of two parents. A mutation child is formed by introducing a mutation on a single gene of a parent. An elite child is a direct copy of an elite parent, which are the parents with the best fitness values.

   Mutated individuals allow for a search outside the search area covered combinations of genes of the initial population. The mutation occurs random on top of an existing gene value. The mutation magnitude decreases in the course of the optimization process, allowing the algorithm to zoom in on the optimal solution.

5. **Repetition of evaluation, selection and creation process**
   Repeating the process of creating and evaluating populations could result an approximation of the optimal solution. The algorithm stops this process when one of the stopping criteria are met. Either a maximum amount of generations is reached, a certain computation time limit is reached, or the algorithm has converged. The latter means that no change is observed in the optimal objective value for a certain number of succeeding generations.

4.4.3 Evaluation design option

The evaluation of a design options occurs through a series of steps. These steps have been visualized in figure 4.10.

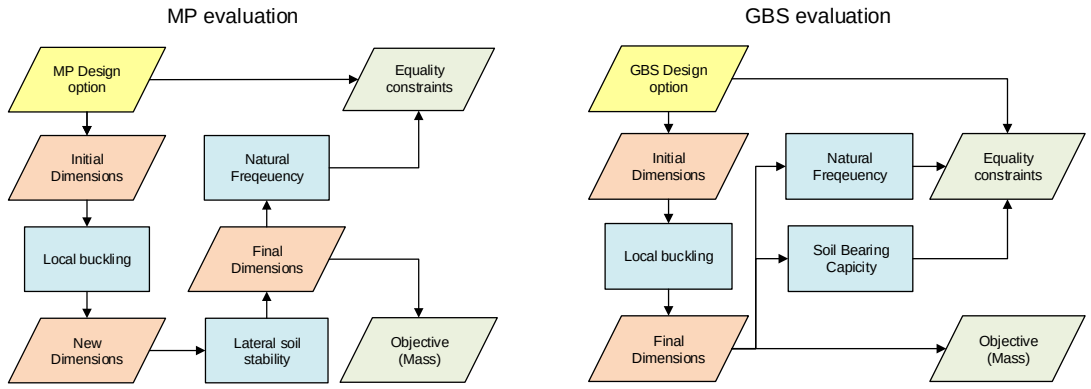

(a) Evaluation of a single MP design option

(b) Evaluation of a single GBS design option

Figure 4.10: Evaluation of a single MP and/or GBS based support structure

.

Initial support structure: The initial support structure dimensions are created, based on the values given to the optimization variables. For the MP support structure the wall thicknesses and pile penetration length are not defined for this initial support structure. For the GBS structure only the tower wall thickness is not defined.

Constraint based variables The local buckling and lateral soil stability design requirements are performed in an iterative loop, until the corresponding constraint based variables have obtained a minimum allowable value. During each iteration the dimensions of the entire support structure are redefined. As a result of this process the MP, TP and tower wall thickness and the pile penetration depth are not required as optimization variables. Hence, less iterations of the genetic algorithm are required, resulting in a faster optimization process. A justification for using these constraint based variables is presented in Appendix G.3.

Constraints used by Genetic Algorithm: The resulting design requirements are used as constraints to evaluate a design option. For the MP based support structure only the natural frequency design requirement remains. For the GBS based support structure the natural frequency and soil bearing capacity design requirements are used. Furthermore, for both the MP and GBS based support structure the lower diameter is required to be larger than the upper diameter, see table 4.11.

Objective: The objective of the optimization problem is to find the lowest structural mass. However, the ultimate goal of a micro siting model is to calculate the revenues and expenses

Table 4.11: Constraints used by genetic algorithm

	Constraint		
MP and GBS	First natural frequency	<	three times the lower boundary of the WT operation frequency
	First natural frequency	>	the upper boundary of the WT operation frequency
	Wall thickness (of each steel segment)	<	maximum wall thickness
MP	Lower MP diameter	>	Upper MP diameter
	Pile penetration depth	<	Maximum pile penetration depth
GBS	Soil Bearing Capacity to unity	<	1
	Base slab diameter	>	Diameter cylindrical section GBS

of OWF components. Fortunately, the objective of the optimization problem can be replaced without affecting the principles behind this research. For example different material prices can be assigned to the steel used for the MP and TP.

Chapter 5

Installation Process Model

In this chapter the installation process model is described. Firstly, the variables used to describe an installation process are listed. For the implmentation of each variable a short description is given. Secondly, two different installation time computation methods are presented.

5.1 Theory on installation process

An overview of the independent variables used to describe the installation process is presented in table 5.1. Furthermore, for each variable it is stated whether or not it is affected by the substructure type and installation vessel properties. A description of the use of each variables is given in the course of this section. Variables that not have been included within the model are listed in Appendix A. The reason for not including these variables is to limit the scope and complexity of the installation process model.

Table 5.1: Independent variables to describe installation process per installation vessel

Variables included in the model	**Differs per installation vessel**	**Differs per substructure type**
Earliest start date	No	Yes
Number of turbines	No	No
Distance to harbour	No	Yes
Installation vessel properties		
- Crane lifting capacity	Yes	No
- Number of components on board	Yes	Yes
- Run for shelter conditions	Yes	No
- Traveling speed	Yes	No
Description of installation cycle		
- Installation strategy	Yes	No
- Activity time	Yes	Yes
- Allowable environmental conditions	Yes	Yes
- Linking activities	Yes	Yes
- Grouting	No	Yes
- Inner array traveling time	Yes	No
- Loading time at harbour	Yes	Yes
Contingency factor on required weather window time	No	No
Risk of not finishing on time	No	No

Brief description of all variables listed in table 5.1:

- **Earliest start date**
  The installation starting date determines which weather conditions are present throughout the entire installation process. Preferably one only works in the months with the best weather conditions. In Europe the best weather conditions occur in the summer months. When the total net installation time is high it is not always possible to install all substructures during the summer months. Therefore, depending on the total net installation time there is an optimal day to start the installation. The model is able to calculate this ideal start date resulting in the lowest total installation time. However, due to other external factors, such as legislation of noise production, required sea temperature for grouting, availability of the installation vessel or overall planning of entire OWF installation, at least an earliest start date is required. Considering these external factors the start date could differ per substructure type.

- **Number of turbines**
  The amount of substructures that are needed to be installed mainly determines the overall length of the entire installation process.

- **Distance to harbour**
  The distance to the harbour together with the vessel traveling speed determine the traveling time from harbour to offshore site. Per substructure type a different harbour can be

chosen. The performed analysis only focuses on the use of a single harbor. No analysis is performed considering a set of multiple harbors.

- **Installation vessel properties**

  - **Crane lifting capacity**
    If the heaviest substructure component exceeds the main installation vessel crane capacity, then this installation vessel is discarded as a viable design option. Alternative options, such as using more than one crane, are not considered.
  - **Number of components on board**
    The number of components on board of the main installation vessel is only applicable for the transiting installation strategy. The total amount of components fitting on the deck can be calculated by using the deck size and deck loading capacity. As not every square meter of deck can be used and not all decks are the same, the number on board component will be assigned manually.
  - **Run for shelter conditions**
    These conditions dictate the maximum allowable environmental conditions of a vessel to still be safely at sea. Before these conditions are met the installation vessel needs to be in a safe place, such as a bay or the harbour. In the model the nearest shelter locations is assumed to be the harbour.
  - **Traveling speed / Traveling time**
    The traveling time to the harbour, $t_{trav,main}$, is used when the vessel needs to travel to the harbour. This can be calculated by dividing the distance to harbour, $d_{harbour}$, by the vessels speed, v_{main}, see Equation 5.1. Reasons for traveling to the harbour are running for shelter or having to reload components. The assumption is made that the traveling time does not depend on the vessel's location within the wind farm. For simplicity no influence on the traveling time is assumed as a result of water currents, wind or traveling direction.

$$t_{trav,main} = \frac{d_{harbour}}{v_{main}} \tag{5.1}$$

- **Description of installation cycle**

  - **Installation strategy and the number of supply vessels**
    The installation strategy is automatically determined by choosing an installation vessel. WIV and multipurpose jack-up vessels are assumed to use the transiting strategy. The jack-up barges and crane vessel are assumed to use the feeding strategy.

    For the feeding strategy the assumption is made that a substructure component is always available at the main installation vessel. The highest amount of supply vessels is required when the main installation vessels installs substructures without any time delays. To calculate the amount of supply vessels required in this situation first the net cycle time of the supply vessel needs to be calculated. This is the summation of the loading in harbour time of a batch of substructures, $t_{load,batch}$, the traveling time

to the main installation vessel and back to the harbour, $t_{trav,sup}$, and the time it takes until the last substructure is handed over to the main installation vessel with respect to the start of the first installation cycle of batch, t_{ho}, see equation 5.2.

$$t_{sup,cycle} = t_{load,batch} + 2 \cdot t_{trav,sup} + t_{ho} \tag{5.2}$$

Here, the traveling time can be calculated by diving the distance from the harbour to the offshore site by the speed of the supply vessel, v_{sup}, see equation 5.3. No distinction is made between the directions of travel. For simplicity, a slower vessel traveling speed as a result of an increased drag due to the increased weight is not accounted for.

$$t_{trav,sup} = \frac{d_{harbour}}{v_{sup}} \tag{5.3}$$

The total loading at harbour time of a batch depends on the loading time per substructure, $t_{load,sub}$, and the carrying capacity of the supply vessel, cc_{supply}, see equation 5.4.

$$t_{load,batch} = cc_{supply} \cdot t_{load,sub} \tag{5.4}$$

When the supply vessel carries more than one substructure, it is assumed that it needs to wait in the proximity of the main installation until all substructures have been handed over. The supply vessel cycle time is increased with a number of installation cycle times. Furthermore, a back up vessel is required to mitigate the risk of time delay as a result of a failure of one of the supply vessels. The miminium required number of installation vessels can then be found by using equation 5.5.

$$n_{sup} \geq \frac{t_{sup,cycle} + (cc_{supply} - 1) \cdot t_{main,cyle}}{t_{main,cyle} \cdot cc_{sup}} + 1 \tag{5.5}$$

– **Activity time**
The installation process of one single substructure is called an installation cycle. An installation cycle differs per substructure type and installation vessel. An installation cycle can be split into smaller parts, called activities. Each activity can have its own maximum allowable environmental conditions. Improving the installation cycle time is a complex process, that is often based on a company's experience. Therefore, no estimation concerning the installation cycle time, as function of the substructure type and dimensions and the installation vessel, will be performed. Instead, the activity time will need to be inserted manually. Activity times are usually in the order of one to several hours.

– **Allowable environmental conditions**
Each activity also has its own maximum allowable environmental conditions. These are defined by the significant wave height, wave period and wind speed. During

an activity the allowable conditions are not allowed to be exceeded. The required period of time, during which these conditions are not allowed to exceed the allowable environmental conditions, is called a weather window. The environmental conditions are assumed to be the same within the entire OWF.

- **Linking activities**
  It is possible to link certain activities together. This means that a second activity needs to be performed straight after the first activity is finished. However, since both activities could have different required weather windows they cannot be combined into one activity. The required length of the weather window now becomes the combined length of both weather windows, according to section 5.2.2.
- **Grouting**
  When a TP is connected to a MP, usually a grouted connection is used. After the grout is inserted inside the cavity between the MP and the TP, it requires some time to cure. During this curing process the substructure is not allowed to undergo severe wave loading for a specified amount of time. Default values chosen for this grout curing process are a maximum significant wave height of 2.0 meters for 24 hours.
- **Traveling time within the OWF**
  The traveling time within the OWF is assumed to be constant throughout the entire OWF substructure installation process. Further it is considered as an activity part of the installation cycle, with its allowable environmental conditions being equal to the run for shelter conditions.
- **Loading time at harbour**
  The transiting installation strategy on commuting between the offshore site and the harbour. At the harbour new foundation components needs to be loaded onto the vessel. The loading at harbour time should depend on the number of on-board components. However, for simplification purposes it needs to be manually inserted.

- **Contingency factor on required weather window time**
  A contingency factor is used to account for the uncertainties during the installation process. The main uncertainties are a delay in performing an activity and an unexpected change in weather conditions. The required weather window of one single activity or multiple activities is increased by multiplying the activity time with a contingency factor. The default value for this contingency factor is 1.5.

5.2 Calculating the total installation time

In this section two methods are presented to calculate the total substructures installation time. In section 6.4 a comparison is made between these two methods via a sensitivity analysis.

5.2.1 Workability percentages method

Calculation method: The workability percentages method uses the workability of the installation steps to predict the total substructures installation time. An installation step is considered

to be either an offshore installation activity, traveling activity or loading at the harbor activity. Workability, W, is defined as the relative amount of time an installation step can take place. The workability depends on the location specific environmental conditions, E_{loc}, the allowable environmental conditions for an installation step, E_{max}, and the net time of an installation step, $t_{n,step}$, see equation 5.6. Site specific environmental conditions constantly change throughout the year. Therefore, the workability is chosen to be calculated per month of the year. The allowable environmental conditions depend on the properties of the main installation vessel and substructure type.

$$W = f(E_{loc}, \quad E_{max}, \quad t_{n,step}) \tag{5.6}$$

By using a workability percentage a net activity time, t_n, can be converted to a gross activity time, t_g, [44] [36]. Such a conversion can be performed on all required installation steps. This results in the gross time for an installation activity, $t_{g,act}$, traveling of the main installation vessel, $t_{g,trav}$, and loading at harbor of the main installation vessel, $t_{g,load}$, see respectively equation 5.7a up to 5.7c. When activities are linked the workability percentage of an activity is multiplied with all workability percentage of all following activities to which it is linked.

$$t_{g,step} = \frac{t_{n,step}}{W_{step}} \begin{cases} t_{g,act} = \dfrac{t_{n,act}}{W_{act}} & \text{(5.7a)} \\ t_{g,trav} = \dfrac{t_{n,trav}}{W_{trav}} & \text{(5.7b)} \\ t_{g,load} = \dfrac{t_{n,load}}{W_{load}} & \text{(5.7c)} \end{cases}$$

The time spent offshore, at the main installation vessel to install one substructure, is called the cycle time. The gross cycle time, $t_{g,cycle}$, consist of the summation of each gross activity time over the number over installation activities, n_{act}, see equation 5.8.

$$t_{g,cycle} = \sum_{i=1}^{n_{act}} t_{g,act\,i} \tag{5.8}$$

Combining the gross cycle-, traveling- and loading time per substructure results in the gross installation time per substructure, $t_{g,sub}$. For the transiting installation strategy a correction is applied to account for the carrying capacity of the main installation vessel, cc_{main}, see equation 5.9. For the feeding installation strategy the gross installation time per substructure equals the gross installation cycle time, see equation 5.10. This is a simplification because the main installation vessels needs to travel to the offshore location at least one time throughout the entire installation season.

Transiting installation strategy:

$$t_{g,sub} = \frac{cc_{main} \cdot (t_{g,cycle} + t_{g,load}) + 2 \cdot t_{g,trav}}{cc_{main}} \tag{5.9}$$

Feeding installation strategy:

$$t_{g,sub} = t_{g,cycle} \tag{5.10}$$

The number of substructures that can be installed within a month results from dividing the number of hours in a month, h_{month}, by the corresponding gross time in hours to install a substructure, see equation 5.11. This calculation can be performed for each month of the year.

$$n_{sub,month} = \frac{h_{month}}{t_{g,sub}} \tag{5.11}$$

The total installation time for all substructures can be calculated by combining the start date of installation with the amount of substructures to be installed within a month.

Obtaining Workability Data: All workability data needs to be converted from measurement or hind cast data. However, measurement or hind cast data is considered valuable information which companies are often not likely to share openly. Therefore, they convert the measurement or hind cast data into a set of workability percentages. These percentages are presented in a number of tables. Each table shows the workability percentages per month of the year for either a specific maximum wind speed or a specific wave height. An example of workability data for OWF Hohe See is given in table 5.2.

Two different methods to obtain workability data can now be distinguished:

- Measurement or hind cast data is available from which workability data can be derived.
- Pre-processed measurement or hind cast data is available and presented in a number of tables.

It is preferable to use directly used measurements or hind cast data. For then an exact description of the activity can be used to find the corresponding monthly workability percentage. This will be illustrated again by a theoretical example. Assumed is an activity with the following properties; activity time of 8 hours, allowable significant wave height of 1.25m and allowable wind speed of 15 m/s. In table 5.3 the results of three scenarios are presented. Firstly, there is the case where measurement or hind cast data is available. Here, all activity properties can be used to obtain a workability percentage. Secondly, there is the case where the use of pre-processed data is required. Here, a choice needs to be made concerning the installation time and significant wave height due to the lack pre-processed data. To account for this, a conservative and optimistic

Table 5.2: Example of a selection of pre-processed workability percentages for Hohe See location.

	Vw lim [m/s]	Vw ≤ 15.0						
Window	Hs lim [m]	Hs ≤ 0.25	Hs ≤ 0.50	Hs ≤ 0.75	Hs ≤ 1.0	Hs ≤ 1.5	Hs ≤ 2.0	Hs ≤ 3.0
3 hr	Jan	0,0%	0,0%	0,9%	6,1%	22%	47%	70%
	Apr	0,0%	0,0%	18%	33%	67%	82%	96%
	Jul	0,0%	4,7%	19%	53%	82%	93%	98%
	Oct	0,0%	0,0%	0,5%	6,1%	24%	43%	73%
6 hr	Jan	0,0%	0,0%	0,9%	5,7%	20%	47%	70%
	Apr	0,0%	0,0%	18%	32%	67%	82%	96%
	Jul	0,0%	4,0%	19%	52%	82%	93%	98%
	Oct	0,0%	0,0%	0,0%	6,1%	24%	43%	72%
12 hr	Jan	0,0%	0,0%	0,0%	5,7%	18%	46%	69%
	Apr	0,0%	0,0%	17%	28%	67%	82%	96%
	Jul	0,0%	3,2%	19%	52%	82%	93%	98%
	Oct	0,0%	0,0%	0,0%	6,1%	24%	40%	70%
24 hr	Jan	0,0%	0,0%	0,0%	3,2%	14%	38%	69%
	Apr	0,0%	0,0%	14%	28%	65%	82%	95%
	Jul	0,0%	3,2%	5,8%	42%	79%	93%	98%
	Oct	0,0%	0,0%	0,0%	3,6%	22%	32%	65%

* *The values of the cells marked gray are used in table 5.3*

scenario are defined. For the conservative scenario the installation time is rounded up and the allowable significant wave height is rounded down to the nearest available data point of table 5.2. For the optimistic scenario the opposite is done.

A large difference in workability percentages can be observed between the three scenarios of table 5.3. It can therefore be concluded that the use of pre-processed workability data could lead to an inaccuracy of the workability method.

Table 5.3: Difference between workability percentages derived from hind cast data and pre-processed workability data of Hohe See OWF

	Direct use of hind cast data	**pre-processed data conservative**	**pre-processed data optimistic**
	t ≤ 8.0 h Hs ≤ 1.25 m Vw ≤ 15.0 m/s	t ≤ 12 h Hs ≤ 1.0 m Vw ≤ 15.0 m/s	t ≤ 6.0 h Hs ≤ 1.5 m Vw ≤ 15.0 m/s
Jan	13%	5.7%	20%
Apr	55%	28%	67%
Jul	72%	52%	82%
Oct	15%	6.1%	24%

5.2.2 Time series method

Working principle: The time series method is not described in literature as far as the author is aware of. This method is based on a method used by the Ballast Nedam offshore wind department. In this research the amount of design variables has increased compared to the models present at Ballast Nedam. Furthermore, the use of Matlab instead of Microsoft Excel, as software package, allowed for a much smaller computation time. The time series method uses measurement or hind cast data to predict the total OWF substructure installation time. It walks step by step through the environmental data samples, hence the name "time series method". During each step the main installation vessel is either performing an activity (installation, loading or traveling) or waiting on the weather to improve.

The basis of a decision lies in the evaluating of weather windows. A summarize of possible situations is presented in table 5.4.

Table 5.4: Decision made by TS model based on vessel location and weather window requirements

Location of main installation vessel	**Decision to be made**	**Required weather window time**	**Required weather window conditions**	**Performing time**
harbour	start traveling	$2 \cdot t_{travel}$	run for shelter	t_{travel}
harbour	start loading	t_{load}	no restrictions	t_{load}
Offshore site	start activity	$t_{n,act} \cdot \alpha + t_{travel}$	specific activity and run for shelter	$t_{n,act}$
Offshore site	start grouting activity	$t_{n,act} \cdot \alpha + t_{grout} + t_{travel}$	grouting activity, grout curing and run for shelter	$t_{n,act}$

Once a decision is made, the main installation vessel start to perform the corresponding activity (installation, loading, traveling or waiting). Since the criteria of table 5.4 have already been evaluated, the main installation vessel will always be able to perform the activity without the allowable environmental conditions being exceeded. After completing an activity, the main installation vessel will also have enough time to run for shelter. A schematic overview of the processes that are included within this method can be seen in figure 5.1.

Step size: The step size is the highest common time interval in which all weather windows can be evaluated. In theory all step sizes are possible. It has been found out that a linear increase in step size will lead to an exponentially longer computation time. Hence, a minimum step size of 15 minutes has been chosen. Resulting in an activity time with an accuracy of 30 minutes (due to contingency factor $\alpha = 1.5$). Once the step size is chosen or calculated the measurement or hind cast data sample time needs to be corrected for the step size. In this research data has been obtained with a sample time of one hour, which becomes the maximum steps size. If a step size of 15 minutes is required, the environmental conditions values of each 15 minute sample have the same values of the original one hour sample.

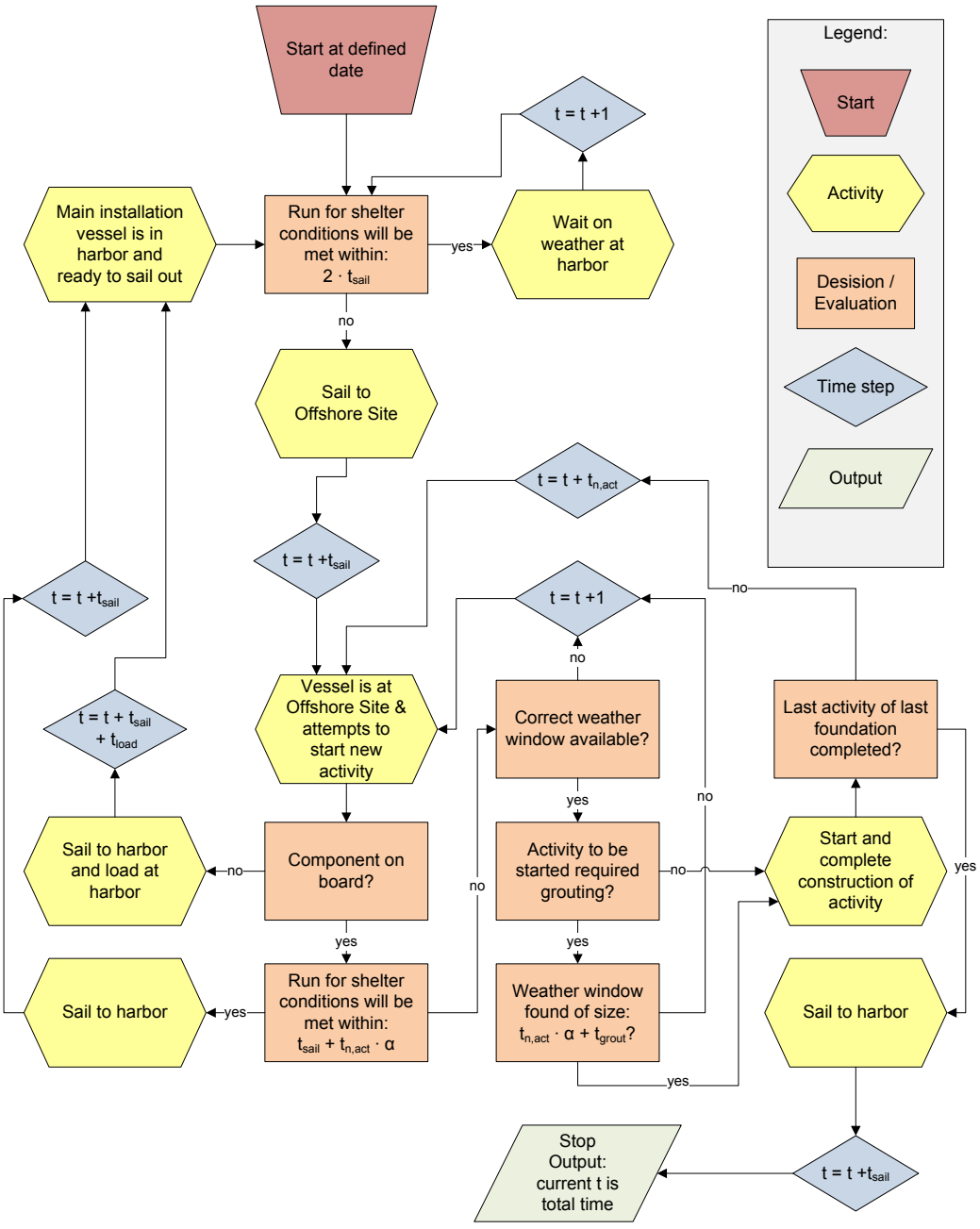

Figure 5.1: Flow diagram of the processes involved in the Time Series Model

Linking of activities: The schematic overview of figure 5.2 explains the computation of the correct weather window when activities are linked. Because activities can have different maximal allowable environmental conditions, care should be taken to correctly implement a contingency factor when activities are linked. Linking activities together does not mean that the activity times can be simply added up and multiplied with a contingency factor to find the correct weather window. An example is given for an installation cycle composed of three activities that take respectively 2, 8 and 6 hours to complete, see figure 5.2. For the unlinked situation, the required weather window time for each activity is calculated by adding the activity time with a contingency time, see figure 5.2(a) and table 5.5. For the linked situation one can only start the first activity when one is certain that the second and third activity can be performed straight afterward. Therefore, at the start of the first activity all three weather windows need to be available at the right moment, see figure 5.2(b) and table tab:Linking. On top of that the length of the second and third weather windows increase as a result of the addition of the contingency time of previous activities.

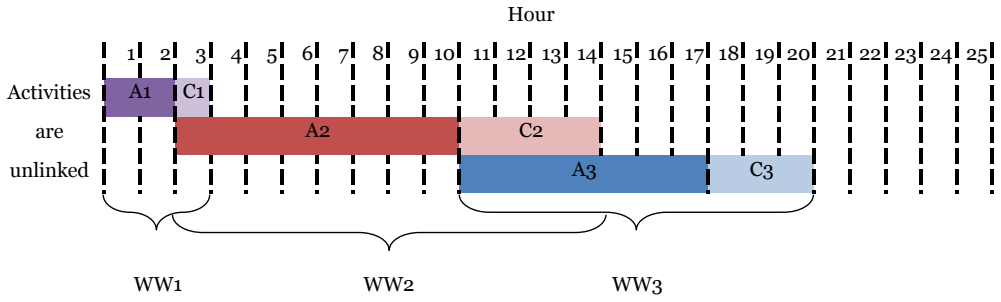

(a) Example of required weather window times for installation cycle with unlinked activities

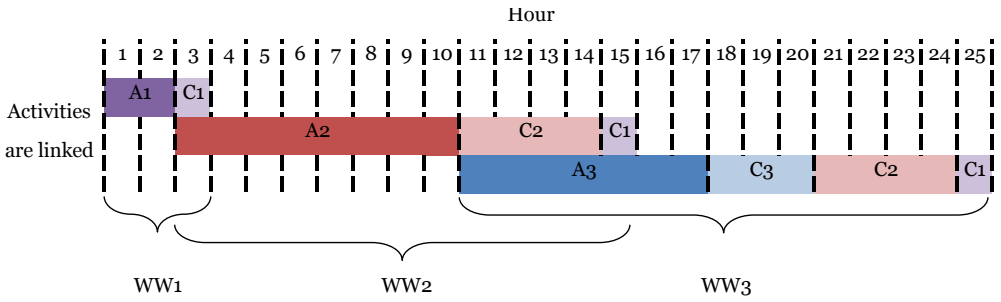

(b) Example of required weather window times for installation cycle with linked activities

Figure 5.2: Examples of installation cycles to illustrate the effect of linking activities
A = Activity, C = Contingency, WW = Weather Window

Table 5.5: Requirements to start activity according to example illustrated by figure 5.2

	Start	Requirement
Unlinked	Activity 1	Weather window 1 must be available
	Activity 2	Weather window 2 must be available
	Activity 3	Weather window 3 must be available
Linked	Activity 1	Weather windows 1, 2 and 3 most be available
	Activity 2	Automatically complies if activity 1 is allowed to start
	Activity 3	Automatically complies if activity 1 is allowed to start

Chapter 6

Verification

In this chapter the accuracy of the structural design and installation process model is verified. Two preliminary designs of monopiles and transition pieces and two hind cast data sets have been provided by Ballast Nedam Offshore. Firstly, the structural design model's components are evaluated based on the reference data. Furthermore, the accuracy of the optimization solver is assessed. Then a sensitivity analysis is performed to assess the effects of changing values of independent variables defined by the OWF's location, an individual substructure location and choices made by the micro siting model. Secondly, the accuracy of the installation process model is evaluated. This is done by a theoretical comparison between the WP and TS method. Finally, a sensitivity analysis is performed on both installation time calculation methods by using hind cast data of two OWF locations.

6.1 Data provided by Ballast Nedam Offshore

Ballast Nedam Offshore has provided data to verify the model. Since the beginning of Dutch offshore wind energy Ballast Nedam Offshore is involved in installation substructure components at various projects. Their installation vessel the HLV Svanen has installed over 350 monopiles [58]. Together with their engineering department Ballast Nedam Offshore tries to provide the entire scope from the design to the installation of substructures.

The provided data consists of:

- Preliminary monopile and transition piece design for OWF Butendiek
- Preliminary monopile and transition piece design for OWF Baltic I
- Hind cast data set of OWF Hohe See
- Hind cast data set of OWF Wikinger

6.2 Verification Structural Design Module

In this section most structural design components are evaluated for their accuracy. Some structural design components are not evaluated, for example the soil bearing capacity requirement, because no data is found to perform such an evaluation.

6.2.1 Reference Designs

The purpose of verifying the structural design of an individual support structure is to assess the accuracy at which the dimensions of that support structure are scaled. A small number of reference design, with their corresponding site specific conditions, is used for this process. Two reference designs have been obtained for a MP based support structure. These reference designs have been provided by Ballast Nedam and correspond to the preliminary structural design for the Butendiek [21] and Baltic I [20] OWFs, see table 6.1. The reference design for the GBS case corresponds to that for the Thornthon Bank OWF and is publicly available online [13], see table 6.2. Site specific conditions and WT properties can be found in Appendix H.2.

Table 6.1: Dimensions and masses of preliminary MP design of Butendiek OWF [21] and Baltic I OWF [20]

OWF	**Optimization variables**		**Constraint based variables**				**Structural mass**		
	$D_{MP,low}$ [m]	$D_{MP,up}$ [m]	$t_{MP,mud}$ [m]	$t_{TP,low}$ [m]	$t_{tow,low}$ [m]	L_p [m]	MP [ton]	TP [ton]	Tower [ton]
Butendiek	6.00	5.19	0.095	0.080	0.045[a]	28.5	635	256	226
Baltic I	5.05	4.50	0.080	0.060	0.035[a]	40.0	410	161	139

[a] *wall thickness required to obtain correct tower mass, see section 4.1.5*

Table 6.2: Dimensions and masses GBS design Thornton Bank [13]

OWF	**Optimization variables**		**Constraint based variables**	**Structural mass**		
	$D_{MP,low}$ [m]	$D_{MP,up}$ [m]	$t_{tow,low}$ [m]	GBS [ton]	Ballast [ton]	Tower [ton]
Thornton Bank	23.5	6.5	unknown	3000	4000[a]	unknown

[a] *estimated based on the volume of ballast sand and a ballast sand density of 1800* kg/m^3

Note that there is a difference between a preliminary design and a final design. Preferably final designs are used in the verification process. For the purpose of this research preliminary designs are used as reference designs, because no final design data is available. The assumption is made that the preliminary designs comply to the most important design requirements. Obtaining a final design would require a more detailed design process, using more design requirements. Still, an final design for a specific wind turbine location does not have to be the lightest design. Other factors such as manufacturability, transportability and installability could result in deviations from the lightest individual design.

6.2.2 Verification Support Structure Dimensions

Independent Variables The submodel responsible for the dimensioning of the support structure is used to generate a matrix describing the support structure's dimensions. The three cases described in tables 6.1 and 6.2 are used, which means using the same optimization variables and constraint based variables. Furthermore, a number of assumptions is shown in table 4.1. To asses the accuracy of the support structure dimensioning model two different sets of assumptions is used. These are the default set of independent variables and a set which represents the reference design as closely as possible, see table 6.3.

Table 6.3: Values for independent values for Default, Butendiek and Batic I case

Independent variable	Default value	Butendiek value	Baltic I value	Thornton Bank value	Unit
Grout thickness	0.75	0.75 [21]	0.090 [20]		[m]
Grout length	$1.5 \cdot D_{MP,up}$ [a]	11.0 [21]	8.0 [20]		[m]
Air gap	1.5	1.5 [21]	1.5 [20]		[m]
Length conical section MP	5.0	7.0 [21]	3.0 [20]		[m]
Length conical section TP	4.0	6 .0 [21]	4.0 [20]		[m]
Difference in wall thickness MP pile toe	0.035	0.035 [21]	0.030 [20]		[m]
Difference in wall thickness MP top part	0.02	0.015 [21]	0.020 [20]		[m]
Difference in wall thickness TP top part	0.02	0.020 [21]	0.015 [20]		[m]
Difference in outer pile diameter TP top part	0.50	0.50 [21]	0.77 [20]		[m]
Wall thickness of pile toe	0.09	0.080 [21]	0.100 [20]		[m]
Distance LAT to to top part of MP	3.0	6.5 [21]	-5.3 [20]		[m]
Highest wave during boat landing	2.5			2.5 [b]	[m]
Draft boat landing vessel	3.0			3.0 [b]	[m]
Wall thickness GBS	0.5			0.5 [13]	[m]
Bottom base slab w.r.t. mud-line	4.5			4.5 [13]	[m]

[a] *Rounded to nearest integer, since segment length equals 1.0 m*
[b] *Assumption*

Monopile based Support Structures Using these sets of independent variables and the reference values for the optimization variables and constraint based variables, see tables 6.1 and 6.2, a matrix containing the support structure dimensions is generated. The masses of the support structure components are shown in table 6.4. Here, it can be seen that for the Butendiek case the model is capable of producing an accuracy output when the non-default independent variables are used. For the Baltic I case larger differences can be observed. These differences mainly emerge from the error in wall thickness distribution. Consequently, the assumed wall thickness distribution results in a good match for the Butendiek case, but not for the Baltic I case. When

default values for the independent variables are selected larger mass differences emerge. Hence, the choice of independent variables greatly affects the outcome of the dimensioning model. Finally, note that even though it is possible to obtain an accuracy match of component mass (Butendiek with non-default independent variables), still differences exist that can have an effect on the structural performance. For example the natural frequency is determined by the mass and stiffness distribution. A support structure with the same mass or even mass distribution can have a difference in the stiffness distribution.

Table 6.4: Output dimensions model, with manually inserted values for constraint based variables

OWF	**Reference**			**Output Default**			**Output Non-Default**		
	MP [ton]	TP [ton]	Tower [ton]	MP [ton]	TP [ton]	Tower [ton]	MP [ton]	TP [ton]	Tower [ton]
Butendiek	635	256	226	586 [a]	244	226	634 [a]	254	226
Baltic I	410	161	139	497	114	146	437	174	137

[a] *Pile penetration depth of 28.0 m is chosen, because only segments with a length of 1.0 m are allowed*

GBS based Support Structure The same process is performed for the GBS based support structure, see table 6.5. However, no constraint based variables are used to dimension the GBS based support structure. Also no non-default scenario is present.

Table 6.5: Output dimensions model, with manually inserted values for constraint based variables

OWF	**Reference**			**Output Default**		
	GBS [ton]	Ballast [ton]	Tower [ton]	GBS [ton]	Ballast [ton]	Tower [ton]
Thorntonbank	3000	4000	unknown	2876	4387	215

6.2.3 Verficitation Environmental Loads

Wind Loads A simple comparison is performed between the ULS turbine thrust force, stated within the documentation of the reference designs, and the computed turbine thrust force, see table 6.6. For these two cases the wind force is overestimated by 13-15%. This is a rather good approximation considering the huge simplifications made to obtain the turbine thrust force.

Table 6.6: Output wind load model

	Turbine Thrust [MN]	
	Reference	Computed
Butendiek	1.5	1.7
Baltic I	1.0	1.3

Wave Loads A suitable wave theory can be chosen according to figure 6.1. The dimensionless wave steepness, $H/g\,T_{app}^2$, and relative depth, $d/g\,T_{app}^2$ for Butendiek and Baltic I OWF are shown in table 6.7. In figure 6.1 it can be seen that the appropriate wave theory would be Stokes 5th order or Stream function. Nevertheless, linear wave theory has been chosen in order to provide fast computation time. According to DNV page 57 [74] a simulation using the linear wave theory in shallow waters may significantly underestimate the wave loads. Hence, an underestimation of the actual wave load is to be expected.

Table 6.7: Dimensionless wave steepness

	Water depth	**Wave height**	**Wave Period**	$\frac{H}{g\,T_{app}^2}$	$\frac{d}{g\,T_{app}^2}$
Butendiek	25.0 m	18.6 m	15.6 s	0.0078	0.0105
Baltic	25.0 m	13.1 m	13.1 s	0.0078	0.0150

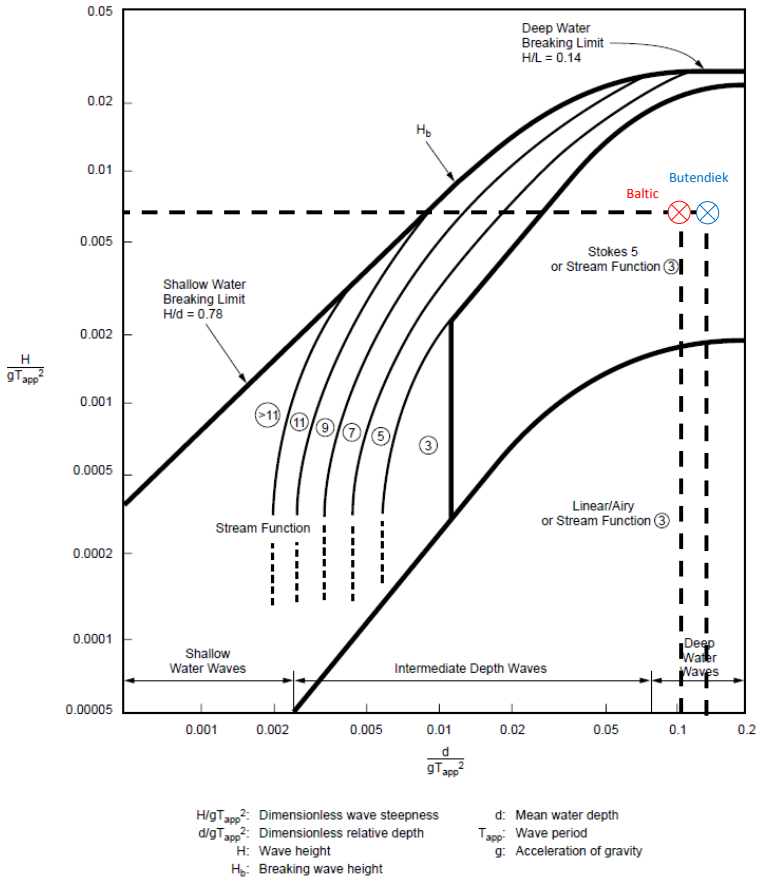

Figure 6.1: Overview of wave kinetic models and their range of applicability [76]

For the verification of the wave loads reference data of Butendiek location 48 is used. Here, the shear force and bending moment diagram have been obtained by using the stream function. Now a comparison is made between these diagrams and the output of the model, see figure 6.2. Initially the expected underestimation of model based on linear wave theory is observed. When an empirical calibration factor of 1.45 is used to increase the wave loads an almost exact match between the reference data and the models output is obtained. Note that from the mud line to the

pile toe the shear forces and bending moment diagrams are calculated by the lateral soil stability model of section 4.3.1. Also note that this empirical calibration factor is applied on top of the already applied ULS load factor of 1.35, see section 4.2.4. In conclusion the wave loads model

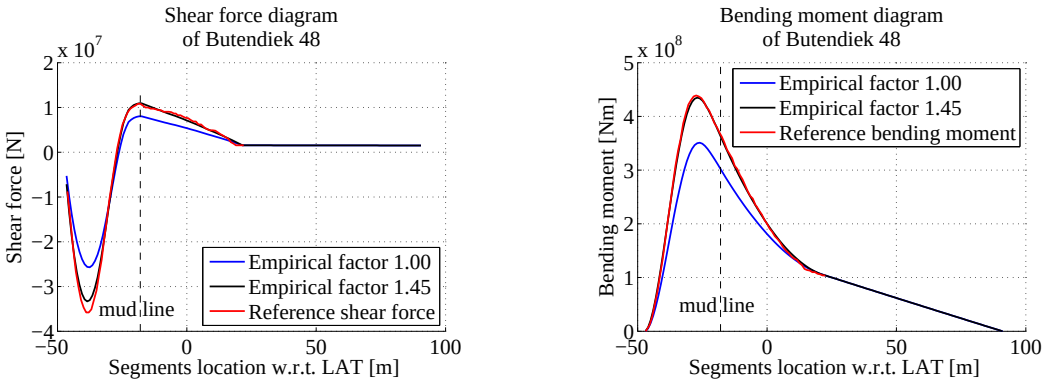

Figure 6.2: Comparison reference data and model output of shear force and bending moment diagram of Butendiek location 48

does not compute the correct extreme wave loads. This has been expected, due to the fact that this model has been chosen for its simplicity and small computation time. An increase of the wave loads with an empirical calibration factor resulted in a good match with the reference shear force and bending moment diagrams. However, this empirical calibration factor cannot be used for all combinations of water depths and wave heights. Therefore, either more information on the calculation of this empirical factor is required or an more accurate wave kinematics model is required.

The Baltic I ULS is not based on extreme wave loading, but on ice load. Therefore, no representative empirical wave load factors is found. For the structural design verification of the next sections an empirical wave load factor of 4.5 has been chosen, since it provides the correct shear force and bending moment at the mud-line. Using this wave load factor it is still possible to assess the lateral pile stability and local buckling requirement for verification purposes.

6.2.4 Lateral soil stability verification

Comparison with an analytical solution An analytical solution for a beam, lying on a elastic foundation and subjected to external forces, was described by Winkler in 1867. Here, a beam (representing the part of the MP from the mud-line down to the pile toe) lies on a elastic foundation and is subjected to external forces. The distribution of the reaction forces depends linearly on the deflection of the beam. For the purpose of this model the external loads are only applied at the begin of the beam, which represents the mud-line. The analytical solution to this problem, based on the lecture notes of S. Parvanova [59], is described in Appendix H.2.1. In this paragraph a comparison between the numerical model of section 4.3.1 and this analytical model are presented.

The analytical solution is only valid for non-varying soil stiffness. In reality this situation will never occur, because the soil stiffness depends on the soil pressure, which is a function of depth.

However, the analytical solution can be used to check the numerical model. The values for the parameters used are stated in table 6.8. Differences between both models can occur as a result of the step size used by the numerical model. Hence, several step sizes are evaluated to obtain the appropriate amount of accuracy, without requiring too much computational power. Eventually, a step size of 0.10 m is chosen to be incorporated within the FIT model.

Table 6.8: Properties used in verification of numeral model lateral soil stability by using analytical solution

Property	Value	Unit
Spring stiffness	$1.00 \cdot 10^8$	[N/m^2]
Flexural rigidity of pile	$1.6942 \cdot 10^{12}$	[Nm^2]
Pile penetration depth	30.0	[m]
Lateral force	$1.00 \cdot 10^7$	[N]
Bending moment	$3.00 \cdot 10^8$	[M]

Table 6.9: Relative displacement and rotation compared to analytical solution

	Δ L = 1.0 m	**Δ L = 0.10 m**	**Δ L = 0.050 m**
Displacement at mud-line	-8.2%	-0.94%	-0.47%
Displacement at pile toe	-12%	-1.4 %	-0.47%
Rotation at mud-line	-5.5%	-0.72%	-0.24%
Rotation at pile toe	-16%	-2.4 %	-1.6%
Computation time[a]	10^{-1} s	10^0 s	$10^1 s$

[a] *values indicate the order of magnitude*

Comparison with reference design Three design requirements have been presented in section 4.3. The pile tip displacement should be smaller than 0.12 m and $3D/100$ and its rotation should be smaller than 0.25 degrees. Furthermore, the pile toe displacement should be smaller than 0.02 m. The pile dimension of six reference design of Butendiek OWF have been inserted in the lateral pile stability model, see table 6.10. It is observed that the pile tip displacement requirement is not fulfilled for the two longest pile lengths. None of the designs complies with the pile tip rotation requirement, but that all designs comply with the pile toe displacement requirement. Therefore, only the pile toe displacement criteria will be used to address the later soil stability design requirement.

A final check is performed to see whether or not the correct pile penetration depth is computed. The dimensions of the TP and tower are also computed. Here, soil properties are either obtained from the reference data set [21] [19] or computed based on basic soil properties, see Appendix C.2. The only design requirement used is a maximum pile toe displacement of 0.02 m. The results are provided in table 6.11.

Here, it can be seen that the use of reference soil data result in an accuracy of -1.5 to +0.5 m pile penetration depth for six locations within Butendiek OWF. When the soil properties are calculated according to Appendix C.2, an underprediction of -5.5 up to -3.5 m is obtained. Comparing the computed soil properties with the reference data revealed that the properties clay

soils is not calculated as accurate as for sand soil layers. Furthermore, the reference soil data contains mixed layers of sand and clay. It is not possible to compute the properties of such layers using the relations described in the API standards [41]. For the Baltic I case an overprediction of the pile penetration depth is observed. A reason for this overprediction could be the fact that the reference soil data properties have been computed using a pile diameter of 4.3 m, while the actual pile diameter is 5.05 m. The method used in Appendix C.2 always uses the actual pile diameter.

Table 6.10: Computed pile displacement and rotation using reference designs and reference shear force and bending moment at the mud-line

	Soil Indication	Reference pile length [m]	Pile tip displacement [m]	Pile tip rotation [deg]	Pile toe displacement [m]
Butendiek 1	Stiff	28.5[a]	0.094	0.408	0.015
Butendiek 2	Stiff	29.5[a]	0.097	0.409	0.014
Butendiek 3	Moderate	31.5[a]	0.112	0.443	0.014
Butendiek 4	Stiff	30.5[a]	0.107	0.434	0.014
Butendiek 5	Stiff	30.5[a]	0.100	0.423	0.017
Butendiek 6	Weak	39.5[a]	0.211	0.593	0.016
Baltic I	Weak[b]	40.0	error[c]	error[c]	error[c]

[a] *Value will be rounded to nearest integer. For example a pile length of 28.5 m will become 29.0 m.*

[b] *No soil indication is found in reference design documentation. Comparison of soil data with that of OWF Butendiek suggests that a weak soil indication is applicable to this MP location.*

[c] *Pile penetration depth is to short. As a result a very large displacement in the order of* 10^{13} *m is obtained. A larger pile penetration depth of 43 m results in reasonably displacements, see table 6.11.*

Table 6.11: Computed pile length for two scenario's

	Reference pile penetration depth [m]	Computed pile penetration depth	
		Reference soil properties [m]	Computed soil properties [m]
Butendiek 1	28.5	28.0	25.0
Butendiek 2	29.5	28.0	25.0
Butendiek 3	31.5	30.0	28.0
Butendiek 4	30.5	30.0	26.0
Butendiek 5	30.5	31.0	28.0
Butendiek 6	39.5	39.0	34.0
Baltic I	40.0	43.0[a]	41.0

[a] *A pile diameter of 4.3 m is used for the computation of the reference soil properties. This does not comply with actual pile diameter of 5.05 m.*

In conclusion the pile penetration depth is computed with a minimum accuracy of 3 m (8%) using reference soil properties and only the pile toe deflection design requirements. Because

this inaccuracy of the pile penetration depth computation only leads to an inaccuracy in the number of pile segments, this will have a limited effect on the overall MP mass. Furthermore, this submodel is also used to compute the lateral and rotational soil spring stiffness, which is used for the computation of the natural frequency. An increment in pile penetration length of +0.5m could lead to an increase of the natural frequency of +0.5%, see Appendix H.3.2. From these points of view the pile penetration computation's accuracy is sufficient for a micro siting model. However, when the soil properties are computed according to Appendix C.2, a larger inaccuracy is observed. Therefore, future research could be directed a more accuray computation of the soil properties of both sand and clay layers.

6.2.5 Natural Frequency Verification

Reference Data The natural frequency model will be verified using reference designs of the preliminary design of OWFs Butendiek en Baltic I. For the several reference structures the first natural frequency has been computed using a FEM based model, consisting of the support structure divided in segments of 1.0 meters, see Column A of table 6.12. At some points the segment length is changed to accommodate important structural transitions. The soil interactions also consist of segment with a length of 1.0 meter each connected to a linear spring. Furthermore, the MP, TP and tower dimensions, the soil properties and the WT properties are known, except for the tower dimensions of the Baltic support structure.

The Butendiek data consists of six support structures for six different locations within the Butendiek OWF. Each location has a different water depth and different soil properties. The Baltic I data consist of one location for which two calculations are performed. One for a scour hole of 1.0 meters and one for a scour hole of 5.0 meters. In both cases the foundation pile starts at the bottom of the scour hole, which results in a different pile penetration depth for both cases.

Results The model used to calculate the natural frequency has been described by section 4.3.2. The support structure dimensions, soil properties and WT properties are manually inserted in the structural design model. As a result the the model has computed the first natural frequency for all support structures, see Column B of table 6.12. The difference between the natural frequency of the reference designs and the model is shown in Column C of table 6.12. The model over predicts the natural frequency for the Butendiek reference designs by 7.0% to 8.9% and for the Baltic I data by 2.1% to 3.3%. Other properties concerning these computations can be found in Appendix H.3.

Table 6.12: Comparison output natural frequency computation with reference data

	Column A	**Column B**	**Column C**	**Column D**	**Column E**
WT location	**Reference frequency [Hz]**	**Model frequency [Hz]**	**Difference w.r.t. to reference [-]**	**Structure clamped at mud line [Hz]**	**Difference w.r.t. model [-]**
Butendiek 1	0.305	0.331	+8.5%	0.371	- 12.1%
Butendiek 2	0.302	0.326	+7.9%	0.366	- 12.3%
Butendiek 3	0.299	0.324	+8.4%	0.366	- 13.0%
Butendiek 4	0.301	0.328	+9.0%	0.369	- 12.5%
Butendiek 5	0.298	0.324	+8.7%	0.366	- 13.0%
Butendiek 6	0.293	0.317	+8.2%	0.367	- 15.8%
Baltic I 1 [a]	0.336	0.355	+5.7%	0.385	- 8.5%
Baltic I 2 [b]	0.331	0.346	+4.5%	0.374	- 8.1%

[a] *Scour hole of 1.0 m*
[b] *Scour hole of 5.0 m*

A list of different reasons that could explain the inaccuracy of the natural frequency computations is presented in table 6.13. A description of each of these explanations is given in Appendix H.3.2.

Table 6.13: Explanations inaccuracy of natural frequency computations, see Appendix H.3.2

	Explanation	Effect
1.	The natural frequency of the structure clamped at the mud-line is over predicted	unknown
2.	Tower dimensions	+ 5.0% [a]
3.	Inaccurate mode shape	unknown
4.	RNA as point mass	unknown
5.	Use of uncoupled spring method	+ 2.0% [b]
6.	Difference in dimensions with respect to the reference design	unknown [c]
7.	Difference in pile penetration depth	+/- 0.5%
8.	Location of springs representing soil interaction	+/- 0.1%
9.	Corrosion at splash zone	+/- 0.1%
10.	Location of other point masses	+/- 0.1%

[a] *only applicable to Baltic I reference design*
[b] *according to research by Zaaijer [81]*
[c] *mass change of +/- 1% observed with respect to reference design*

In conclusion a list of reasons that could explain the difference between the modeled natural frequency and the reference natural frequency have been stated. For some of these reasons a percentage difference has been calculated. The combination of all explanations for which the effect on the natural frequency computation is known, does not account for the inaccuracy of approximately 8 - 9%. Other explanations, for which effects are unknown, could account for

the obtained inaccuracy. Therefore, future research is required to improve the natural frequency computations. Such a research could focus on implementing the method used in this research and compare its outcome with the outcome of a model used by the industry, which is built in a finite element method software package. Using this approach the effect of each individual provided explanation can be investigated, which is impossible by using only the results these reference designs.

An underestimation of the natural frequency results in a higher computed natural frequency. As a result for Butendiek location number 1, the computation of the upper and lower MP pile diameter will be underestimated by approximately 10%.

6.2.6 Verification Wall Thickness computation using Local Buckling requirement

The wall thickness is scaled as a constraint based variable using local buckling as design requirement. Both the Butendiek and Baltic I structures are subjected to the reference bending moment and shear force distribution. As a result the model will select the wall thickness in such a way that the material stress is lower than the allowable local buckling stress, see table 6.14. Here, it can be observed that the wall thicknesses are underpredicted. The use of the lo-

Table 6.14: Results non-calibrated structural design model with reference design variables as input

Location number	**Reference Optimization variables**		**Non-calibrated model output**						
			Constraint based variables				**Structural mass**		
	$D_{MP,low}$ [m]	$D_{MP,up}$ [m]	$t_{MP,mud}$ [m]	$t_{TP,low}$ [m]	$t_{tow,low}$ [m]	L_p [m]	MP [ton]	TP [ton]	Tower [ton]
Butendiek	6.00	5.19	0.058	0.028	0.025	28	370	82	152
Baltic I	5.05	4.05	0.072	0.045	0.022	43	413	126	103

* *Note: None of the designs fulfilled the natural frequency requirements*

cation buckling requirement to scale the wall thicknesses does not result in a good match with the reference data. This means that local buckling is not the dominant design requirement for wall thickness determination. Two solutions can be used to solve this problem; a new design requirement or a new calibration factor in combination with the local buckling requirement can be implemented. Within this research the latter solution is chosen. A calibration factor is applied to increase the bending moment and normal forces experienced by each structural segment. As a result the stress within the structure increases, which requires a larger wall thickness to prevent local buckling.

The calibration factor is divided in three individual parts, one for each support structure component. The calibration factors for the Butendiek and Baltic I support structure are shown in table 6.15. Using these calibration factors the same wall thicknesses are obtained as shown in table 6.1.

Table 6.15: Empirical factors applied to the bending moment and normal force distribution to correct for the inaccuracy of the wall thicknesses computations

	Empirical factor	
	Butendiek	Baltic I
MP	1.97	1.02
TP	2.81	1.21
Tower	1.80	1.72

Using these calibrated factors results in an quick and easy fix to obtain the wall thicknesses. However, it is very likely that the values for these calibration factors are not applicable to other OWF sites. Different water depths, wave and wave conditions, wind turbine types (and corresponding hub heights) are the most likely dominant factors for the value of these calibration factor. In Appendix H.4 a brief argumentation is given for which design requirements could be dominant for the wall thickness computation. Here, fatigue is considered to be the most promising design requirement required to obtain an accurate wall thickness distribution.

6.2.7 Verification Support Structure Dimensioning using Calibrated Model

Unfortunately, all these data sets have already been used to define the scaling rules and to verify the natural frequency and wave loads models. Therefore, no representative verification of the entire MP and GBS support structures can be performed. Nevertheless, a comparison can be made concerning the accuracy of translating the reference data into the structural design model. For the MP based support structure both the constraints based variables and the mass of each structural component (MP, TP and tower) is compared. Furthermore, the first natural frequency can be compared with reference data. For the GBS based support structure the computed GBS and ballast material mass is compared with the reference data. Also the computed structure must comply with the natural frequency and soil bearing capacity requirements. In the interest of obtaining comparable results, corrections concerning the environmental loads and natural frequency calculations are performed, see table 6.16. Using these corrections the computed designs are subjected to the same ULS loads as the reference designs.

Table 6.16: Values for the optimziation variables for the reference designs

	Butendiek	Baltic I	Thornton Bank
Empirical wave load factor (multiplication factor)	1.45 (section 6.2.3)	4.50[a] (section 6.2.3)	1.45[b]
Natural frequency factor (multiplication factor)	0.925 (section 6.2.5)	0.925 (section 6.2.5)	0.925
Turbine thrust (ULS) (manually inserted)	1.5 MN [21]	1.0 MN [20]	no correction
Empirical wall thickness correction factor	table 6.15 (section 6.2.6)	table 6.15 (section 6.2.6)	1.8 for tower only

[a] *calibrated for ice loading*
[b] *assumption*

Table 6.17: Result calibrated structural design model

		MP [ton]	TP [ton]	Tower [ton]	L_p [m]	f [Hz]
Butendiek	Reference	635	256	226	28.5	0.309
	Non-Default	634	254	226	28.0	0.311
	Default	599	258	226	28.0	0.312
Baltic I	Reference	410	161	139	40.0	0.331
	Non-Default	457	174	137	43.0	0.314
	Default	474	101	139	44.0	0.302

Table 6.18: Modeled GBS based support structure masses

OWF	**Reference**			**Output Default**		
	GBS [ton]	Ballast [ton]	Tower [ton]	GBS [ton]	Ballast [ton]	Tower [ton]
Thorntonbank	3000	4000	unknown	2876	4387	287

6.2.8 Verification Genetic Algorithm Solver

In this section the accuracy and speed of the search towards the ideal design solution is evaluated. The model is run with the same configuration as is used to obtain the data of table 6.17 and 6.18 for the non-default cases of the Butendiek MP an Thornton Bank GBS support structures. Furthermore, an evaluation has been performed of all design options within the boundary conditions with an interval of the optimization variables of 0.005 m. For the same scenario the genetic algorithm is used ten times to find the optimal solution. The results are visualized in figure 6.3. It is observed that the solutions found by the genetic solver are located closely to the best brute force computation solution. The genetic algorithm even finds a better solution five out of ten times, see table 6.19. For this particular example the brute force computation method uses approximately $2 \cdot 10^3$ times more iterations than the genetic solver.

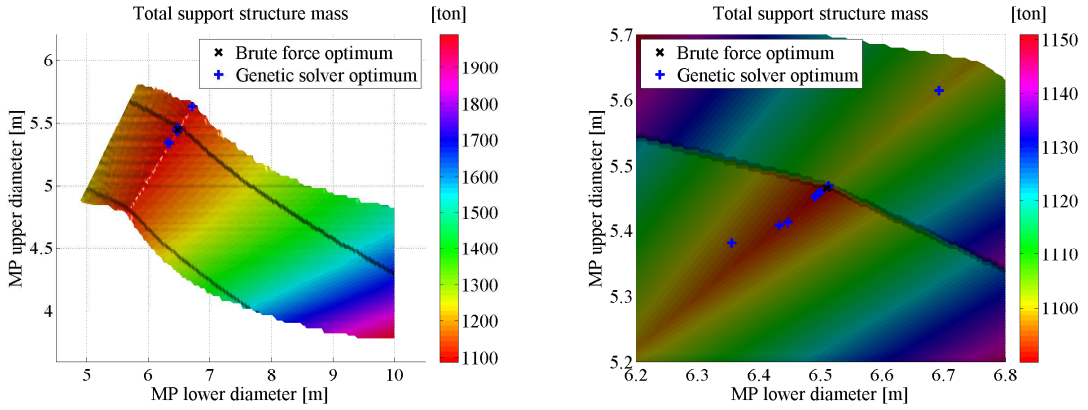

(a) Overview viable design solutions

(b) Detailed view of area of optimal solutions

Figure 6.3: Brute force optimization MP based support structure for Butendiek location 1

Table 6.19: Brute force optimization MP based support structure for Butendiek location 1 and 10 solutions found by the genetic solver

Computation Method	$D_{MP,low}$ [m]	$D_{MP,up}$ [m]	m_{tot} [ton]	Number of iterations
Brute force	6.510	5.465	1090.0	$1.2 \cdot 10^6$
Genetic Solver	6.340	5.336	1085.8	550 to 750
	6.466	5.434	1086.0	
	6.338	5.337	1086.3	
	6.339	5.334	1088.7	
	6.469	5.429	1088.7	
	6.479	5.462	1092.0	
	6.709	5.630	1093.1	
	6.330	5.340	1094.1	
	6.465	5.431	1095.8	
	6.479	5.430	1098.9	

6.3 Sensitivity Analysis Structural Design

Thus far the structural design model has been verified using a limited amount of reference data. Therefore, a sensitivity analysis is performed to assess the effect of changing the values of independent variables set by the micro siting model and determined by the OWF's site.

Reference set of independent variables The independent variables and their reference values are presented in table 6.20.

Table 6.20: Reference values independent variables for sensitivity analysis

Defined by	Independent variable	Reference value
OWF specific conditions	50 year recurrence wave height	16.0 m
	50 year recurrence wave crest	12.0 m
	Water level difference due to tidal	2.0 m
	Water level difference due to storm	3.0 m
WT location specific conditions	Soil type	Uniform Sand
	Sand friction angle	37.5 degrees
	Sand effective unit weight	11.0 kN/m^3
	Water depth (LAT)	20.0 m
Set by micro siting model	Hub Height	100.0 m
	WT type	Siemens 3.6 MW
Set by structural design model	MP and GBS scaling	default, see table 6.3
	MP boundaries	4.0 m $\leq$ Lower MP diameter $\leq$ 10.0 m
		3.0 m $\leq$ Upper MP diameter $\leq$ 8.0 m
	GBS boundaries	10.0 m $\leq$ Base slab diameter $\leq$ 40.0 m
		4.0 m $\leq$ GBS top diameter $\leq$ 10.0 m

Water Depth The TP and tower shear force and bending moment distribution do not change as a result of an increase in water depth, see figure 6.4(a). Therefore, no change in mass is observed for these components. The MP mass increases as a result of a number of combined phenomena. Since the bending moment at the mud line increases a longer pile penetration depth is required to provide stability. Furthermore, a longer pile length is required to overcome the distance from the mud line to the sea surface. Also it is observed that thicker bottom pile diameters are selected as optimum design solutions, see table H.4. This is to be expected since the wave forces scale to the third power with an linear increase of the pile diameter and water depth. Likewise, the area moment of inertia scales to the third power with an linear increase of the pile diameter. Furthermore, a thicker MP wall thickness is required to maintain a certain pile diameter over wall thickness ratio. As a result an increase of the MP mass is observed, due to the combination of higher pile diameters, wall thicknesses and a higher pile length. Because the natural frequency decreases as a result of a longer total support structure length, viable design solutions are not present beyond a water depth of 55 m (for this particular case).

The GBS mass and volume also increase as a result of an increasing water depth, see figure 6.4(b). To overcome a higher mud-line bending moment a larger base slab diameter is required. Also a longer GBS construction is required to overcome from the distance from the mud line to platform. As a result also the average GBS diameter increases, due to a longer conical section. The combination of these factors results in an increase of the GBS mass and ballast mass. The tower mass remains unchanged. The soil bearing capacity requirements in combination with the upper boundary of the base slab diameter prevent the presence of viable design options in water depth beyond 55 m (for this particular case). However, not filling the entire GBS structure with ballast sand increases the water depth range. Therefore, it is prudent to consider the implementation of the ballast sand mass as a constraint based variable in future research.

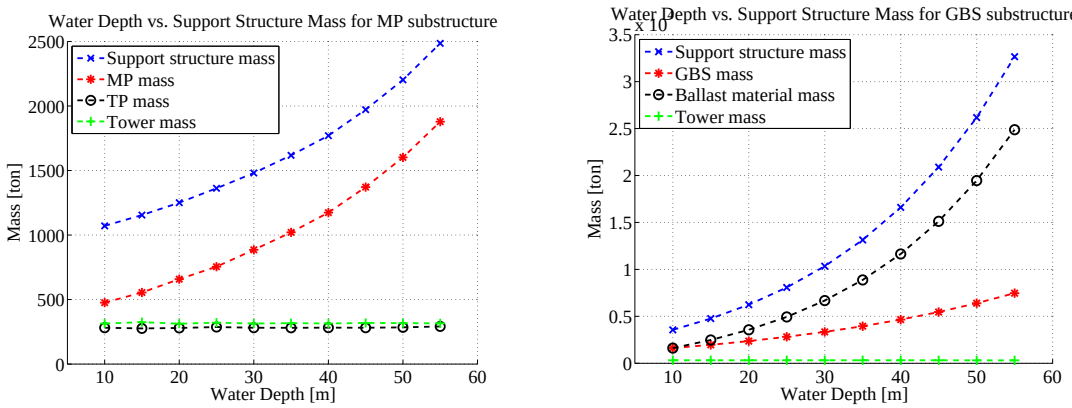

(a) (b)

Figure 6.4: Effect of the water depth on the support structure's mass

Wave Height A higher wave height requires a longer TP and shorter tower structure as a result of a higher platform location. Both the lower and upper MP diameter are decreased by the algorithm for higher wave heights to limit the extreme wave loads, see table H.6. As a result the wall thickness of the MP and TP increases resulting in higher masses for these three components and higher natural frequencies. The increase of the tower thickness in limited due to the smaller bending moment at the tower base, which results from a short tower length. The MP also requires a longer pile penetration depth. Longer and thicker walls results into an increase of the MP and TP mass, see figure 6.5(a). The tower mass almost linear decreases mainly as a result of a shorter tower length.

For the GBS based support structure a higher wave height results in an increase of the base slab diameter to resist overturning. A small increase of the GBS top diameter is required to increase the natural frequency, see table H.7. This is required to compensate the decrease in natural frequency due to an increase of the amount of ballast mass. The same behavior of the tower is observed as for the MP case, see figure 6.5(b). The total support structure length remains constant, because the GBS length increases and the tower length decreases. Hence, a large extreme wave height can be resisted, without being restricted by any natural frequency requirements. The base slab diameter provides the required stability, which means that even higher wave height than 75 m can be resisted. This is believed to be unlikely and is probably the result of using the linear wave theory. The results of the linear wave theory become more inaccurate for a higher wave height over water depth ratio's.

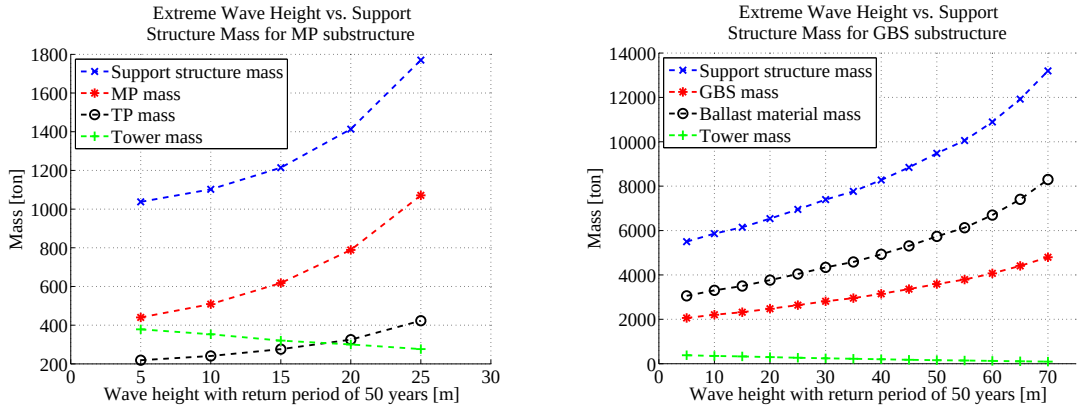

Figure 6.5: Effect of the extreme wave height on the support structure's mass

Hub Height A higher hub height results in a heavier tower, see figure 6.6(a). Consequently, the MP and TP are subjected to higher gravitational loads. Despite higher wave loads, the lightest design solution is provided by increasing the MP upper and lower diameters. Higher pile diameters reduce the effect of a decreasing natural frequency, see table H.8. All supports structure component show an increase of their mass. For the MP this is a result of an increase of the pile penetration depth and pile diameter, but despite a decrease of the wall thickness. For the TP an increase of the TP diameter also results in a higher mass, despite a decrease of the TP wall thickness. The tower wall thickness roughly remains constant due to the combination of a higher turbine thrust generated bending moment and an increase of the tower base diameter. Nevertheless, the total tower mass increases due to an increase of the average tower diameter and total tower length.

The GBS based support structure requires a large base slab diameter to limit the decrease of the natural frequency as a result of an increase in hub height, see table H.9. Consequently, the GBS mass and ballast mass increase, see figure 6.6(b). The tower mass increases according to the same principles applicable to the MP based support structure.

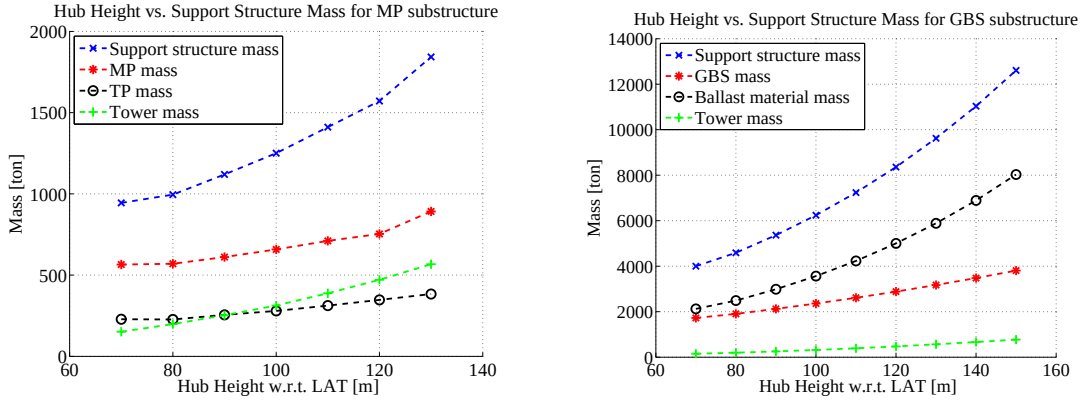

Figure 6.6: Effect of the hub height on the support structure's mass

Soil Properties The TP and tower mass do not change as a result of changing soil properties, see figure 6.7(a). This is because the bending moment and shear for distribution are not affected by the soil properties. The pile penetration depth decreases as a result on an increase of the soil friction angle, see table H.10. The change in MP mass is solely due to the change pile penetration depth.

The base slab diameter can be decreased as the soil friction angle increases, see figure 6.7(b). As a result the GBS and ballast material masses decrease. The tower mass remains unchanged for the same reasons as it is unchanged at the MP based support structure.

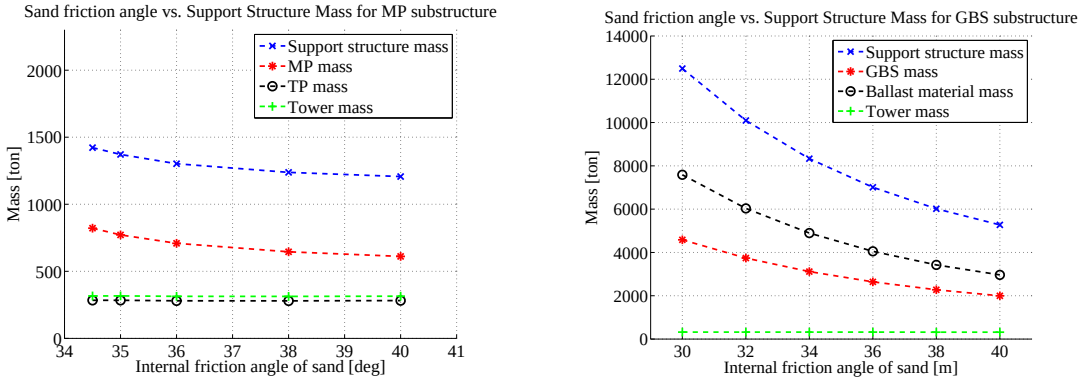

(a) (b)

Figure 6.7: Effect of the sand friction angle on the support structure's mass

6.4 Installation Model Verification

In Chapter 5 two methods, called the TS and WP method, have been described to predict the required amount of time for the installation of all substructures. The ideal way to assess the accuracy of each method would be to obtain installation time data of an actual installation process and compare the model results. The required input for the model would be the same environmental data as experienced during the actual installation process. However, this data could not be found. Instead a comparison between both methods will be made on a theoretical level and by changing the input parameters.

6.4.1 Theoretical comparison

The WP method uses workability percentages, which are obtained from processing a set of measurement data, to calculate the gross installation time. The total amount of substructures installed per month is calculated by dividing the number of hours in a month by the gross installation time. The TS method uses the measurement data directly and fits the activity within the weather windows of the measurement data.

Two main differences exist between the WP and TS method. Firstly, the WP method does not use the order in which activities are performed. Secondly, a workability percentage consist of

all data samples that are part of a suitable weather window, even though some samples cannot be used usefully. For example a weather window of 4.0 hours is fully used to calculate a the workability percentage of an activity taking 3.0 hours. Also the WP method does not account for the overlap of weather windows of different activities.

To demonstrate these two differences, two different theoretical scenarios have been created. No contingency factor is used in assessing the required weather windows. Therefore, the activity time equals the weather window time. Here, the installation process consists of two activities taking respectively 3.0 and 6.0 hours to complete. In the first case the allowable significant wave height of activity 1 is lower than for activity 2. In the second case this is the other way around. In both cases the TS method computes the completion of exactly one installation cycle as output, see figure 6.8.

Figure 6.8: Two theoretical scenarios resulting in the same output of the TS model but a different output of the WP model

On the other hand the WP method produces two different results. Two different gross cycle times emerge as a result of different workability percentage. These workability percentage are the relative amount of time it is possible to perform an activity, see figure 6.8. The gross cycle time for both scenarios is computed according to equation 5.2.1. The results of these calculations are presented in table 6.21.

The amount of completed cycles calculated per method differs significantly. The scenario's are chosen in such a way that the TS method can perform exactly one installation cycle. The WP methods computes the completion 1.7 and 0.67 cycles for respectively the first and second scenario, see table 6.22. According to figure 6.8 it is not possible to perform 1.7 installation cycle in scenario 1. Also it is possible to perform more than 0.67 installation cycle in the second scenario. Hence, the time series method provides a better description of the installation process. Therefore, it is expected that the TS model provides an exact description of the installation process for an installation process as described by the section 5.1. This installation process is a simplification of the real life installation process.

Table 6.21: Workability percentage and gross installation time for two scenario's described in figure 6.8

	Scenario 1		**Scenario 2**	
	Workability percentage	Gross time [h]	Workability percentage	Gross time [h]
Activity 1	80.0%	3.75	15.0%	20.0
Activity 2	75.0%	8.00	60.0%	10.0
Entire cycle		11.75		30.0

Table 6.22: Amount of installation cycles that can be performed according to figure 6.8

Calculation method	**Amount of installation cycles that can be performed within 20 hours according to figure 6.8**	
	Scenario 1	Scenario 2
WP method	1.7	0.67
TS method	1.0	1.0

6.4.2 Sensitivity Analysis for Installation Process

The effect of changing input parameters on the average installation time is described in this paragraph. Here, a comparison will be made between the WP and TS method. Two hourly hind cast data sets will be used for this comparison. The two different locations, from which hind cast data is obtained, are the Wikinger and Hohe See wind farms. The Wikinger location is positioned in the German Baltic Sea and the Hohe See can be found in the German North Sea. The wind and wave conditions are higher at the Hohe See location, see table 6.23. The results presented in this section indicate the average total installation time for the entire set of yearly hind cast data.

	Winkinger [1]	Hohe See [2]
Average significant wave height	0,66 m	1,74 m
Average wave period	2,97 s	6,04 s
Average wind speed [3]	6,18 m/s	8,33 m/s

[1] *hourly hind cast data from 1979 - 2009*
[2] *hourly hind cast data from 1981 - 2006*
[3] *corresponding altitude unknown*

Table 6.23: Environmental hind cast data of two offshore locations

For an appropriate comparison first some reference properties concerning the installation vessel and installation cycle need to be established, see table 6.24. Finally note that the data shown in all graphs in this section represents the average or standard deviation of all yearly hind cast data sets.

Property	Value	Unit
Start date	1 march	[-]
Number of substructures	80	[-]
Activy time	[4 8 6 2]	[h]
Hs,max	[1.75 1.25 1.5 1.0]	[m]
Vw,max	[12 12 12 12]	[m/s]
Tp,max	[8.0 8.0 8.0 8.0]	[s]
Ship's carrying capacity	5	[-]
Grouting constraints	not included	[-]
Vessels traveling speed	12	[kts]
Distance to harbor	24	[NM]
Loading at harbour time	4 hours per substructure	[h]
Run for shelter conditons	not included	[-]
Contingency factor	1.5	[-]

Table 6.24: Reference data input used to describe the installation process

Installation time throughout the years: Environmental conditions change throughout the years. This results in a different installation time per year, see figure 6.9. It is observed that the WP method computes a lower installation time than the TS method for each year of the date set. Hence, one can state that the WP method underpredicts the total installation time for all years of the data set.

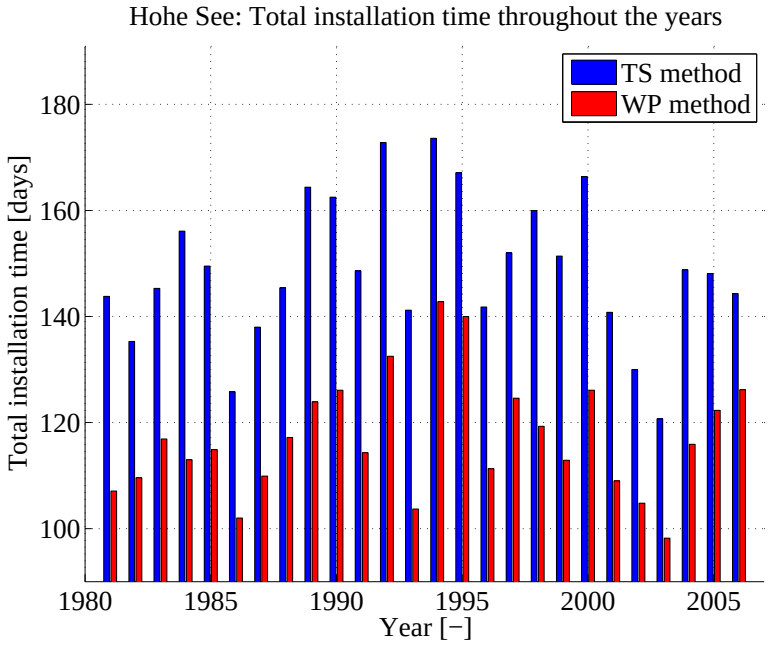

(a)

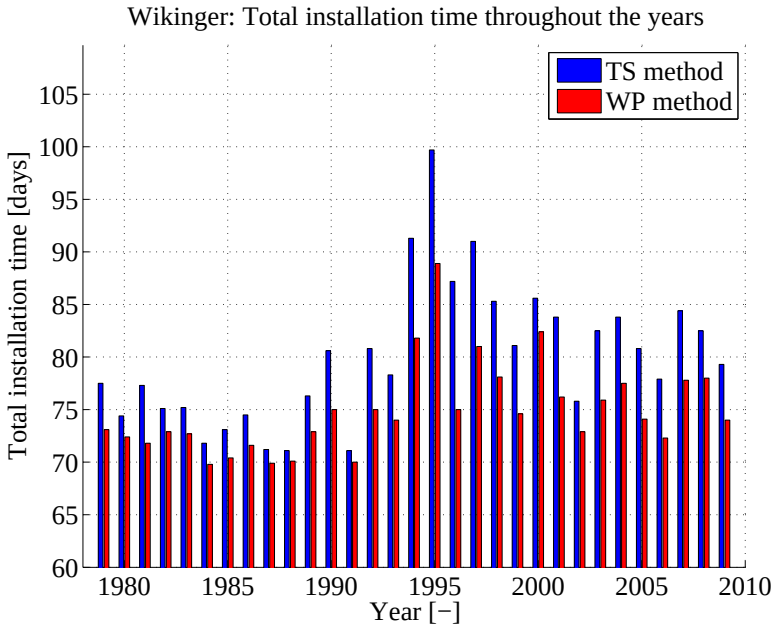

(b)

Figure 6.9: Effect of contingency factor and linking of activities on total installation time

Start date: The start date of installation determines in which months the installation process will take place and therefore the environmental conditions during installation. The ideal start date depends on a properties described in table 6.24. The output results of the model are presented in figure 6.10 and 6.11. Starting on the first day of the year will result in a very high total installation time for both sites. Starting later in the year reduces the total installation time as a result of improving environmental conditions. This is valid up to a point where the completion of the last substructure enters the autumn months. After that the total installation time increases as a result of the worse environmental conditions in the autumn months. The standard deviation also follows the same trends, resulting in a high standard deviation when a large part of the total installation process is performed during bad environmental conditions. For the Wikinger it is possible to start installation further ahead in the year than for the Hohe See location due to the milder environmental conditions.

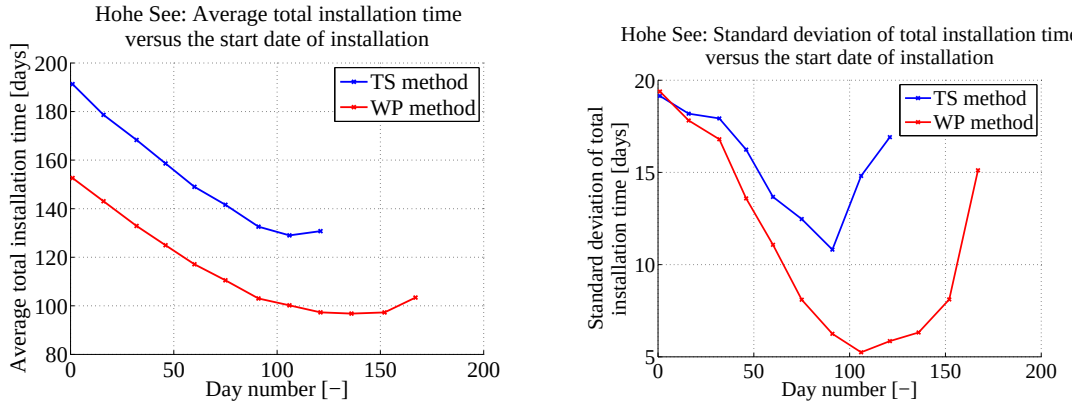

Figure 6.10: Hohe See: Effect of start date on total installation time

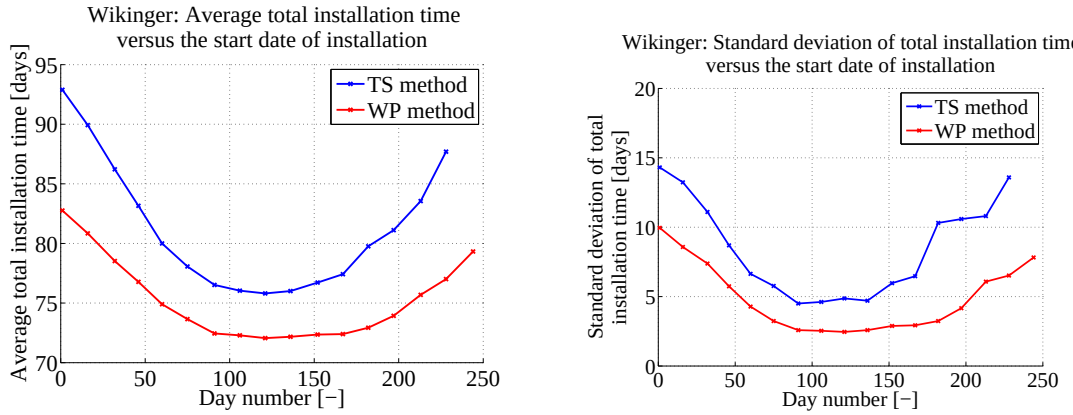

Figure 6.11: Wikinger: Effect of start date on total installation time

Allowable significant wave height during grouting: For a grout curing time of 24 hours the effect of the allowable significant wave height on the installation time is shown in figure 6.12 and 6.13. The average total installation time decreases and approaches the limit of the installation time corresponding to no-grouting requirements, when the allowable significant wave height increasing. The standard deviation also decreases with increasing allowable significant wave

height after grouting. Again the WP method underestimates the installation time. This results in the fact that a lower allowable significant wave height still result in completing installation of all substructures within one calender year for all years of data.

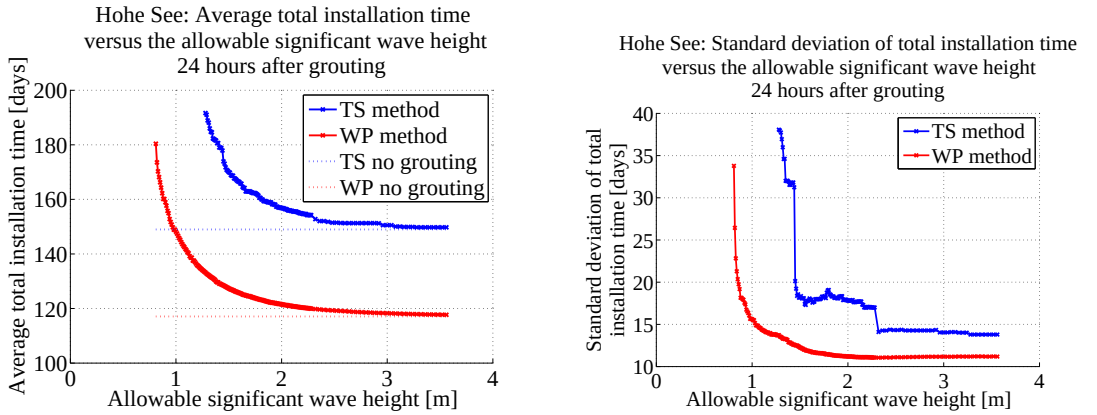

Figure 6.12: Hohe See: Effect of allowable significant wave height after grouting on the total installation time

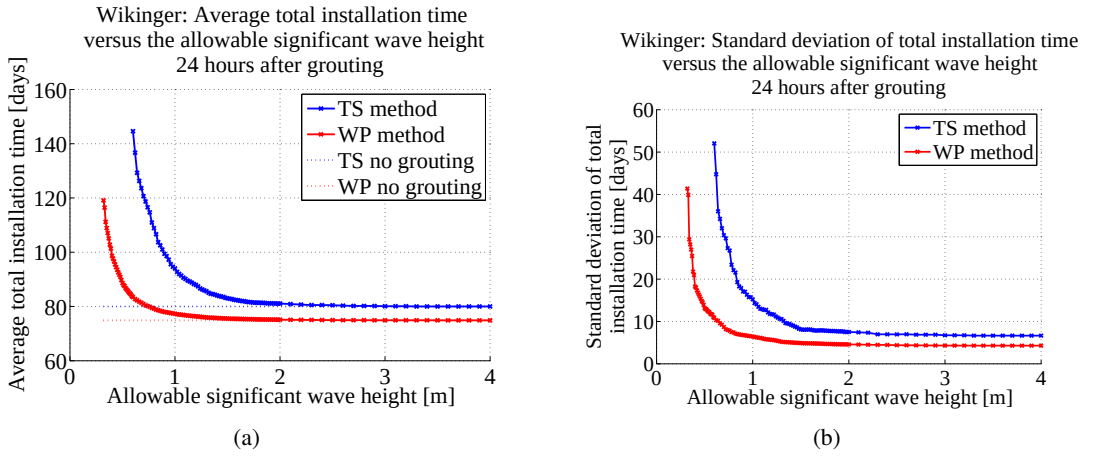

Figure 6.13: Wikinger: Effect of allowable significant wave height after grouting on the total installation time

Number of substructures: A larger number of substructures to be installed will result in a higher total installation time, see figure 6.14 and 6.15. For the Hohe See location, with its heavier environmental conditions, a larger difference with respect to the nett installation time is computed compared to the Wikinger location. This fits with the fact that the allowable environmental conditions for performing activities weighs heavier on the location with the most severe environmental conditions.

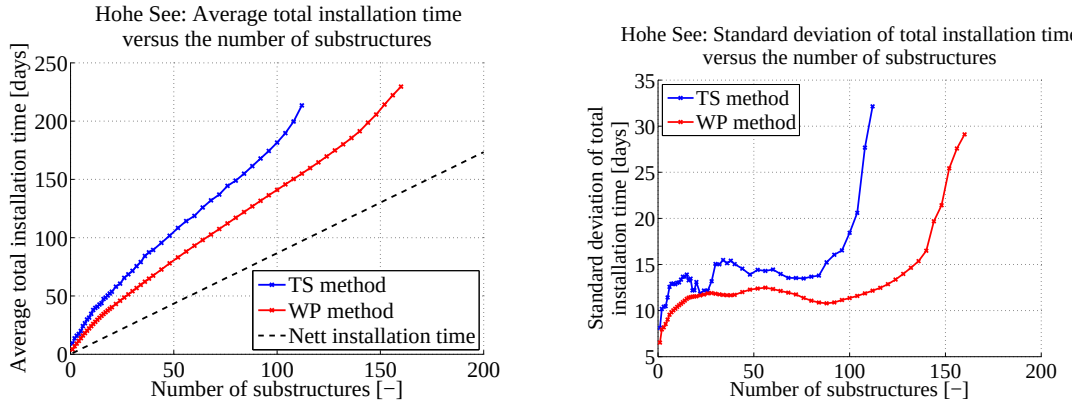

Figure 6.14: Hohe See: Effect of the number of substructures to be installed on the total installation time

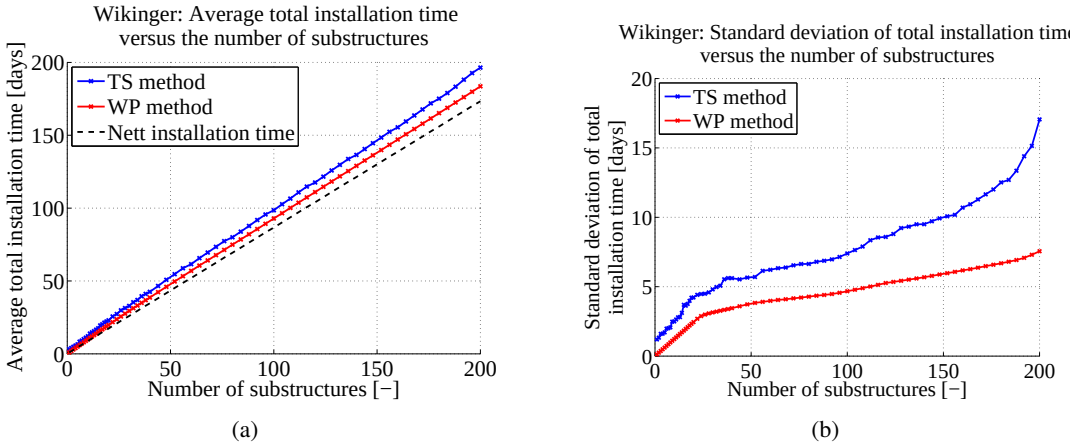

Figure 6.15: Wikinger: Effect of the number of substructures to be installed on the total installation time

Allowable significant wave height: Here the allowable significant wave height off all four activities is multiplied with an factor to see the effect of change this parameter. As to be expected the installation time increase with the allowable significant wave height is reduced.

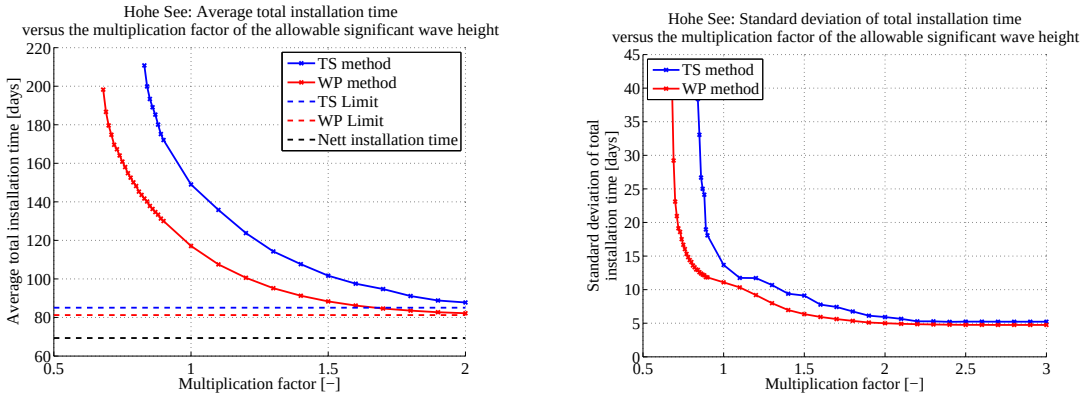

(a) (b)

Figure 6.16: Hohe See: Effect of the allowable significant wave height on the total installation time

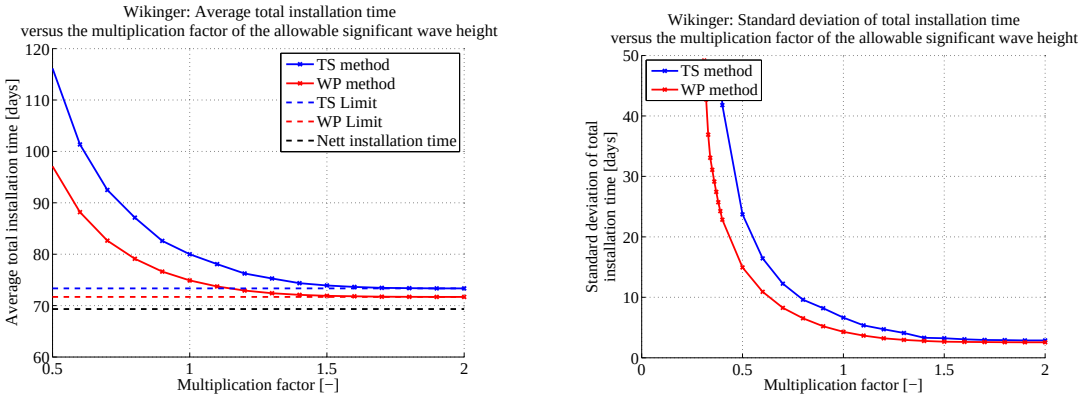

(a) (b)

Figure 6.17: Wikinger: Effect of the allowable significant wave height on the total installation time

Other independent variables: The effect of changing three other independent variables is presented in Appendix I. Here, similar results are obtained as discussed in this section. These other three variables are:

- Installation strategy and distance to harbor
- Contingency factor and linking of activities
- Grout curing time

Chapter 7

Validation

In this chapter the validation of the model is discussed. Firstly, an example is given how the model could perform within a micro siting model. Secondly, the thesis objective and research question are evaluated.

7.1 Theoretical case study

A micro siting model uses an iterative approach to compute the ideal OWF configuration. To illustrate the incorporation of the developed model within a micro siting model, the output of the developed for two iterations of a micro siting model is presented in this section.

7.1.1 Input defined by micro siting model

In this section the evaluation of two OWF design options is performed from a micro siting model point of view. The design variables, defined by the micro siting model, are displayed in table 7.1. The chosen design variables are the wind turbine type, number of turbines, hub height and location of each turbine. Eleven sets of soil and water depth properties are defined in table 7.1. For each set of wind turbine location specific data a number of turbines is assigned. Hence, the assumption is made that multiple wind turbines are subjected to similar water depth and soil conditions. Wave, water level and water current values corresponding to the OWF site can be found in table 6.20. For the installation of each substructure type eight different installation vessel can be used. The installation strategy used is a transiting method for the MP and a feeder method for the GBS installation process, see tables L.1 up to L.3. The structural design model is implemented as described according to the default model of table 6.3. However, now the substructure costs are evaluated instead of the substructure mass. The material, labour, equipment and other costs corresponding to the substructure components are presented in table 7.3. Finally, the OWF site specific properties are displayed in table 7.4.

Table 7.1: Properties set by micro siting model

Design Variable	Iteration 1	Iteration 2
OWF capacity	155 MW	155 MW
WT type	Vestas V112 3.0 MW	Repower 5.0 MW
Number of turbines	55	33
Hub Height	90.0 m	97.0 m
Wind turbine location specific properties	see table 7.2	see table 7.2

Table 7.2: Location specific properties of 11 soil and water depth categories

Location number	LAT [m]	Sand friction angle [deg]	Sand effective unit weight [kN/m^3]	Number of turbines	
				Iteration 1	Iteration 2
1	10.0	30.0	9.50	5	1
2	12.0	31.0	9.65	5	2
3	14.0	32.0	9.80	5	3
4	16.0	33.0	9.95	5	4
5	18.0	34.0	10.10	5	4
6	20.0	35.0	10.25	5	5
7	22.0	36.0	10.40	5	4
8	24.0	37.0	10.55	5	4
9	26.0	38.0	10.70	5	3
10	28.0	39.0	10.85	5	2
11	30.0	40.0	11.00	5	1

Table 7.3: Substructure costs

Material	Applies to:	Costs
Steel cost	MP, TP and tower	1200 €/ton
Reinforced concrete	GBS, outer	400€/ton
Ballast material	GBS, inner volume	50 €/ton

Table 7.4: Offshore wind farm properties

Independent variable	Value
50 year recurrence wave height	20.0 m
50 year recurrence wave crest	15.0 m
Water level difference due to tidal	2.0 m
Water level difference due to storm	3.0 m
Sub surface current velocity at still water level	1.0 m/s

7.1.2 Output and discussion

The model successfully produces an output. In both cases the MP design option result in the lowest overall cost, see table 7.5. A part of the output of the structural design model model is presented in table 7.6. It seems that the genetic algorithm does not always approach the optimal

design solution, because large differences exist between the costs of different GBS designs. The output of the installation process is computed by the time series model and displayed in table 7.7. Here, it can be seen that the MP installation process is limited by its earliest starting date of July 1. For the first case vessel number 3 provides the lowest installation cost. Using vessel 4 results in the lowest installation cost for the second case.

The exact output values are not of importance, since they are mainly based on the assumed material and vessel costs. Nevertheless, this case study gives an idea of the use of the model developed in this research.

Table 7.5: Output developed model

Iteration number	**MP cost [M€]**		**GBS cost [M€]**	
	Support structure	**Installation process**	**Support structure**	**Installation process**
Iteration 1	90.6	15.7	100.3	12.0
Iteration 2	60.1	8.5	71.3	8.2

Table 7.6: Output structural design model

Location number	MP based support structure				GBS based support structure			
	Iteration 1		Iteration 2		Iteration 1		Iteration 2	
	Mass [ton] [ton]	Cost [M€]	Mass [ton]	Cost [M€]	Mass [ton]	Cost [M€]	Mass [ton]	Cost [M€]
1	1306	1.57	1430	1.72	5962	1.70	6737	1.94
2	1343	1.61	1546	1.85	6117	1.66	7340	2.00
3	1372	1.65	1484	1.78	6281	1.64	7463	1.95
4	1366	1.64	1527	1.83	7181	1.77	7498	1.89
5	1352	1.62	1518	1.82	6689	1.63	8368	2.01
6	1358	1.63	1479	1.77	8910	2.00	10218	2.31
7	1368	1.64	1562	1.87	10168	2.19	9588	2.14
8	1382	1.66	1505	1.81	7803	1.74	10816	2.32
9	1390	1.67	1524	1.83	9878	2.07	10588	2.25
10	1416	1.70	1576	1.89	7200	1.60	12812	2.55
11	1449	1.74	1583	1.90	10179	2.05	13728	2.68

Table 7.7: Offshore wind farm properties

Iteration number	Vessel number	MP installationn:			GBS cost		
		Ideal Start date	Time [days]	Cost [M€]	Ideal Start date	Time [days]	Cost [M€]
Iteration 1	1 / 5 [a]	Crane capacity exceeded			Crane capacity exceeded		
	2 / 6 [a]	Crane capacity exceeded			June 19	58.4	14.6
	3 / 7 [a]	July 1	80.6	16.1	June 24	43.7	13.1
	4 / 8 [a]	July 1	62.7	15.7	July 9	34.3	12.0
Iteration 2	1 / 5 [a]	Crane capacity exceeded			Crane capacity exceeded		
	2 / 6 [a]	Crane capacity exceeded			Crane capacity exceeded		
	3 / 7 [a]	July 1	42.6	8.5	May 15	28.3	9.2
	4 / 8 [a]	July 1	35.6	8.9	May 25	21.4	8.2

[a] *First number is applicable to MP installation. Second number is applicable for GBS installation.*

7.1.3 Computation time

In this section an indication is given of the computation time of the model developed in this research. The computation time depends on the type of computer that available. For this research a Hewlett Packard laptop has been used, which properties are described in table 7.8. Matlab version R2013b is used for a 64-bit operating system.

Table 7.8: Properties laptop used for this research

Laptop	Hewlett Packard - Elitebook 8530w
Processor	Intel(R)Core(TM)2 Duo CPU T9600 2.80GHz 2.80GHz
RAM	4.00 GB
System	64-bits

Performing the two micro siting iterations, as presented in the case study of previous subsection, required a total computation time of 9 hours and 13 minutes. An overview of the division of this computation time is provided in table 7.9.

Table 7.9: Computation time of theoretical case study

Model	Computation time	Number of computations	Time per computation
MP optimization	5 hours and 58 minutes	13084	1.64 s
GBS optimization	2 hours and 33 minutes	19598	0.47 s
Installation process	42 minutes	101	24.95 s

This is a large amount of computation time considering that the developed model needs to be implemented within an iterative design process used by a micro siting model. Consequently,

it is not desired to use the developed model, in its current form, within a micro siting model. However, some measures can be taken to reduce the computation time. These measures are listed below.

- Use parallel computing
- Reduce computation time for evaluation of individual design option

Both these measures are explained in Appendix J. Here, it is shown that using a parallel computation process could in theory reduce the computation time from 9 hours and 13 minutes to only 12 minutes.

7.2 Thesis objective and research questions

7.2.1 Thesis objective

The thesis objective, as stated in section 1.3, is repeated below.

Develop a model that provides data to a micro siting model, concerning the manufacturing and installation costs of offshore wind farm substructures. The model should be able to analyze different combinations of substructure types and installation vessel types.

Based on the performed research, it can be stated that the objective has been met. Below a short elaboration is provided.

A model has been developed, that uses the substructure mass and total substructure installation time to estimate the corresponding manufacturing and installation costs. Two different types of substructures are implemented within the structural design model. Each substructure type uses a different set of design requirements, optimization variables and constraints based variables to create the support structure dimensions in an iterative optimization process. The use of offshore wind farm site and wind turbine location specific data results in individually optimized support structures per wind turbine location. Furthermore, a wide range of installation vessel types can be used within the model. For each installation vessel a small data set is required that describes the installation vessel and supply vessel properties, and the installation process of a single substructure. Data concerning the environmental conditions is used to determine the total installation time and find the ideal installation start date. The software program Matlab is used to develop the model. Since only simple data sets are required to initiate the developed model, it is assumed that communication with a micro siting model is possible. The current required computation time is found to be insufficient, but the computation time of individual submodels is found to be sufficient. Using a parallel computation process will result in a significant computation time reduction and a small increase in accuracy. When implemented correctly the current computation methods are expected to provide a suitable manufacturing and installation costs analysis for a micro siting model.

7.2.2 Research questions

1. Can the developed model provide a contribution to current micro siting models concerning the estimation of the substructure's manufacturing and installation cost?
In this research a large amount of design variables is incorporated within the developed model. Two sensitivity analyzes have shown that those design variables have a great influence on the outcome of the support structure mass and the total installation time. To improve the accuracy of a micro siting model these design variables need to be included within the model that computes the substructure manufacturing and installation costs. Furthermore, a computation time can be obtained that is sufficient for iterative design process used by a micro siting model. However, the accuracy of the current structural design model is not good enough for an accurate cost estimation. The wall thickness computation needs to be improved for the MP based support structure. For the GBS based support structure a wall thickness computation needs to be added. Also more reference data or insight in the design process is required to eliminate, improve or justify certain assumptions. Nevertheless, using the current approach it is easy to improve current and add new computations within the developed model.

2. Is it useful to integrate the estimation of the substructure's manufacturing and installation process cost into one model?
The support structure's mass and installation time are computed in series. No integrated design process is used to combine these two computations. Within this project only the crane capacity has been used as restriction of the choice of installation vessel. Future research could also implement the use to the main installation vessels deck area and deck loading capacity in combination with the substructure's dimensions to assess the amount of components a vessel can carry. However, a further increase in the integration between these computations increases the computation time drastically, because the in series computations will then have to be replaced by an iterative design loop. Such an amount of details is probably not required by a micro siting algorithm, since the difference in outcome will have a very small effect on the overall OWF levelized cost of electricity. In conclusion it is not required to combine the support structure design and installation process computations into one single integrated model.

Chapter 8

Conclusions and Recommendations

8.1 Conclusions

In this thesis a model has been successfully developed that estimates the offshore wind farm substructure manufacturing- and installation cost for the purpose of a micro siting model. It is believed that the current approach can contribute to the micro sitings models described in literature by improving these cost estimations. Because the verification process of the structural design model uses a very limited amount of reference data, the direct implementation of the current structural design model in a micro siting model is not advisable. However, with some minor adjustments the installation process model can in its current form be implemented in an existing micro siting model. Integrating the substructure manufacturing- and installation process cost in one single model is not required for the purpose of micro siting modeling. Nevertheless, a number of interactions between these two cost components exist, but they can be described by individual models. Here, the outcome of the structural design process determines the outcome to the installation process, but not the other way around.

In a theoretical case study the developed model is able to compute the manufacturing and installation cost of two offshore wind farm design solutions provided by a micro siting model. Here, the model was capable of selecting the installation vessel, substructure type and corresponding substructure's dimensions per wind turbine location resulting in the lowest overall costs.

Two methods have been used to compute the installation time of all offshore wind farm substructures, called the workability percentage method and the time series method. The time series method is not describes in literature as far as the author is aware of. A similar approach is used by Ballast Nedam. An altered and more comprehensive version is used within the installation process model. A theoretical example showed a more realistic installation time estimation potential of the time series method compared to the workability method. Furthermore, a sensitivity analysis using two sets of hind cast data, provided by Ballast Nedam, revealed a significant difference between the outputs of both methods. The time series method produces a more accurate estimation of the installation time. Each computation method can use a large number of installation vessels, all described by a set of independent variables specific for a substructure type and an installation vessel. Both methods are able to compute the ideal start date of installation,

resulting in the lowest total installation time.

The structural design model can evaluate and choose between two different substructure types; the monopile substructure and the gravity base substructure. For each of these substructures the dimensions are determined by a combination of knowledge based engineering rules, constraint based variables, assumptions and two optimization variables. Data on the preliminary design of monopile substructures for offshore wind farms Butendiek and Baltic I, provided by Ballast Nedam, was used for verification of structural design model.

The extreme wave loads are computed by using the Morison equations in combination with Airy wave theory and Wheeler stretching. Only the Butendiek data set provided a single shear force and bending moment distribution as a result of ULS wave loading. The wave loads model underpredicted the reference load distribution by 31%.

The model overpredicted the structure's first natural frequency with approximately 8 - 9 % compared to six preliminary monopile design of Butendiek Wind farm. The same computation resulted in an overprediction of 4 - 6% for two the Baltic I preliminary monopile designs. However, no tower data was available for this support structure. Using the tower dimensions as defined in this thesis a 5% lower natural frequency was found compared to the situation in which actual tower data was used. No satisfying answer was found for the overprediction of the natural frequency.

The pile penetration depth computation process was verified using an analytical description of a Winkler foundation using homogenous soil and pile properties. The model computed the pile rotation and deflection with an accuracy of 2.0% and 0.5% for a pile segment length of 0.05 m. To increase the models speed a segment size of 1.0 m was chosen, the preliminary monopile reference designs used segment lengths of 0.5 m. Nevertheless, the model computed the pile penetration depth with an accuracy of 2% for 6 soil profiles. Here, only a maximum allowable pile toe deflection of 0.02 m was used for ULS soil properties and loads. A 10% accuracy was found when the soil properties also were calculated instead of inserted as a data set.

The wall thickness scaling is performed using a local buckling during a ULS load scenario as design requirement. This leads to a large underprediction of the wall thickness distribution. For the purpose of this thesis an empirical factor was applied to the ULS bending moment and normal loads distribution. This resulted in the same wall thicknesses as for one of the preliminary monopile, transition piece and towers designs of Butendiek offshore wind farm. This factor is not applicable for different combinations of wind turbine type, wave loading, hub height and water depth. Therefore, other analysis are required to improve the wall thickness computation.

By applying these empirical factors to the wave loading, natural frequency and bending moment- and normal force distribution the model is able to recreate the dimensions of the preliminary monopile designs and the gravity base structure design. All these created support structure dimensions comply with the design requirements. No detailed design data have been found for a gravity base structure. A copy of the Thorntonbank gravity base structure dimensions resulted in a support structure that complied with all the gravity base structure design requirements.

The genetic solver is able to successfully find the design option resulting in the lowest costs or structural mass. This method provides a higher accuracy than a brute force computation using

a grid size of 0.005 m. Using two optimization variables results in viable design options for a large range of offshore wind farm site conditions and wind turbine properties.

8.2 Recommendations

Further research is required to improve the developed model, making its output more accurate and its applicability more comprehensive. In this section the most important improvements are presented and divided into three categories; overall model, structural design and installation process.

Overall model:

- This research describes most requirements for the implementation of substructure manufacturing and installation cost computation model for the use within a micro siting model. Future research should be directed towards the actual implementation of the developed model within a micro siting model. In that case a desired cost computation accuracy needs to be defined. This requires the assessment of a minimum desired accuracy for the developed model and all its submodels.
- Using a parallel computation process is expected to reduce the computation time significantly. The developed model requires to much computation time for performing of a substructure optimization process. Hence, implementing a parallel computation process is required when connecting the developed model to a micro siting model. As a result the number of individuals, of a population created by the genetic algorithm, can be increased. This results in an increase in accuracy of the structural design model, while maintaining a low computation time.
- The computation time required to evaluation a single monopile or gravity based support structure should also be reduced. The monopile lateral soil stability requires the most computation time within the monopile design process. Hence, reducing the computation time of this component provides the most potential in a significant computation time reduction.

Structural design model:

- The accuracy of the wall thickness computations is insufficient. An improvement of the wall thickness computation should have the highest priority in obtaining an accurate support structure mass description. Using fatigue as design requirement is considered to be the most promising solution to this problem for steel cross-sections. For the segments, consisting of reinforced concrete, other analyzes might be required. This can be combined with an investigation for the use of a larger number of load cases. Furthermore, the wall thickness should then be computed per structural segment instead of being based on knowledge based engineering rules.
- The current model assumes a linear relation between the mass and cost of the entire support structure. An investigation should be performed to assess the effect of the manufac-

turing process on the support structure's cost. Then the costs can be divided into different components; such as labour, materials and required equipment. The output of such a new cost computation function can then be used as the objective of the optimization algorithm.

- The current wave load computation model is used for both the monopile and gravity base substructure. Due to the large difference in diameter it is expected that different wave load models are applicable to each of these substructure types. For extreme wave heights the current wave load computation approach will not result in an accurate description of the wave loads. A more accurate wave load model is therefore required. This will (most probably) result in a larger computation time. It might be possible to apply a parallel computation process to prevent this from happening.
- The computation accuracy of the natural frequency model needs to be increased. Recommended is to do this side by side next to a model used by the industry. This way the effect of individual phenomena on the structure's natural frequency can be investigated. Furthermore, the implementation of the computation of the second natural frequency should also be added as a design requirement.
- The computation of the soil properties needs to be improved. Currently only sand and clay layers can be used. A more comprehensive soil properties analysis can be made when the model has the ability to use more different soil types.
- Although the current natural frequency model provides reasonably accuracy, it is believed that further improvements can be made without increasing the computation time. These improvements are advised to be made using an model, used by the industry for certified natural frequency computations, commonly built in a finite element software package, as reference. Using this approach the reason for the current inaccuracy can be isolated.
- When an improvement of at least the wall thickness computation is realized, more reference designs can be used to evaluate the output of the structural design model. If a large number of reference designs is available, then a number of knowledge based engineering rules can be improved.
- The addition of other substructure types is required to obtain a more comprehensive analysis for the ideal location specific substructure type. A jacket substructure is expected to provide the greatest potential, since it is currently the most implemented substructure type next to the monopile substructure.

Installation process model:

- Data of an actual installation process is required to assess the accuracy of the time series method. A list of variables, that have not been included in the time series model, has been listed. Of these variables the failure of equipment is the most likely reason for a potential differences between the output of the time series method and the results of the actual installation process.
- The current time series model can provide a lot of data concerning the description of the entire installation process. Most of this data is not used for the installation cost computation. A new cost computation function could make use of the number of vessel movements, a vessel's operation cost and a vessel's waiting on weather cost.

- The current installation process model requires an elaborate description of an installation cycle. It is unlikely that a micro siting model possesses information of the installation cycle properties for a fleet of installation vessels and different substructure types. Therefore, a database is need for a comprehensive fleet analysis. It is also possible to create a function that calculates or estimates the installation cycle properties based on the installation vessel's properties.

Bibliography

[1] 4Coffshore. Heavy maintenance and construction vessels, 2013. Web. http://www.4coffshore.com/windfarms/vessels.aspx?catId=3.

[2] Acteon. How menck predicts and reduces underwater noise, 2013. http://www.acteon.com/s2s-magazine/s2s-issue-11/sound-solutions-for-offshore-piledriving-347.

[3] Sir G. B. Airy. Tides and waves. *Encycl. Metrop. Art 192*, 1845.

[4] J. Bard and F. Thalemann. Offshore infrastructure: Ports and vessels. Technical report, Offshore Renewable Energy Conversion platforms âĂŞ Coordination Action (ORECCA), 2011. Chapter 3, Page 11-15, Web. http://www.orecca.eu/c/document_library/get_file?uuid=6b6500ba-3cc9-4ab0-8bd7-1d8fdd8a697a&groupId=10129.

[5] J. Bard and F. Thalemann. Offshore infrastructure: Ports and vessels. Technical report, Offshore Renewable Energy Conversion platforms âĂŞ Coordination Action (ORECCA), 2011. Chapter 2, Page 7-8, Web. http://www.orecca.eu/c/document_library/get_file?uuid=6b6500ba-3cc9-4ab0-8bd7-1d8fdd8a697a&groupId=10129.

[6] M. Blanco. The economics of wind energy. *Renewable and Sustainable Energy Reviews*, 13:1372–1382, 2009. Web. http://www.sciencedirect.com/science/article/pii/S1364032108001299.

[7] T. Burton, D. Sharpe, N. Jenkins, and E.Bossanyi. *Wind Energy Handbook*. John Wiley & Sons, 2001. Chapter 3: Aerodynamics of Horizontal-Axis Wind Turbines, Page 46.

[8] A.K. Chopra. *Dynamics of structures, Theory and Applications to Earthquake Engineering*. Prentice Hall, Inc., 1995.

[9] R. Clough and J. Penzien. *Dynamics of structures*. Computers & Structures, Inc., 3 edition, 2003. Chapter 8: Generalized single degree-of-freedom systems, Page 158.

[10] Global Wind Energy Council. Global offshore: Current status and future prospects, 2013. Web. http://www.gwec.net/global-offshore-current-status-future-prospects/.

[11] W. de Vries. Foundation pile analysis tool, 2010. Delft University of Technology course OE5662 Offshore Wind Farm Design 2011-2012, Matlab code, https://blackboard.tudelft.nl/bbcswebdav/pid-1736165-dt-content-rid-4817341_2/xid-4817341_2.

[12] W.E. de Vries and D.J. Cerda Salzmann. Morison calc auto v06.xls. Delft University of Technology course OE5662 Offshore Wind Farm Design 2011-2012, Excel file, https://blackboard.tudelft.nl/bbcswebdav/pid-1736167-dt-content-rid-4817356_2/xid-4817356_2.

[13] Environmental Dreging and Marine Engineering. Far offshore wind thorntonbank belgium. http://www.deme.be/projects/documents/Brochure_GB.pdf.

[14] C.N. Elkinton, J.F. Manwell, and J.G. McGowan. Offshore wind farm layout optimization (owflo), project: introduction, 2005. Tech. rep. University of Massachusetts. Web. http://www.umass.edu/windenergy/publications/published/2005/COW05_OWFLO.pdf.

[15] C.N. Elkinton and J.F. Manwelland J.G. McGowan. Algorithms for offshore wind farm layout optimization. *Wind Engineering Volume*, 32:67–83, 2008. Web. http://multi-science.metapress.com/content/y14xl29nu6565rp1/fulltext.pdf.

[16] A. Emami and P. Noghreh. New approach on optimization in placement of wind turbines within wind farm by genetic algorithms. *Renewable energy*, 35:1559–1564, 2010. Web. http://www.sciencedirect.com/science/article/pii/S0960148109005023.

[17] Les energies de la mer. Thornton bank : Repower et c-power finalisent une transaction pour livrer 325mw, 2013. http://energiesdelamer.blogspot.nl/2010/12/thornton-bank-repower-et-c-power.html.

[18] Dong Energy. Newsletter no. 1 - april 20, 2013. http://www.dongenergy.com/Walney/News/data/Pages/Newsletterno1-April2010.aspx.

[19] Ballast Nedam Engineering. Geotechnical design. Technical Report 10080006-30-00-CA-006, Ballast Nedam, . Project Offshore Windfarm Baltic I.

[20] Ballast Nedam Engineering. Preliminary design foundation wtg 14. Technical Report 10080006-20-00-CA-008, Revision A, Ballast Nedam, . Project Offshore Windfarm Baltic I.

[21] Ballast Nedam Engineering. Preliminary design steel foundations for a siemens 3.6 mw-120. Technical Report 10090094-10-00-CA-008, Revision B, Ballast Nedam, . Project Butendiek.

[22] S. Engström, T. Lyrner, M. Hassanzadeh, T. Stalin, and J. Johansson. Tall towers for large wind turbines. Technical Report , Report from Vindforsk project V-342 Högatorn för vindkraftverk - Elforsk rapport 10:48, 2010. Page 28.

[23] H.J.T. Kooijman et al. Cost and potential of offshore wind energy on the dutch part of the north sea., 2001. EWEC. Copenhagen, DK, 2001. pp. 218-21. Web http://www.ecn.nl/docs/library/report/2001/rx01063.pdf.

[24] T. Fischer, W. de Vries, and A. Cordle. Executive summary; wp4: Offshore foundations and support structures). Technical report, Upwind, 2011. Chapter 1, Page 40, http://www.upwind.eu/Publications/~/media/UpWind/Documents/Publications/4%20-%20Offshore%20Foundations/WP4_Executive_Summary_Final.ashx.

[25] D. Gielen. Renewable energy technologies: Cost analysis series. Technical Report Volume 1: Power sector, Issue 5/5, International Renewable Energy Agency (IRENA), june 2012. Web. https://www.irena.org/DocumentDownloads/Publications/RE_Technologies_Cost_Analysis-WIND_POWER.pdf.

[26] Germanischer Lloyd WindEnergie GmbH. Guideline for the certification of offshore wind turbines. Technical Report edition 2005, Germanischer Lloyd WindEnergie GmbH, 2005. Chapter 3, http://onlinepubs.trb.org/onlinepubs/mb/Offshore%20Wind/Guideline.pdf.

[27] Germanischer Lloyd WindEnergie GmbH. Guideline for the certification of offshore wind turbines. Technical Report edition 2005, Germanischer Lloyd WindEnergie GmbH, 2005. Chapter 4, Section 4.2.4.1, Page 4-21, http://onlinepubs.trb.org/onlinepubs/mb/Offshore%20Wind/Guideline.pdf.

[28] Germanischer Lloyd WindEnergie GmbH. Guideline for the certification of offshore wind turbines. Technical Report edition 2005, Germanischer Lloyd WindEnergie GmbH, 2005. Chapter 6, Section 6.6.5.2.2, Page 6-25 up to 6-32, http://onlinepubs.trb.org/onlinepubs/mb/Offshore%20Wind/Guideline.pdf.

[29] Germanischer Lloyd WindEnergie GmbH. Guideline for the certification of offshore wind turbines. Technical Report edition 2005, Germanischer Lloyd WindEnergie GmbH, 2005. Chapter 5, Section 5.4.4.2, Page 5-19, http://onlinepubs.trb.org/onlinepubs/mb/Offshore%20Wind/Guideline.pdf.

[30] Germanischer Lloyd WindEnergie GmbH. Guideline for the certification of offshore wind turbines. Technical Report edition 2005, Germanischer Lloyd WindEnergie GmbH, 2005. Chapter 4, Section 4.3.3.4, Page 4-36, http://onlinepubs.trb.org/onlinepubs/mb/Offshore%20Wind/Guideline.pdf.

[31] Germanischer Lloyd WindEnergie GmbH. Guideline for the certification of offshore wind turbines. Technical Report edition 2005, Germanischer Lloyd WindEnergie GmbH, 2005. Chapter 4, Section 4.2.3.1.4, Page 4-17, http://onlinepubs.trb.org/onlinepubs/mb/Offshore%20Wind/Guideline.pdf.

[32] Germanischer Lloyd WindEnergie GmbH. Guideline for the certification of offshore wind turbines. Technical Report edition 2005, Germanischer Lloyd WindEnergie GmbH, 2005. Chapter 4, Section 4.2.3.2, Page 4-19, http://onlinepubs.trb.org/onlinepubs/mb/Offshore%20Wind/Guideline.pdf.

[33] Germanischer Lloyd WindEnergie GmbH. Guideline for the certification of offshore wind turbines. Technical Report edition 2005, Germanischer Lloyd WindEnergie GmbH, 2005. Chapter 4, Section 4.2.2.4.1, Page 4-10, http://onlinepubs.trb.org/onlinepubs/mb/Offshore%20Wind/Guideline.pdf.

[34] Germanischer Lloyd WindEnergie GmbH. Guideline for the certification of offshore wind turbines. Technical Report edition 2005, Germanischer Lloyd WindEnergie GmbH, 2005. Chapter 6, Section 6.6.5.4.2, Page 6-28 up to 6-32, http://onlinepubs.trb.org/onlinepubs/mb/Offshore%20Wind/Guideline.pdf.

[35] Germanischer Lloyd WindEnergie GmbH. Guideline for the certification of offshore wind turbines. Technical Report edition 2005, Germanischer Lloyd WindEnergie GmbH, 2005.

Chapter 4, Section 4.2.2.3.2, Page 4-8, http://onlinepubs.trb.org/onlinepubs/mb/Offshore%20Wind/Guideline.pdf.

[36] J. S. Gonzalez, M. B. Payan, and J. R. Santos. A new and efficient method for optimal design of large offshore wind power plants. *IEEE Transactions on Power Systems*, 28:3075–3084, 2013. http://ieeexplore.ieee.org/xpl/articleDetails.jsp?arnumber=6502287.

[37] S.A. Grady, M.Y. Hussaini, and M.M. Abdullah. Placement of wind turbines using genetic algorithms. *Renewable energy*, 30:259–270, 2005. Web. http://www.sciencedirect.com/science/article/pii/S0960148104001867.

[38] A. Grilli, M. Spaulding, C. O'Reilly, and G. Potty. Offshore wind farm macro and micro siting protocol application to rhode island. *Coastal Engineering*, 2012. Web. http://journals.tdl.org/icce/index.php/icce/article/view/6831/pdf.

[39] L. Harland and J. Vugts. Analytic expression for the first natural frequency of a stepped tower, October 1996. Project: OPTI-OWECS, Memo: sent to Tim Cockerill, Murray Ferguson, Martin Kühn, Wim Bierbooms and Anita Sanström, http://ocw.tudelft.nl/fileadmin/ocw/courses/OffshoreWindFarmEnergy/res00070/NF_stepped_monotower__Rayleigh_.pdf.

[40] A.R. Henderson. Design methods for offshore wind turbines at exposed sites, hydrodynamic loading on offshore wind turbines, owtes task 4.2, owec tools task b.1 - b.2. Technical report, Duwind, 2003. Chapter 2, Page 16-28, http://www.citg.tudelft.nl/fileadmin/Faculteit/CiTG/Over_de_faculteit/Afdelingen/Afdeling_Waterbouwkunde/sectie_waterbouwkunde/people/personal/gelder/publications/citations/doc/citatie184.pdf.

[41] American Petroleum Institute. Recommended practice for planning, designing and constructing fixed offshore platforms - working stress design, api recommended practice 2a-wsd. Technical report, American Petroleum Institute, 2005. Chapter 6, Section 6.8, Page 68-71, oc.its.ac.id/ambilfile.php?idp=1765.

[42] Mark J. Kaiser and Brian Snyder. Offshore wind energy installation and decommissioning cost estimation in the u.s. outer continental shelf. Technical report, U.S. Dept. of the Interior, Bureau of Ocean Energy Management, Regulation and Enforcement, November 2010. Chapter 2, Page 19, Web. http://www.bsee.gov/uploadedFiles/BSEE/Research_and_Training/Technology_Assessment_and_Research/648aa.pdf.

[43] Mark J. Kaiser and Brian Snyder. Offshore wind energy installation and decommissioning cost estimation in the u.s. outer continental shelf. Technical report, U.S. Dept. of the Interior, Bureau of Ocean Energy Management, Regulation and Enforcement, November 2010. Chapter 2, Page 23-26, Web. http://www.bsee.gov/uploadedFiles/BSEE/Research_and_Training/Technology_Assessment_and_Research/648aa.pdf.

[44] M.J. Kaiser and B. Snyder. Modeling the decommissioning cost of offshore wind development on the u.s. outer continental shelf. *Marine Policy*, 36:153–164, 2010. Web. http://www.sciencedirect.com/science/article/pii/S0308597X11000807.

[45] M. Kühn, T.T. Cockerill, L.A. Harland, R. Harrison, C. Schöntag, G.J.W. van Bussel, and J.H. Vugts. Methods assisting the design of offshore wind energy conversion systems. Technical Report , Institute for Wind Energy, Delft University of Technology, Renewable

Energy Centre, University of Sunderland, Workgroup Offshore Technology, Delft University of Technology, 1996. Page 5-10.

[46] MathWorks. gaoptimset, 2013. http://www.mathworks.nl/help/gads/gaoptimset.html.

[47] MathWorks. Genetic algorithm - what is the genetic algorithm?, 2013. http://www.mathworks.nl/help/gads/what-is-the-genetic-algorithm.html.

[48] MathWorks. Genetic algorithm- nonlinear constraint solver algorithm, 2013. http://www.mathworks.nl/help/gads/description-of-the-nonlinear-constraint-solver_bqf8bdd.html.

[49] MathWorks. How the genetic algorithm works, 2013. http://www.mathworks.nl/help/gads/how-the-genetic-algorithm-works.html#f11083.

[50] MathWorks. Weibull parameter estimates, 2013. http://www.mathworks.nl/help/stats/wblfit.html.

[51] MathWorks. Wind power, 2013. http://www.mathworks.nl/energy-production/wind-power.html.

[52] A. Moeller. Efficient offshore wind turbine foundations, 2008. http://homes.civil.aau.dk/rrp/BM/BM8/o.pdf.

[53] J. R. Morison, M.P. O'Brien, J. W. Johnson, and S. A. Schaaf. The forces excerted by surface waves on piles. *Petroleum Transactions*, 189:149, 1950.

[54] G. Mosetti, C. Poloni, and B. Diviacco. Optimization of wind turbine positioning in large wind farms by means of a genetic algorithm. *Journal of Wind Engineering and Industrial Aerodynamics*, 51:105–116, 1994. Web. http://www.sciencedirect.com/science/article/pii/0167610594900809.

[55] W. Musial and B. Ram. Large-scale offshore wind power in the united states, assesment of opportunities and barriers. Technical report, National Renewable Energy Laboratory (NREL), september 2010. Web. http://www.nrel.gov/wind/pdfs/40745.pdf.

[56] Official Journal of the European Union. Directive 2009/28/ec of the european parliament and of the council of 23 april 2009, 2009. Web. http://eur-lex.europa.eu/LexUriServ/LexUriServ.do?uri=Oj:L:2009:140:0016:0062:en:PDF.

[57] Department VI of the Royal Belgium Institute of Natural Sciences. Forecast of the water level at thorntonbank center, 2014. http://www.mumm.ac.be/EN/Models/Operational/Tides/series.php?station=thorntonbankcenter.

[58] Ballast Nedam Offshore. Ballast nedam offshore, 2013. http://www.bnoffshore.com/public/offshore/hlv-svanen/Pages/default.aspx.

[59] S. Parvanova. Beams on elastic foundation - lecture notes, 2011. Lecture Notes: Structural Analysis II, University of Architecture, Civil Engineering and Geodesy - Sofia http://www.uacg.bg/filebank/att_1324.pdf.

[60] B. Pérez, R. Mínguez, and R. Guanche. Offshore wind farm layout optimization using mathematical programming techniques. *Renewable energy*, 53:389–399, 2013. Web. http://www.sciencedirect.com/science/article/pii/S0960148112007628.

[61] B. P. Rašuo and A. Č. Bengin. Optimization of wind farm layout. *FME Transactions*, 38:107–114, 2010. http://www.mas.bg.ac.rs/istrazivanje/biblioteka/publikacije/Transactions_FME/Volume38/3/01_BPRasuo.pdf.

[62] Repower. Repower 5.0 mw offshore. Brochure: http://www.ceoe.udel.edu/windpower/resources/5m_uk.pdf.

[63] S. Rodrigues, P. Bauer, and J. Pierik. Modular approach for the optimal wind turbine micro siting problem through cma-es algorithm. *Proceeding of the fifteenth annual conference companion on Genetic and evolutionary computation conference companion*, pages 1561–1568, 2013. http://dl.acm.org/citation.cfm?id=2482736.

[64] B. Saavedra-Moreno, S. Salcedo-Sanz, A. Paniagua-Tineo, L. Prieto, and A. Portilla-Figueras. Seeding evolutionary algorithms with heuristics for optimal wind turbines positioning in wind farms. *Renewable Energy*, 36:2838–2844, 2011. http://www.sciencedirect.com/science/article/pii/S096014811100190X.

[65] S. Salisbury. Numerically calculating beam deflections, 2010. Matlab code: http://www.eng.uwo.ca/people/ssalisbury/Programs/MatlabBeamDeflection.pdf.

[66] M. Segeren. Foundation design guide of owss, 2012-2013. Delft University of Technology course OE5665 Offshore Wind Support Structures https://blackboard.tudelft.nl/bbcswebdav/pid-2012757-dt-content-rid-6859268_2/courses/26935-121304/Foundation%20Design%20Guide%20for%20OWSS.pdf.

[67] Siemens. Siemens 3.6 mw offshore - technical specifications. http://www.energy.siemens.com/hq/en/renewable-energy/wind-power/platforms/g4-platform/wind-turbine-swt-3-6-120.htm#content=Technical%20Specification.

[68] The Engineering Toolbox. Modulus of elasticity - young modulus for some common materials, 2014. http://www.engineeringtoolbox.com/young-modulus-d_417.html.

[69] Unknown. Barge abjv4 with monopiles and system tower elements for offshore wind farm âĂđlondon arrayâĂIJ, 2013. http://www.flickr.com/photos/cuxclipper1/7124015089/.

[70] Emre Uraz. Offshore wind turbine transportation & installation analyses, planning optimal marine operations for offshore wind projects. Master's thesis, Gotland University, Sweden, 2011. https://www.yumpu.com/en/document/view/10277494/offshore-wind-turbine-installation-analyses.

[71] J. van der Tempel. *Design of Support Structures for Offshore Wind Turbines*. PhD thesis, Delft University of Technology, 2006. Chapter 3, Page 85-86. Web. http://repository.tudelft.nl/assets/uuid:ae69666e-3190-4b22-84ed-2ed44c23e670/ceg_tempel_20060426.pdf.

[72] J. van der Tempel. *Design of Support Structures for Offshore Wind Turbines*. PhD thesis, Delft University of Technology, 2006. Chapter 2, Page 18. Web. http://repository.tudelft.nl/assets/uuid:ae69666e-3190-4b22-84ed-2ed44c23e670/ceg_tempel_20060426.pdf.

[73] J. van der Tempel. *Design of Support Structures for Offshore Wind Turbines*. PhD thesis, Delft University of Technology, 2006. Chapter 2, Page 55-57. Web. http://repository.tudelft.nl/assets/uuid:ae69666e-3190-4b22-84ed-2ed44c23e670/ceg_tempel_20060426.pdf.

[74] Det Norske Veritas. Offshore standard DNV-OS-J101, design of offshore wind turbine structures. Technical report, Det Norske Veritas, 2007. https://exchange.dnv.com/publishing/Codes/download.asp?url=2011-09/os-j101.pdf.

[75] Det Norske Veritas. Offshore standard DNV-OS-J101, design of offshore wind turbine structures. Technical report, Det Norske Veritas, 2007. App. G, Page 197, https://exchange.dnv.com/publishing/Codes/download.asp?url=2011-09/os-j101.pdf.

[76] Det Norske Veritas. Offshore standard DNV-OS-J101, design of offshore wind turbine structures. Technical report, Det Norske Veritas, 2007. Section 3C, Page 35, https://exchange.dnv.com/publishing/Codes/download.asp?url=2011-09/os-j101.pdf.

[77] Vestas. Vestas v112 3.0 mw offshore. Brochure: http://www.vestas.com/Files/Filer/EN/Brochures/Productbrochure_V112_Offshore_UK.pdf.

[78] Vestas. Vestas v90 3.0 mw offshore. Brochure: http://www.vestas.com/Files/Filer/EN/Brochures/Vestas_V_90-3MW-11-2009-EN.pdf.

[79] N. Wang. A parallel computing application of the genetic algorithm for lubrication optimization. *Tribology Letters,*, 18:105–112, 2004. http://link.springer.com/article/10.1007%2Fs11249-004-1763-x.

[80] J.D. Wheeler. Method for calculating forces produced by irregular waves. , 1969. Proceedings of First Offshore Technology Conference, Houston, Texas, OTC 1006.

[81] M. B. Zaaijer. Foundation modelling to assess dynamic behaviour of offshore wind turbines. *Applied Ocean Research*, 28:45–57, 2006. http://www.sciencedirect.com/science/article/pii/S0141118706000289.

[82] M.B. Zaaijer. Comparison of monopile, tripod, suction bucket and gravity base design for a 6 mw turbine. In *Offshore Windenergy in Mediterranean and Other European Seas (OWEMES conference), Naples, Italy, April 2003.*, 2003. https://www.ecn.nl/fileadmin/ecn/units/wind/docs/dowec/2003-OWEMES-Support-structures.pdf.

[83] M.B. Zaaijer. Great expectations for offshore wind turbines. emulation of wind farm design to anticipate their value for customers, 2013. Page 85, http://repository.tudelft.nl/assets/uuid:fd689ba2-3c5f-4e7c-9ccd-55ddbf1679bd/PhD_thesis_MB_Zaaijer_Final_-_pdf.pdf.

[84] M.B. Zaaijer and J. van der Tempel. Scour protection: a necessity or a waste ofmoney?, 2004. Proceedings of the 43rd IEA Topical Expert Meeting âĂŞ Critical Issues Regarding Offshore Technology and Deployment: 43-51. Skaerbaek, Denmark. Web. http://www.lr.tudelft.nl/fileadmin/Faculteit/LR/Organisatie/Afdelingen_en_Leerstoelen/Afdeling_AEWE/Wind_Energy/Research/Publications/Publications_2004/doc/Tempel_scour.pdf.

Appendix A

Variables not included in installation process model

In this Appendix variables are presented that contribute to the total installation time computation results, but are not incorporated within the installation process model. The reason for not including these variables is to limit the scope and complexity of the installation process model.

- **Learning processes**
  Throughout the installation season the installation cycle time could decrease as a result of learning.

- **Failure of equipment or vessels**
  It is assumed that no failure occurs of any offshore installation equipment, the main installation vessel, a supply vessel, the onshore cranes or other required components. Furthermore, it is assumed that a fully capable crew is responsible for and available during the entire installation process.

- **Loading restrictions at harbour**
  No restrictions concerning the wind conditions at the harbour are considered. Substructure components are commonly prepared onshore. This requires the use of cranes, which cannot be operate above a certain wind speed.

- **Multiple weather data sets**
  When a large distance from harbour to OWF site exist there could be a difference in weather conditions between these locations. For example at the OWF site it could be perfect weather, but the supply vessel at the harbour are not allowed to sail out. Multiple sets of weather data would be required to incorporate this in the model.

- **Effect of components weight on activity time**
  The crane's lifting cable can be connected to one or several winches. By doing so the lifting speed and crane lifting capacity can be changed. This results in a slower lifting speed. The effect of the substructure component weight on the installation speed is neglected.

- **Pile penetration depth and soil properties**
  The pile driving time could be influenced by the required pile penetration depth and the soil properties. A constant pile driving time, independent of these properties, is assumed.

- **Installation in multiple phases**
  The installation of the substructures could be performed in two or more phases. For example, all MPs of an OWF can be installed first, after which all TPs are installed. This could be beneficial when one considers the required sea temperature. The installation of the second phase could be performed by a second installation vessel. All possible combinations of installation vessels and installation in phases are not taken into account.

- **Installation with more than one main installation vessel**
  The installation of the substructures in only one season can also be performed by two or more installation vessels. All possible combinations of installation vessels running in parallel are not considered. Current OWF substructures are mostly installed with one installation vessel.

- **Supply vessels with different properties**
  The calculation of the required number of supply vessels for the feeding strategy assumes homogeneous supply vessel properties. The possibility of different supply vessel properties is not considered.

- **Loading during run for shelter**
  When the main installation vessel, using the traveling installation strategy, needs to shelter and it does so at the harbour it could resupply. However, for the porpuse of simplification this is not considered.

- **Accuracy predicting of environmental conditions**
  Environmental conditions cannot be predicted perfectly. Hence, a contingency factor is used to calculate the required weather window time. This is not exactly the same as perfectly predicting the environmental conditions. For example look at an activity time of 2 hours and 8 hours. In the first case a weather window of 3 hours is required, which means an accurate weather prediction of 3 hours. In the latter case a prediction of 12 hours is required. A solution to this problem could be to split the contingency factor in two components; one related to a delay in performing an installation activity and one related to uncertainties in future weather conditions. This last contingency factor can now be expressed as a function of the prediction time. Since this would require an extensive statistical analysis in the change of environmental conditions, the contingency factor is assumed to be constant.

- **Variation in of activity time**
  The required time to complete an activity can slightly fluctuate per installation cycle. Currently, this is partly incorporated by using a contingency factor. However, a more accurate method could be to see each activity as a process with a mean time and standard deviation.

- **Variable speed of vessels**
  A main installation vessel or supply vessel can have a higher or lower traveling speed depending on the magnitude, direction of the current and amount of load. This is not included within the model.

- **Vessel's location within the wind farm**
  Despite the fact that an inner OWF traveling time is incorporated within the model, it is assumed that the traveling time from OWF site to harbour is independent of a vessels location within the OWF.

- **Restrictions in supply of components**
  The feeding installation strategy assumes a constant supply of substructure components. The transiting methods assumes substructure components always to be available in the harbour. Restriction due to supply chain limitations, harbour weather conditions or failures during transport are not accounted for.

- **Complying to a deadline**
  The current model uses a start date to on which the installation process commences. By analyzing different start date the ideal start date resulting in the least installation time can be obtained. However, it could also be the case that installation activities need to be finished before a end date. The end date can, for example be determined by the vessel's owner.

Appendix B

Wind Loads

B.1 Wind speed conversion

The 5 and 50 year highest wind speed, obtained by the Weibull distribution, are only valid for a certain time period and altitude. Commonly a data set of wind data consist of sample with a sample time of 1.0 hour or 10 minutes. To convert this wind speed to the highest wind speed within that particular sample table B.1 can be used [33].

Table B.1: Conversion factors for averaging values of the wind speed

Time	**1 h**	**10 min**	**1 min**	**5 s**	**3 s**
Factor	0.91	1.00	1.10	1.21	1.25

The wind speed at any height, Vz, can be calculated using equation B.1 from the GL [33]. Here, V_{ref} is the reference wind speed corresponding to the reference height, z_{ref}. The height of a structural segment at which the wind speed is calculated, z, is equal to the distance from the water level to the location of the corresponding segment.

$$V_z = V_{ref}\left(\frac{z}{z_{ref}}\right)^{0.14} \tag{B.1}$$

The wind loads are required to assess the ULS scenario. Within this research only simple relations are used to calculated the wind loads for extreme wind speed. However, more eleborate and complex relations will result in a higher accuracy assessment of the wind loads. It is also possible to use the wind farm simulation toolbox, which is available within the MATLAB program [51].

Within this research the wind loads is calculated for a operating turbine and a idle turbine. The scenario resulting in the highest wind loads in chosen to be used for the assessment of the local buckling design requirement.

B.2 Operating turbine

When operating the turbine blades produce a thrust force, which is required to extract energy from the wind. The structure experiences this forces pointing in the direction of the wind flow.

$$F_{T,turb} = C_T \, 1/2 \cdot \rho_{air} \cdot A_{R,plane} \cdot V_{hub}^2 \tag{B.2}$$

Where:

$$A_{R,plane} = \pi \, R^2 \tag{B.3}$$

Within this equation all variables are known, except for the thrust coefficient, C_T. The thrust coefficient of the can be derived from the induced wind speed, a, equation B.4 [7].

$$C_T = 4a(1-a) \tag{B.4}$$

The highest thrust force during operational mode is obtained when the turbine is operating at rated wind speed and is hit by a wind gust. Here, it is assumed that the turbine is operates at the Betz limit. The induction factor at rated wind speed equals $a = 1/3$. Using this induction factor the thrust force can be calculated, which is multiplied by a factor 1.5 to account for a sudden gust.

B.3 Tower drag

A tower drag force is the result of interaction between the wind particles and the tower. This can be expressed by the following simple relation;

$$F_{tower\ segment} = C_D \, 1/2 \cdot \rho_{air} \cdot A_{segment} \cdot V(z)^2 \tag{B.5}$$

With:

$$A_{segment} = D(z) \cdot dl \tag{B.6}$$

$$V(z) = V_{hub} \left(\frac{z}{z_{hub}} \right)^{\alpha} \tag{B.7}$$

Here, α, is called the power law exponent. According to the Germanischer Loyd α is approximately 0.14 [-] for offshore rough sea conditions [35]. During extreme wind conditions it is likely this α-value for rough sea conditions will be suitable. The hub height wind speed is chosen as a the reference wind speed. Further, the drag coefficient, C_D, can be a function of the Reynolds number. However, (at the moment) a constant value of $C_D = 1,2$ is chosen. The tower diameter as function of the height, $D(z)$, is defined by the structural dimensions, see section 4.1.

Appendix C

Lateral Soil Stability

C.1 Example Stiffness Matrix

The soil and structure stiffness matrix, **K**, is composed of a combination of the structural stiffness and soil stiffness. In combination with a force vector, **F** and a displacement vector, **u** a description of the pile deflection and rotation as a result of a shear force and bending moment is obtained. The size of these vectors and this matrix depends on the amount of structural elements, n, see equation C.1 up to C.3.

$$\mathbf{F} = [n+1 \times 1] \tag{C.1}$$
$$\mathbf{u} = [n+1 \times 1] \tag{C.2}$$
$$\mathbf{K} = [n+1 \times n+1] \tag{C.3}$$

An example of the Here, an example for a **K** matrix of a structure of two elements is given. The corresponding **F** and **u** vectors are also showed.

$$\mathbf{F}_2 = \begin{bmatrix} F_{mudline} \\ M_{mud\ line} \\ 0 \\ 0 \\ 0 \\ 0 \end{bmatrix} \quad \mathbf{u}_2 = \begin{bmatrix} u_1 \\ \theta_1 \\ u_2 \\ \theta_2 \\ u_3 \\ \theta_3 \end{bmatrix} \tag{C.4}$$

$$\mathbf{K}_2 = \begin{pmatrix} \frac{12EI_1}{L^3}+k_1 & -\frac{6EI_1}{L^2} & -\frac{12EI_1}{L^3} & -\frac{6EI_1}{L^2} & 0 & 0 \\ -\frac{6EI_1}{L^2} & \frac{4EI_1}{L} & \frac{6EI_1}{L^2} & \frac{2EI_1}{L} & 0 & 0 \\ -\frac{12EI_1}{L^3} & \frac{6EI_1}{L^2} & \frac{12EI_1}{L^3}+\frac{12EI_2}{L^3}+k_2 & \frac{6EI_1}{L^2}-\frac{6EI_2}{L^2} & -\frac{12EI_2}{L^3} & -\frac{6EI_2}{L^2} \\ -\frac{6EI_1}{L^2} & \frac{2EI_1}{L} & \frac{6EI_1}{L^2}-\frac{6EI_2}{L^2} & \frac{4EI_1}{L}+\frac{4EI_2}{L} & \frac{6EI_2}{L^2} & \frac{2EI_2}{L} \\ 0 & 0 & -\frac{12EI_2}{L^3} & \frac{6EI_2}{L^2} & \frac{12EI_2}{L^3} & \frac{6EI_2}{L^2} \\ 0 & 0 & -\frac{6EI_2}{L^2} & \frac{2EI_2}{L} & \frac{6EI_2}{L^2} & \frac{4EI_2}{L} \end{pmatrix}$$

C.2 Load deflection curves for Sand and Clay

The load deflection (p-y) curves are required to determined the stiffness of the soil. The soil properties required to obtain p-y curves for are described by API [41]. In this section the calculation method used to obtain the p-y curves of sand and clay is showed.

C.2.1 Sand

Each soil layer requires a set of data describing the properties of this particular layer. The required input for a sand layer consist of the effective unit weight of the soil, γ, the depth (distance with respect to the mud-line), H, and the angle of internal friction, ϕ'. Now the ultimate soil resistance can be calculated for deep, p_{ud}, and shallow, p_{us}, depth conditions, see equation C.5. For the depth of each structural segment the lowest of these two values is chosen to be the final ultimate soil resistance, p_u, see equation C.6.

$$p_{us} = (C_1 \cdot H + C_2 \cdot D) \cdot \gamma \cdot H \tag{C.5a}$$

$$p_{ud} = C_3 \cdot D \cdot \gamma \cdot H \tag{C.5b}$$

$$p_u = \begin{cases} p_{us} & \text{if} \quad p_{us} < p_{ud} \\ p_{ud} & \text{if} \quad p_{ud} < p_{us} \end{cases} \tag{C.6}$$

The non-dimensional coefficients C_1, C_2 and C_3 are obtained by fitting a forth order polynomial, see equation C.7, to the data in figure C.1(a). The polynomial coefficient p1 up to p5 are presented in table C.1.

$$C_x = p1 \cdot \phi'^4 + p2 \cdot \phi'^3 + p3 \cdot \phi'^2 + p4 \cdot \phi'^2 + p5 \tag{C.7}$$

The load deflection curve for sand can now be described by equation C.8.

	p1	p2	p3	p4	p5
C_1	0.0000057228	-0.0005238638	0.0233014354	-0.4237261794	3.1643475564
C_2	0.0000066539	-0.0009039276	0.0473457978	-0.9709162734	8.2279829893
C_3	0.00063961	-0.06697406	2.78481979	-51.64257405	361.52232411

Table C.1: Polynomial coefficients obtained from data of figure C.1(a)

$$P = A \cdot p_u \tanh\left[\frac{k \cdot H}{A \cdot p_u} y\right] \tag{C.8}$$

Here, A, is a factor that account for the static or cyclic loading. Cyclic loading is always assumed. Further, k, is the initial modulus of subgrade reaction, which is a function of the angle of internal friction, see equation C.10. Here, a second degree polynomial fit is made through data provided by figure C.1(b). Note that the calculated values are converted from lb/in^3 to kN/m^3.

$$A = 0.9 \text{ for cyclic loading} \tag{C.9}$$

$$k = 0.4295\phi'^2 + 17.806\phi' + 179.10 \tag{C.10}$$

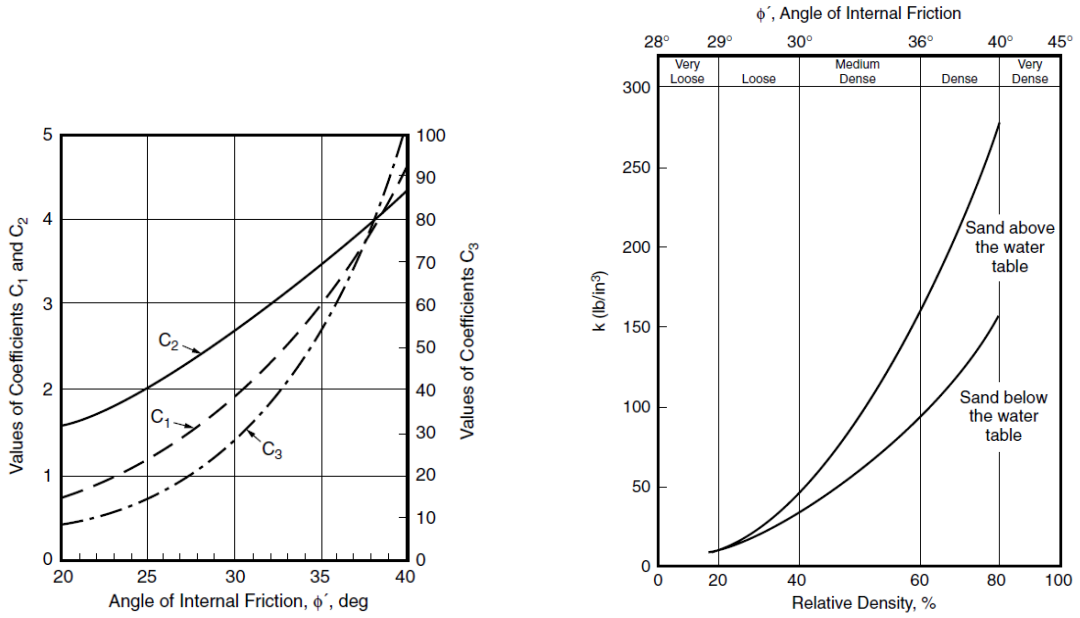

(a) Coefficients as function of angle of internal friction

(b) Initial modulus of subgrade reaction as function of angle of internal friction

Figure C.1: Soil properties of sand layer as function of angle of internal friction [41]

C.2.2 Clay

The ultimate soil resistance, p_u, can be calculated by combining the effective unit weight of the soil, γ, the depth (distance with respect to the mud-line), X, the undrained shear strength for

undisturbed claysoil samples, c, a dimensionless empirical constant, J, and the pile diameter, D, see equation C.11. When the depth of the soil segment is higher than the depth below soil surface to bottom of reduced resistance zone, X_R, than equation C.12 is appliclable.

$$p_u = 3c + \gamma X + J\frac{cX}{D} \tag{C.11}$$

$$p_u = 9c \qquad \text{for} X \geq X_R \tag{C.12}$$

The depth below soil surface to bottom of reduced resistance zone can be calculate using equation C.13. Suitable values for the dimensional constant are in the range between 0.25 and 0.5. A constant values of 0.5 is chosen to be used within this thesis, see equation C.14.

$$X_R = \frac{6D}{\frac{\gamma D}{c} + J} \tag{C.13}$$

$$J = 0.5 \tag{C.14}$$

From de Vries [11] a relation between the soil resistance and displacement is obtained, see table C.2. Dimensionless coefficients A1 and B1 are obtained using the empirical obtained relations described in equations C.16 and C.17.

Sort Clay		Stiff Clay	
p	y	p	y
0	0	0	0
$0.3p_u$	$0.55y_{50}$	$0.51B_1p_u$	$0.46A_1y_{50}$
$0.5p_u$	$2.5y_{50}$	$0.82B_1p_u$	$0.92A_1y_{50}$
$0.72p_u$	$7.5y_{50}$	B_1p_u	$1.85A_1y_{50}$
$0.72p_u\frac{X}{X_r}$	$37.5y_{50}$	$(0.936B_1 - 0.418A_1)p_u$	$7.38A_1y_{50}$
$0.72p_u\frac{X}{X_r}$	D	$(0.936B_1 - 0.418A_1)p_u$	D

Table C.2: Used PY relations of different soil types [11]

$$y_50 = \varepsilon_{50}D \tag{C.15}$$

$$A1 = 0.6 - \frac{0.4}{3.0^2}\cdot\left(\frac{X}{D} - 3.0\right)^2 \qquad \text{for} \quad X/D < 3.0 \tag{C.16a}$$

$$A1 = 0.6 \qquad \text{for} \quad X/D \geq 3.0 \tag{C.16b}$$

$$B1 = 0.3 - \frac{0.1}{1.8^2}\cdot\left(\frac{X}{D} - 1.8\right)^2 \qquad \text{for} \quad X/D < 1.8 \tag{C.17a}$$

$$B1 = 0.3 \qquad \text{for} \quad X/D \geq 1.8 \tag{C.17b}$$

Appendix D

Improved Rayleigh Method

The improved Rayleigh method is used to compute the first natural frequency of the structure clamped at the mud-line. This method is described by Clough and Penzien in their "Dynamics of Structures" [9].

The basics behind the improved Rayleigh method lies in the maximum kinetic and potential energy involved in a vibration. Both these energies depends on the vibration shape of the structure. Further more, the kinetic energy also depends on the structure's vibrational frequency. Now a certain frequency exist for which the maximum kinetic energy equals the maximum potential energy, which means that no energy is lost during such a vibration. Rayleigh has derived an expression for such a situation, see equation 4.38.

The problem with this expression is the unknown mode shape function, $\phi(x)$. A solution lies in the implementation of the improved Rayleigh method, see equation D.1. An iterative process, of n being the number of iterations, is used to find the correct natural angular frequency, ω_n.

Here, $\phi^{(n-1)}$ is the mode shape of the previous iteration and $\phi^{(n)}$ is the mode shape of the final iteration. The generalized coordinate amplitude, $\bar{Z}_0^{(n)}$, is found using equation D.2.

$$\omega_n^2 = \frac{Z_0^{(n-1)}}{\bar{Z}_0^{(n)}} \frac{\int_0^L m(x)\ \phi^{(n-1)}\ \phi^{(n)}\ dx}{\int_0^L m(x)\ (\phi^{(n)})^2\ dx} \tag{D.1}$$

$$\bar{Z}_0^{(n)} = \frac{Z_0^{(n)}}{\omega_{n-1}^2} \tag{D.2}$$

The implementation of this iterative procedure is described below for the first two iterations. In the developed model three iterations are sufficient to converge to a final natural frequency.

Initial mode shape: Consequently, two mode shape are required to perform one iteration. A guess for the initial mode shape, $\phi^{(0)}$, is described by equation D.3.

$$\phi^{(0)} = 1 - \cos\left(\frac{\pi x}{2L}\right) \tag{D.3}$$

First mode shape: Using the original Rayleigh method, equation 4.38, an angular frequency, ω_0, can be calculated. Using this angular frequency an initial distributed inertia force, $p^{(0)}(x)$, can be computed, see equation D.4.

$$p^{(0)}(x) = \omega_0^2 \cdot m(x) \cdot v^{(0)} \tag{D.4}$$

The displacement of each structural segment as a result of the distributed inertia force can be obtained using a finite element method approach. A Matlab code, provided by Salisbury [65], is used to obtain a deflection vector, $v^{(1)}$. The corresponding mode shape, $p^{(1)}(x)$, is obtained by dividing the deflection vector by the maximum amplitude, $Z_0^{(1)}$, see equation D.5.

$$\phi^{(1)}(x) = \frac{v^{(1)}}{Z_0^{(1)}} \tag{D.5}$$

Completing first iteration Now the generalized coordinate amplitude, $\bar{Z}_0^{(1)}$, and the first angular natural frequency, ω_n, can be calculated using equation D.1.

Second iteration Now a new angular frequency is know. Therefore, a new distributed inertia force, $p^{(1)}(x)$, can be computed, using equation D.6.

$$p^{(1)}(x) = \omega_1^2 \cdot m(x) \cdot v^{(1)} \tag{D.6}$$

Furthermore, the second displacement vector, $v^{(2)}$, is obtained using the finite element method in combination with the latest distributed inertia force. From the displacement vector a corresponding mode shape is obtained, see equation D.7.

$$\phi^{(2)}(x) = \frac{v^{(2)}}{Z_0^{(2)}} \tag{D.7}$$

Finally, the second iteration is completed by calculation the natural frequency, ω_2.

Appendix E

Soil Bearing Capacity Formulas

The implementation of the soil bearing capacity design requirement is performed according to a description provided by a memo from Zaaijer. The entire memo is presented in the next three pages of this report. Only the use of sand layers is permitted using this approach. Further investigation is required to assess the use of other soil layers as foundation for a GBS based support structure.

Memo

TU Delft

Date:	**24 January 2002**
From:	**Michiel Zaaijer**
To:	**Sergio Herman**
Subject:	**Soil mechanics for gravity base structures**

This memo provides information about the bearing capacity and sliding resistance of a rigid gravity base foundation on a sandy soil. The information is based on [1, Section 42] and [2, Section 11.2], setting c=0 (shear strength) and q=0 (overburden pressure). The sliding resistance and bearing capacity must be sufficient for all load cases and at all instants. It is recommended to check this for several phases of a design wave, because minimum sliding resistance, minimum heave and maximum lateral hydrodynamic loading do not coincide. Particularly the information concerning the bearing capacity of the GBS must be used with care, since there is no firm fundamental theory that supports this equation. Furthermore, the effect of pore pressures under dynamic loading is not included.

Symbols

Φ_{SB}	GBS resistance factor on bearing capacity (=0.67)
Φ_{SS}	GBS resistance factor on sliding capacity (=0.80)
δ	soil-GBS friction angle
φ	(internal) friction angle of the soil
γ'	soil submerged unit weight
D	diameter of cylindrical GBS
F	force
M	moment about horizontal axis on the seabed, intersecting with tower centreline
N_γ	coefficient in bearing equation for GBS
N_q	coefficient in bearing equation for GBS
i_γ	factor for inclined loading
m_γ	factor for reduced effective area of GBS, caused by eccentricity of force
p	(vertical) pressure at contact surface soil-GBS
s_γ	shape factor
t	shear stress at contact surface soil-GBS

Loading

Lateral and vertical forces and overturning moment at the soil-GBS interface are required to determine the stability of the GBS. A GBS may experience a large heave force (vertical) and a pitch moment (hydrodynamic overturning moment). These are caused by pressure variations on the upper surface of the GBS, while the soil-GBS contact surface is at a more or less constant pressure (the slowly varying pressure difference from tidal variation can be levelled off by draining the soil below the GBS. Thus, only the pressure variations during wave passage cause forces on the structure.) Evidently, the hydrodynamic- and aerodynamic loading on the rest of the structure and turbine need to be included.

Sliding Resistance
To have sufficient resistance against sliding, the following criterion must be met:

$t \le \Phi_{SS}\, p \tan\varphi$.

This equation assumes that the internal friction in the soil is dominating the sliding resistance. This is for instance the case when skirts are applied or when the GBS surface is 'very' rough. Use the friction angle of the GBS-soil contact surface, δ, when the friction between the GBS and the soil is less than the internal friction.

In terms of forces (with the z-axis positive downward):

$$F_{lateral} \le \left(F_{gravity} + F_{bouyancy} + F_{heave}\right) \cdot \Phi_{SS} \tan\varphi$$

Note: $F_{lateral}$ and F_{heave} are functions of load case and time, F_{heave} can be a negative value.

Bearing capacity
The vertical pressure of the structure on the soil may not exceed the bearing capacity according to:

$$p \le \Phi_{SB} \frac{1}{2} i_\gamma s_\gamma m_\gamma N_\gamma \gamma' D_{GBS}$$

In terms of forces (with the z-axis positive downward):

$$F_{gravity} + F_{bouyancy} + F_{heave} \le \Phi_{SB} \frac{1}{2} i_\gamma s_\gamma m_\gamma N_\gamma \gamma' D_{GBS} \cdot \frac{1}{4}\pi D_{GBS}^2,$$

with:

$$i_\gamma = \left(1 - \frac{F_{lateral}}{\left(F_{gravity} + F_{bouyancy} + F_{heave}\right)\tan\varphi}\right)^3$$

$s_\gamma = 1 - 0.3\frac{width}{length} = 0.7$ (other coefficients than 0.3 are also used, e.g. 0.4)

$$m_\gamma = \frac{2\alpha}{\pi} - \frac{4M}{F_{gravity} + F_{bouyancy} + F_{heave}} \cdot \frac{1}{\pi \cdot D_{GBS}} \sin\alpha$$ (see next section)

$$\alpha = \arccos\left(\frac{2M}{\left(F_{gravity} + F_{bouyancy} + F_{heave}\right) \cdot D_{GBS}}\right)$$

$N_\gamma = 2\left(N_q - 1\right)\tan\varphi$ (conservative coefficient of 2/3 instead of 2 was originally proposed by Brinch Hansen)

$$N_q = \frac{1 + \sin\varphi}{1 - \sin\varphi} \cdot e^{\pi \tan\varphi}$$

Note that apart from Φ_{SS} the factor i_γ implicitly gives the same requirement at the sliding resistance. Therefore, the criterion for sliding resistance in itself is not driving the design of the GBS.

Reduced effective area of a GBS

An eccentric load caused by a moment, results in a reduced effective bearing-area. The position of the resultant force in the soil-structure contact plane is the centre of the reduced area (see figure).

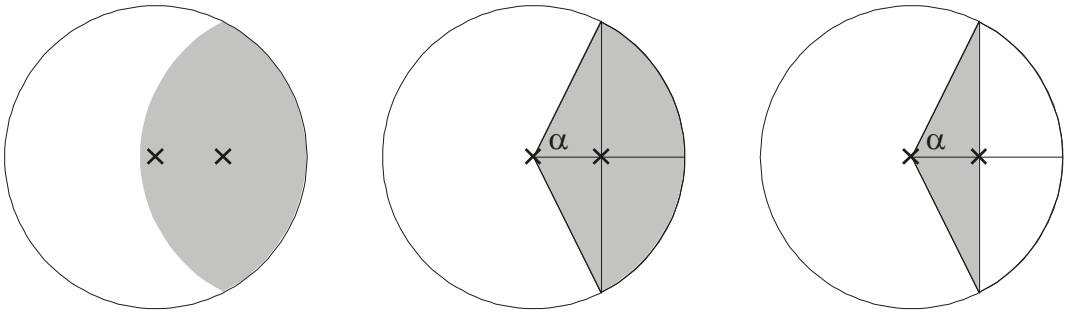

The eccentricity of the force equals $\frac{M}{F_z}$ and must be at least smaller than $\frac{1}{2}D_{GBS}$.

Angle $\alpha = \arccos\left(\frac{2M}{F_z \cdot D_{GBS}}\right)$

Area of pie $\frac{1}{4}\alpha \cdot D_{GBS}^2$

Area of triangle $\frac{M}{F_z} \cdot \frac{D_{GBS}}{2}\sin\alpha$

Reduced area of GBS $\frac{1}{2}\alpha \cdot D_{GBS}^2 - \frac{M}{F_z} \cdot D_{GBS}\sin\alpha$

Reduced area divided by total area $\frac{2\alpha}{\pi} - \frac{4M}{F_z} \cdot \frac{1}{\pi \cdot D_{GBS}}\sin\alpha$

References

[1] Verruijt, A., Grondmechanica, Delftse Universitaire Pers, Delft, 1997.

[2] Verruijt, A., Offshore Soil Mechanics, Delft University of Technology, Delft, August 1998.

Appendix F

Local Buckling

In this section the applied GL method to assess local buckling for shells is showed. This method is applied to all steel structural elements.

F.1 Element's compressive stress

Local buckling is emerges from a compressive stress resulting instability in the deflection shape of a structure. This is compressive stress is composed of a gravity term, σ_N, and a bending moment term, σ_M. The gravity term emerges from the gravitational force, F_g, acting on the mass of all structural and non-structural parts above the evaluated structural segment. This force is divided by element's the cross sectional area, see equation F.1. The bending moment term emerges from the multiplication of the bending moment, M, with the element's radius, R, and diving it by the area moment of inertia, I, see equation F.2.

$$\sigma_N = \frac{F_g}{A} \tag{F.1}$$

$$\sigma_M = \frac{M \cdot r}{I} \tag{F.2}$$

Here, R, is the distance from the center of the circular cross section to the center of the wall thickness, t, see equation F.3.

$$R = \frac{D_{out} - t}{2} \tag{F.3}$$

The stresses generated by the gravitational forces are always compressive. The stresses generated by bending moments could be either tensile or compressive. However, due to the fact that the element's cross section is symmetrical and the fact the buckling occurs as a result of compressive loading, both stress components are added together resulting in the maximum compressive stress, σ_c, see equation F.4.

$$\sigma_c = \sigma_N + \sigma_M \tag{F.4}$$

F.2 Allowable local buckling stress

The compressive stress is not allowed to exceed the critical local buckling stress for each structural segment. The computation of the critical local buckling stress is described by GL [34].

GL section 6.6.5.4.2. Buckling of long unstiffened cylindrical shells:

1. Part 8: "For long cylinders such as tower section sunder combined axial compression and bending moments, C_x, may be taken as defined in equation F.5.

$$C_x = 1.0\frac{\sigma_M}{\sigma} + C_{x,N}\frac{\sigma_N}{\sigma} \tag{F.5}$$

   Here, $C_{x,N}$ is a coefficient defined according to DIN 18800-4: 1990-11. This document has not been obtained, therefore $C_{x,N}$ is unknown. As a result a the assumption is made that equation F.5 result in $C_x = 1.0$. This assumption becomes more valid for structural segments with higher bending stress with respect to axial compressive stress.

2. Part 6: The ideal buckling stress for axial compressive loads, σ_{xi}, can be calculated according to equation F.6.

$$\sigma_{xi} = 0.605 \cdot C_x \cdot E_{steel}\frac{t}{R} \tag{F.6}$$

3. Part 10: Use the reduced slenderness of the shell, λ_{sx}, see equation F.7, to calculate the material safety factor, γ_M, and the reduction factor, $\kappa 1$.

$$\lambda_{sx} = \sqrt{\frac{\sigma_{steel}}{\sigma_{xi}}} \tag{F.7}$$

   The material safety factor depends on the reduced slender of the shell structure, see equation F.8.

$$\gamma_M = 1.1 \quad \text{for:} \quad \lambda_{sx} \leq 0.25 \tag{F.8a}$$
$$\gamma_M = 1.1\left(1 + 0.318\frac{\lambda_{sx} - 0.25}{1.75}\right) \quad \text{for:} \quad 0.25 < \lambda_{sx} \leq 2.0 \tag{F.8b}$$
$$\gamma_M = 1.45 \quad \text{for:} \quad \lambda_{sx} > 2.0 \tag{F.8c}$$

   The reduction factor also depends on the reduced slender of the shell structure, see equation F.9.

$$\kappa_2 = 1.0 \quad \text{for:} \quad \lambda_{sx} \leq 0.25 \tag{F.9a}$$
$$\kappa_2 = 1.233 - 0.993 \cdot \lambda_{sx} \quad \text{for:} \quad 0.25 < \lambda_{sx} \leq 1.0 \tag{F.9b}$$
$$\kappa_2 = \frac{0.3}{\lambda_{sx}^2} \quad \text{for:} \quad 1.0 < \lambda_{sx} \leq 1.5 \tag{F.9c}$$
$$\kappa_2 = \frac{0.2}{\lambda_{sx}^2} \quad \text{for:} \quad \lambda_{sx} > 1.5 \tag{F.9d}$$

The ultimate critical buckling stress, σ_u, is calculated according the equation Here, hoop stress as a result of water level difference between the sea water level and the inner MP water level are neglected.

$$\sigma_u = \frac{\kappa_2 \cdot \sigma_{steel}}{\gamma_M} \tag{F.10}$$

F.3 Result

Finally the element's compressive stress needs to be compared with the ultimate critical buckling stress, see equation F.11.

$$\sigma_u \leq \sigma_c \tag{F.11}$$

Appendix G

Optimization algorithm details

G.1 Gradient base algorithm

The use of gradient based optimization algorithm is incorporated with the Matlab software package. A gradient based algorithm uses the gradient of the objective function to determine the direction of the search towards the optimal solution. The gradient of the objective function is determined by evaluation the effect of changing the value of an optimization variables.

The use of this approach did not result in a close approximation of the optimal solution. In section 6.2.8 a brute force computation resulted in finding the optimal solution for a optimization variable accuracy of 0.005 m. The multistart algorithm, using the settings described in table G.1, has been chosen as gradient based optimization algorithm. The result of using the multistart algortihm are presented in table G.2. It is observed that using the multistart algorithm does not lead to an approximation of the optimal design solution.

Property	Value / setting
Type of solver	fmincon
Algorithm	sqp
Objective	lowest support structure mass
Number of start points	10

Table G.1: Properties of matlab optimization solver

Table G.2: Brute force optimization MP based support structure for Butendiek location 1 and 10 solutions found by the genetic solver

Computation Method	$D_{MP,low}$ [m]	$D_{MP,up}$ [m]	m_{tot} [ton]	Number of iterations
Brute force	6.510	5.465	1090.0	$1.2 \cdot 10^6$
Multistart Algorithm	6.277	5.063	1125.4	378
	6.647	5.192	1137.6	571
	5.378	4.872	1144.6	438
	5.622	5.190	1155.9	324
	6.157	4.791	1160.0	425
	6.611	5.001	1161.8	493
	5.381	4.964	1165.3	558
	6.827	4.988	1182.4	434
	5.194	4.908	1185.5	471
	5.538	5.396	1188.5	432
	6.256	4.679	1188.6	543
	5.120	4.902	1197.0	498
	5.152	4.979	1215.1	538
	6.289	4.416	1243.8	441

G.2 Genetic algorithm options

In this section the non-default settings of the optimization genetics algorithm are stated.[46]

Creation function	Uniform
Mutation function	Adaptive Feasible
Crossover function	Heuristic
Selection function	Stochastic uniform
Stall generation limit	10
Maximum number of generations	5
Population size	29

G.3 Justification constraint based variables

In section 4.1 it is mentioned that a number of design variables are scaled using constraints. This can be done when no conflict exists between the lowest allowable value for this variable, the objective and other design requirements.

The local buckling design requirement is used to scale the wall thickness of the MP, TP and tower. The lowest wall thickness complying to the local buckling constraints will also result in the lowest structural mass. It is assumed that no conflict exists with the natural frequency requirement. The natural frequency emerges from a stiffness and mass distribution. For a single cylindrical structural segment the stiffness and mass are linear proportional to the wall thickness,

see equation G.1 and G.2. Hence, changing the wall thickness only has a small effect on the natural frequency. As a result the amount of valid design options slightly increases when the wall thickness is not set by the local buckling requirement. However, none off these design options will result in the lightest possible support structure.

$$I \propto D^4 - (D-2t)^4 \tag{G.1a}$$
$$I \propto D^3 t \quad \text{ignoring all terms including } t^2, t^3 \text{ or } t^4 \tag{G.1b}$$

$$m \propto A \tag{G.2a}$$
$$m \propto D^2 - (D-2t)^2 \tag{G.2b}$$
$$m \propto Dt \quad \text{ignoring all terms including } t^2 \tag{G.2c}$$

The lateral soil stability is used to determine the pile penetration depth. The interaction with the natural frequency is very limited, see figure G.1. Here, one can see that a minimum pile penetration depth of 29 meters is required to reduce the pile toe deflection in ULS conditions beneath the maximum allowable value, see figure G.1(a). The pile penetration depth can be increased even further to increase the natural frequency. However, only a 0.3% increase of the natural frequency, between the allowable pile penetration depths of 29 and 40 meters, is observed, see figure G.1(b). Hence, a minimum pile penetration depth complying with the lateral soil stability requirements does not conflict with the natural frequency requirements.

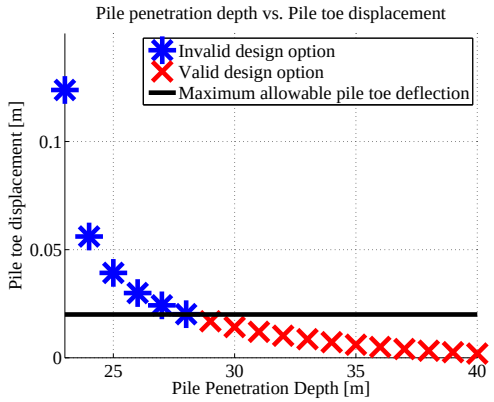

(a) Effect of pile penetration depth on pile toe deflection during ULS conditions

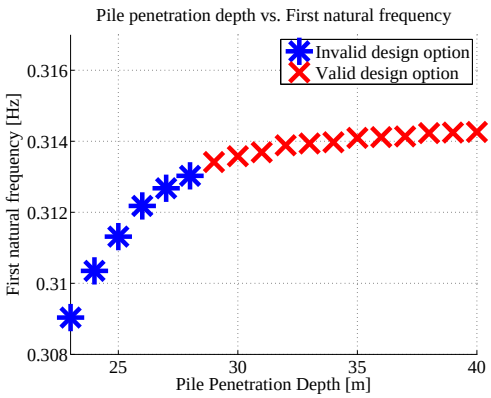

(b) Effect of pile penetration depth on structural natural frequency

Figure G.1: Effect of the pile penetration depth on the pile toe deflection and natural frequency. A lower and upper MP pile diameter of 6.5 and 5.5 meters has been chosen. Soil conditions are equal to those of location 48 of OWF Butendiek [21]

.

Appendix H

Supplements to Structural Design Verification

H.1 Butendiek MP

The properties of six reference designs for monopile based support structures for OWF Butendiek and one set of properties for OWF Baltic I are presented in table H.1.

Table H.1: Dimensions and masses of six reference designs for Butendiek OWF [21] [20]

Location number	**Optimization variables**		**Constraint based variables**				**Structural mass**		
	$D_{MP,low}$ [m]	$D_{MP,up}$ [m]	$t_{MP,mud}$ [m]	$t_{TP,low}$ [m]	$t_{tow,low}$ [m]	L_p [m]	MP [ton]	TP [ton]	Tower [ton]
Butendiek 1	6.00	5.19	0.095	0.080	0.045	28.5	635	256	226
Butendiek 2	6.00	5.19	0.100	0.080	0.045	29.5	680	256	226
Butendiek 3	6.00	5.19	0.100	0.080	0.045	31.5	723	256	226
Butendiek 4	6.00	5.19	0.095	0.080	0.045	30.5	660	256	226
Butendiek 5	6.00	5.19	0.100	0.080	0.045	30.5	692	256	226
Butendiek 6	6.00	5.19	0.095	0.080	0.045	39.5	827	256	226
Baltic I	5.05	4.05	0.080	0.060	0.030	40.0	410	161	139

H.2 OWFs Butendiek, Baltic I and Thornton Bank site conditions

The values of the independent site specific variables of Butendiek, Baltic I and Thorntonbank OWF are presented in table H.2.

Independent variable	Butendiek [1]	Baltic	Thornton Bank	Unit
Hub height	90.75	74.7	95.0 [13] [57]	[m]
Turbine thrust (ULS)	1.5	1.0	0.10 [2]	[MN]
Marine growth thickness	0.10	0.10	0.10	[m]
50 year highest wave	18.6	13.1	16.0[1]	[m]
50 year highest wave crest	15.2	8.6	12.0[1]	[m]
Tidal difference	2.3	3.5	2.2 [57]	[m]
Storm surge difference	2.9	0.64	2.5 [2])	[m]

[1] *asumption, see equation H.1*
[2] *assumption*

Table H.2: Values for independent design variables based data of Butendiek and Baltic I OWF

The 50 year recurrence wave height has been calculated based on the location of the platform. The platform's location is situation 17 m above mean sea level (MSL), which is 18.1 m above LAT. Equation 4.4 can be rewritten to find the 50 year recurrence wave height, which is estimated to be 16.0 m, see equation H.1.

$$0.75 \cdot h_{w,50years} = z_{plat} - z_{tide} - z_{surge} - z_{air} \tag{H.1}$$

H.2.1 Analytical Expression of Beam on Elastic Foundation

Analytical expression: An analytical solution for a beam, lying on a elastic foundation and subjected to external forces, was described by Winkler in 1867. This concept of an elastic foundation is widely used. One description of an beam on a elastic foundation is described in the lecture notes of by S. Parvanova [59]. The distribution of the reaction forces depends linearly on the deflection of the beam. For the purpose of this model the external loads are only applied at the begin of the beam, which represents the mud-line.

$$\frac{d^4u}{dx^4} + 4\frac{k}{EI}u = \frac{q(x)}{EI} \tag{H.2}$$

Since, $q(x) = 0$, only the homogenous solution to equation H.2 is required. The solution to this homogenous equation result in the representation shown in equation H.2.1, also known as the method of initial conditions. The deflection $u(x)$, rotation $\phi(x)$, bending moment M(x) and shear force $Q(x)$ at any point of distance can be obtained by inserting the correct initial displacement y_0, rotation ϕ_0, bending moment M_0 and shear force Q_0.

$$\begin{pmatrix} u(x) \\ \phi(x) \\ M(x) \\ Q(x) \end{pmatrix} = \begin{pmatrix} A(x) & B(x) & -C(x) & -D(x) \\ -4\alpha \cdot D(x) & \alpha \cdot A(x) & -\alpha \cdot B(x) & -\alpha \cdot C(x) \\ EI4\alpha^2 C(x) & EI4\alpha^2 D(x) & EI\alpha^2 A(x) & EI\alpha^2 B(x) \\ EI4\alpha^3 B(x) & EI4\alpha^3 C(x) & -EI4\alpha^3 D(x) & EI\alpha^3 A(x) \end{pmatrix} \begin{pmatrix} u_0 \\ \frac{\phi_0}{\alpha} \\ \frac{M_0}{\alpha^2 \cdot EI} \\ \frac{Q_0}{\alpha^3 \cdot EI} \end{pmatrix} \tag{H.3}$$

Where:

$$\alpha = \left(\frac{k}{4 \cdot EI}\right)^{1/4} \tag{H.4}$$

$$A(x) = \cosh(\alpha x) \cdot \cos(\alpha x) \tag{H.5a}$$

$$B(x) = \frac{\cosh(\alpha x) \cdot \sin(\alpha x) + \sinh(\alpha x) \cdot \cos(\alpha x)}{2} \tag{H.5b}$$

$$C(x) = \frac{\sinh(\alpha x) \cdot \sin(\alpha x)}{2} \tag{H.5c}$$

$$D(x) = \frac{\cosh(\alpha x) \cdot \sin(\alpha x) - \sinh(\alpha x) \cdot \cos(\alpha x)}{4} \tag{H.5d}$$

Derivation displacement and rotation at mud line In order to use equation H.2.1 the unknown values u_0 and ϕ_0 need to be obtained. This is done by using the fact that the bending moment and shear force at the pile toe equals zero, see equation H.6.

$$M(L_p) = 0 \tag{H.6a}$$

$$Q(L_p) = 0 \tag{H.6b}$$

As a result two equation with two unknowns, u_0 and ϕ_0, are obtained, equation H.2.1. Note that the corresponding x-cordinate is located at the pile toe, $x = L_p$.

$$\begin{pmatrix} 0 \\ 0 \end{pmatrix} = \begin{pmatrix} EI4\alpha^2 C(L_p) & EI4\alpha^2 D(L_p) & EI\alpha^2 A(L_p) & EI\alpha^2 B(L_p) \\ EI4\alpha^3 B(L_p) & EI4\alpha^3 C(L_p) & -EI4\alpha^3 D(L_p) & EI\alpha^3 A(L_p) \end{pmatrix} \begin{pmatrix} u_0 \\ \frac{\phi_0}{\alpha} \\ \frac{M_0}{\alpha^2 \cdot EI} \\ \frac{Q_0}{\alpha^3 \cdot EI} \end{pmatrix} \tag{H.7}$$

Finally an analytical expression for u_0 and ϕ_0 can be obtained, see equation H.8. In combination with the already known value M_0 and Q_0 a complete description of the elastic beam problem is given by equation H.2.1.

$$u_0 = \frac{Mo \cdot \alpha \left[4D(L_p)^2 + A(L_p)C(L_p)\right] + Q_0 \left[B(L_p)C(L_p) - A(L_p)D(L_p)\right]}{4EI\alpha^3 \left[B(L_p)D(L_p) - C(L_p)^2\right]} \tag{H.8a}$$

$$\frac{\phi_0}{\alpha} = \frac{Mo \cdot \alpha \left[A(L_p)B(L_p) + 4C(L_p)D(L_p)\right] + Q_0 \left[B(L_p)^2 - A(L_p)C(L_p)\right]}{4EI\alpha^3 \left[C(L_p)^2 - B(L_p)D(L_p)\right]} \tag{H.8b}$$

H.3 Natural Frequency Verification

H.3.1 Supplementary data

Supplementary data concerning the reference designs of the natural frequency verfication process are presented in table H.3.

Table H.3: Properties of locations used for natural frequency verification of table 6.12

WT location	**Pile diameter** [m]	L_p [m]	**LAT** [m]	K_{lat} $\left[10^8 \frac{N}{m}\right]$	K_{rot} $\left[10^{10} \frac{Nm}{rad}\right]$
Butendiek 48	6.00	28.5	18.4	8.44	9.76
Butendiek 62	6.00	29.5	20.0	8.40	10.0
Butendiek 71	6.00	31.5	19.8	6.82	9.58
Butendiek 32	6.00	30.5	18.5	8.53	9.71
Butendiek 14	6.00	30.5	20.0	7.48	9.53
Butendiek 23	6.00	39.5	20.1	2.83	8.27
Baltic I 14a [a]	5.05	39.0 [c]	17.3[d]	4.99	4.83
Baltic I 14b [b]	5.05	35.0 [c]	21.3[d]	5.93	5.43

[a] *Scour hole of 1.0 m*
[b] *Scour hole of 5.0 m*
[c] *Actual pile penetration depth is 40.0 m. However, here it is calculated from the bottom of the scour hole.*
[d] *Actual LAT is 16.3 m. However, here it is calculated w.r.t. to the bottom of the scour hole.*

H.3.2 Possible explanations for natural frequency overprediction

In this section a number of explanations are stated that could partly explain the overprediction of the structure's first natural frequency.

1. **The natural frequency of the structure clamped at the mud-line is over predicted** The natural frequency of the structure clamped at the mud-line is presented in Column D of table 6.12. Column E indicates the difference between this frequency and the models output (of Column A). Here, it is shown that the soil interaction reduces the clamped natural frequency by approximately 11.0% to 13.7% for the Butendiek support structure's and by 9.6% to 9.9% for the Baltic I support structure.

   If the natural frequency of the clamped structure is calculated correctly, then the overprediction of the model would be a result of an error in the soil interaction. In that case the soil interaction should reduce the clamped natural frequency by 18%, which means that the lateral and rotational spring stiffness need to be reduced by a factor 1.72. In the section about the verification of the lateral soil stability, section 6.2.4, a much higher accuracy of the deflection and rotation at the mud line has been obtained. Therefore, it is likely that over prediction of the Butendiek first natural frequency is caused by an over prediction of the natural frequency of the structure clamped at the mud line. On the other hand Clough and Penzien state that *"the process will eventually converge to the exact vibration shape if it is carried through enough cycles and therefore will yield the exact frequency"* [9]. This applicable to the natural frequency of the clamped structure. In the natural frequency computation submodel it is observed that the natural frequency indeed converges after three iterations.

2. **Inaccurate mode shape** An inaccurate mode shape always results in an overprediction of the natural frequency of the support structure clamped at the mud-line. The mode shape is calculated by using the improved Rayleigh method and a finite element model. The improved Rayleigh method should result in the exact solution for the natural frequency [9]. With the model the mode shape converges by using this improved Rayleigh method. This solution is only valid for one frequency (the natural frequency). The soil interaction changes the natural frequency with respect to the clamped structure. As a result it is possible for the assumed mode shape not to be valid anymore.

3. **RNA as point mass** The RNA is assumed to be a point mass. The farther away mass is located from the mud-line the large its effect on the natural frequency. The blade tip of an upwards pointed blade could reduce the natural frequency compared to the point mass it is now assumed to be.

4. **Use of uncoupled spring method** Zaaijer over predicted the first natural frequency by approximately +2.0% by using this uncoupled spring method in combination with the force method [81]. Here, flexible behaving piles with a smaller diameter and wall thickness and a very long pile penetration depth have been used.

5. **Difference in dimensions with respect to the reference design** The dimensions of the reference support structures have been converted to segments with a length of 1.0 meters. As a result the total support length could change by +/-0.5 meters with respect to the

reference design. The support structure's mass also changes slightly. For the designs of Butendiek a maximum total mass change of -1% to +1% is observed.

6. **Difference in pile penetration depth** The model uses a longer pile penetration depth +0.5 meters for all Butendiek support structures. This results in an over prediction of approximately +0.5%.

7. **Location of springs representing soil interaction** In the soil stability model a spring has been attached at the pile toe (bottom of the lowest segment). When no spring at the pile toe is attached than a better calculation of the pile tip deflection is realized. The choice of attaching a spring to the pile to result to an over prediction of the first natural frequency of approximately +0.1%.

8. **Corrosion at splash zone** The Butendiek reference designs have incorporated corrosion at the splash zone. Since this is not incorporated within the research model this will result in an over prediction of approximately +0.1%.

9. **Location of other point masses** Change the location of other point masses by +/-5.0 m results in change in natural frequency of +/- 0.1%. Because these point masses are located in the TP their effect on the natural frequency is much smaller than that of the RNA, which is heavier and located higher.

10. **Tower dimensions** For all the Butendiek support structures a reference tower design has been used. However, for the Baltic I support structure no tower data is found except for the tower height, mass and base diameter. Therefore, a the tower dimensions have been generated by the structural dimensioning submodel. The effect of the tower dimensions can be seen by replacing the reference tower is replaced for one dimensioned by the model itself for the Butendiek support structures. Now a change in the natural frequency is observed. Here, the reference tower support structure has a natural frequency which is 4.5% higher than when the tower is dimensioned according to used the KBE rules. This is likely to explain the natural frequency error difference between the Butendiek and Baltic I support structures.

H.4 Discussion about improving wall thickness computation

Is has been shown that using local buckling as design requirement did not result in an appropriate wall thickness computation. Therefore, a better method should be used to compute the wall thickness. Since wind turbine support structure are subjected a large number of load cycles fatigue could be a design driver. Implementing a fatigue analysis will change the ratio wall thickness to pile diameter. A light support structure with high resistance against fatigue damage can best be obtained by designing using a large diameter and small wall thickness. This will lead to a large area moment of inertia and a low cycle stresses. However, there are limitations to this concept.

1. Higher wave loading
   A larger pile diameter will result in higher wave loads. This results in larger wave loads, increasing the fatigue damage.

2. Structural stability
   When the ratio between the pile diameter over the wall thickness becomes larger the structure becomes more sensitive to buckling.

3. Manufacturing cost
   Higher manufacturing cost of lighter pile segments with a high diameters and small wall thicknesses could become more costly than heavier segment with a smaller diameter.

4. Impact resistance
   The impact resistance will decrease for pile with a larger diameter and smaller wall thickness. Resistance against boat impact or transportation loads could now become the limiting requirement.

H.5 Data Sensitivity Analysis Structural Design

The data corresponding to figures 6.4 up to 6.7 are presented in tables H.4 up to H.11.

Table H.4: Output Sensitivity Analysis: Effect of water depth on MP substructure

LAT $[m]$	$D_{MP,up}$ $[m]$	$D_{MP,low}$ $[m]$	m_{sup} $[ton]$	m_{MP} $[ton]$	m_{TP} $[ton]$	m_{tow} $[ton]$	t_{MP} $[m]$	t_{TP} $[m]$	t_{tow} $[m]$	L_p $[m]$	f $[Hz]$
10	6.22	6.09	1072	476	282	314	0.085	0.078	0.049	29	0.310
10	6.23	6.08	1071	476	281	314	0.085	0.078	0.049	29	0.310
10	5.76	5.64	1077	484	274	320	0.093	0.085	0.054	29	0.292
15	6.67	6.30	1159	563	284	313	0.083	0.076	0.047	30	0.309
15	5.96	5.54	1155	554	276	325	0.093	0.087	0.056	29	0.280
15	5.97	5.52	1158	555	278	324	0.093	0.088	0.056	29	0.280
20	7.10	6.32	1251	658	280	313	0.082	0.075	0.047	31	0.302
20	7.01	6.23	1253	657	280	315	0.083	0.076	0.048	31	0.299
20	7.11	6.31	1251	658	280	313	0.082	0.075	0.047	31	0.302
25	6.96	5.88	1362	754	287	320	0.088	0.082	0.052	31	0.281
25	7.40	6.23	1364	769	280	315	0.083	0.076	0.048	32	0.294
25	7.40	6.24	1364	769	281	315	0.083	0.076	0.048	32	0.294
30	7.59	6.01	1485	883	286	316	0.085	0.080	0.050	33	0.282
30	7.81	6.19	1482	886	282	313	0.083	0.077	0.048	33	0.289
30	7.71	6.08	1481	885	281	314	0.084	0.078	0.049	33	0.285
35	8.07	6.03	1619	1020	283	317	0.085	0.079	0.050	34	0.280
35	8.29	6.15	1617	1020	281	317	0.083	0.077	0.049	34	0.285
35	8.30	6.16	1618	1021	281	317	0.083	0.077	0.049	34	0.285
40	8.82	6.10	1770	1173	282	315	0.083	0.078	0.049	35	0.281
40	8.73	6.08	1773	1177	281	314	0.084	0.078	0.049	35	0.280
40	8.71	6.06	1777	1175	284	318	0.084	0.079	0.050	35	0.280
45	9.69	6.19	1974	1379	282	313	0.082	0.077	0.048	37	0.285
45	9.37	6.08	1971	1372	281	319	0.084	0.078	0.050	37	0.280
45	9.63	6.14	1989	1389	284	316	0.083	0.078	0.049	37	0.284
50	9.95	6.15	2203	1602	284	317	0.086	0.078	0.049	38	0.281
50	9.97	6.33	2240	1645	281	314	0.087	0.075	0.047	39	0.285
50	9.99	6.18	2209	1609	282	318	0.086	0.077	0.049	38	0.282
55	9.93	6.42	2487	1882	293	312	0.094	0.074	0.046	39	0.281
55	9.92	6.39	2485	1878	291	316	0.094	0.074	0.047	39	0.280

Table H.5: Output Sensitivity Analysis: Effect of water depth on GBS substructure

LAT $[m]$	D_{bs} $[m]$	D_{cyl} $[m]$	m_{sup} $[ton]$	m_{GBS} $[ton]$	m_{bal} $[ton]$	m_{tow} $[ton]$	t_{tow} $[m]$	f $[Hz]$
10	18.84	5.56	3557	1622	1615	320	0.053	0.280
10	18.84	5.56	3557	1622	1615	320	0.053	0.280
10	18.84	5.56	3557	1622	1615	320	0.053	0.280
15	20.19	5.64	4760	1964	2477	319	0.052	0.280
15	20.19	5.64	4760	1964	2477	319	0.052	0.280
15	20.19	5.64	4760	1964	2477	319	0.052	0.280
20	21.72	5.71	6240	2358	3563	319	0.051	0.280
20	21.72	5.71	6241	2358	3564	319	0.051	0.280
20	21.72	5.71	6240	2358	3563	319	0.051	0.280
25	23.44	5.77	8070	2814	4938	318	0.051	0.280
25	23.44	5.77	8070	2814	4938	318	0.051	0.280
25	23.44	5.77	8070	2814	4938	318	0.051	0.280
30	25.36	5.83	10335	3340	6678	317	0.050	0.280
30	25.36	5.83	10335	3340	6678	317	0.050	0.280
30	25.36	5.83	10335	3340	6678	317	0.050	0.280
35	27.48	5.88	13138	3948	8874	317	0.050	0.280
35	27.48	5.88	13139	3948	8874	317	0.050	0.280
35	27.48	5.88	13139	3948	8874	317	0.050	0.280
40	29.81	5.93	16605	4650	11640	316	0.049	0.280
40	29.81	5.93	16605	4650	11640	316	0.049	0.280
40	29.81	5.93	16607	4650	11641	316	0.049	0.280
45	32.37	5.97	20891	5460	15116	316	0.049	0.280
45	32.37	5.97	20893	5460	15117	316	0.049	0.280
45	32.37	5.97	20892	5460	15117	316	0.049	0.280
50	35.16	6.01	26172	6394	19463	315	0.048	0.280
50	35.16	6.01	26171	6394	19463	315	0.048	0.280
50	35.16	6.01	26171	6394	19463	315	0.048	0.280
55	38.19	6.05	32659	7468	24876	315	0.048	0.28
55	38.19	6.05	32659	7468	24876	315	0.048	0.28
55	38.19	6.05	32661	7468	24878	315	0.048	0.28

Table H.6: Output Sensitivity Analysis: Effect of extreme wave height on MP substructure

hw_{50} $[m]$	$D_{MP,up}$ $[m]$	$D_{MP,low}$ $[m]$	m_{sup} $[ton]$	m_{MP} $[ton]$	m_{TP} $[ton]$	m_{tow} $[ton]$	t_{MP} $[m]$	t_{TP} $[m]$	t_{tow} $[m]$	L_p $[m]$	f $[Hz]$
5	7.00	6.98	1038	446	217	376	0.061	0.072	0.047	27	0.291
5	6.79	6.76	1037	440	219	378	0.063	0.075	0.049	26	0.284
5	6.80	6.77	1039	441	219	379	0.063	0.075	0.049	26	0.285
10	6.76	6.29	1103	510	241	353	0.071	0.078	0.051	28	0.284
10	6.74	6.29	1102	509	241	353	0.071	0.078	0.051	28	0.284
10	6.66	6.26	1105	511	242	351	0.072	0.079	0.051	28	0.282
15	7.36	6.62	1229	628	283	318	0.076	0.072	0.045	31	0.310
15	6.88	6.19	1214	619	273	322	0.081	0.077	0.049	30	0.294
15	6.96	6.26	1214	618	276	320	0.080	0.077	0.048	30	0.297
20	7.07	6.18	1415	803	320	292	0.096	0.079	0.046	33	0.310
20	6.38	5.49	1414	790	326	298	0.106	0.093	0.053	32	0.284
20	6.44	5.54	1414	789	325	300	0.105	0.092	0.053	32	0.287
25	6.76	5.63	1770	1071	423	276	0.126	0.106	0.049	36	0.312
25	6.77	5.62	1779	1081	422	276	0.127	0.106	0.049	36	0.312
25	6.76	5.62	1771	1072	423	276	0.126	0.106	0.049	36	0.312

Table H.7: Output Sensitivity Analysis: Effect of extreme wave height on GBS substructure

hw_{50} $[m]$	D_{bs} $[m]$	D_{cyl} $[m]$	m_{sup} $[ton]$	m_{GBS} $[ton]$	m_{bal} $[ton]$	m_{tow} $[ton]$	t_{tow} $[m]$	f $[Hz]$
5	20.66	5.74	5500	2061	3057	383	0.057	0.280
5	20.66	5.74	5500	2061	3057	383	0.057	0.280
5	20.66	5.75	5502	2061	3059	382	0.057	0.280
10	21.16	5.73	5860	2206	3304	350	0.054	0.280
10	21.16	5.73	5860	2206	3304	350	0.054	0.280
10	21.16	5.73	5860	2206	3304	350	0.054	0.280
15	21.59	5.71	6147	2321	3500	326	0.052	0.280
15	21.59	5.71	6146	2321	3500	326	0.052	0.280
15	21.59	5.71	6148	2321	3500	326	0.052	0.280
20	22.17	5.69	6539	2477	3765	296	0.049	0.280
20	22.17	5.69	6539	2477	3765	296	0.049	0.280
20	22.17	5.69	6539	2477	3765	296	0.049	0.280
25	22.79	5.68	6953	2641	4044	268	0.046	0.280
25	22.79	5.68	6952	2640	4043	268	0.046	0.280
25	22.79	5.68	6952	2640	4043	268	0.046	0.280
30	23.47	5.67	7396	2814	4340	242	0.044	0.280
30	23.47	5.67	7396	2814	4340	242	0.044	0.280
30	23.47	5.67	7397	2814	4341	242	0.044	0.280
35	24.05	5.66	7765	2956	4586	223	0.041	0.280
35	24.05	5.66	7765	2956	4586	223	0.041	0.280
35	24.05	5.66	7765	2956	4586	223	0.041	0.280
40	24.83	5.67	8280	3151	4930	199	0.039	0.280
40	24.83	5.67	8279	3151	4929	199	0.039	0.280
40	24.83	5.67	8279	3151	4929	199	0.039	0.280
45	25.66	5.69	8846	3360	5308	177	0.036	0.280
45	25.66	5.69	8846	3360	5309	177	0.036	0.280
45	25.66	5.69	8846	3360	5308	177	0.036	0.280
50	26.56	5.74	9483	3589	5738	156	0.033	0.280
50	26.56	5.74	9480	3588	5736	156	0.033	0.280
50	26.56	5.74	9480	3588	5736	156	0.033	0.280
55	27.37	5.79	10057	3790	6125	142	0.031	0.280
55	27.37	5.79	10057	3790	6125	142	0.031	0.280
55	27.37	5.79	10057	3790	6125	142	0.031	0.280
60	28.44	5.90	10893	4072	6696	124	0.028	0.280
60	28.44	5.90	10893	4072	6696	124	0.028	0.280
60	28.44	5.90	10893	4072	6696	124	0.028	0.280
65	29.68	6.05	11922	4406	7408	108	0.025	0.280
65	29.67	6.05	11921	4406	7407	108	0.025	0.280
65	29.67	6.05	11921	4406	7407	108	0.025	0.280
70	31.07	6.28	13194	4799	8301	94	0.022	0.280
70	31.07	6.28	13193	4799	8300	94	0.022	0.280
70	31.07	6.28	13194	4799	8301	94	0.022	0.280

Table H.8: Output Sensitivity Analysis: Effect of hub height on MP substructure

z_{hub} $[m]$	$D_{MP,up}$ $[m]$	$D_{MP,low}$ $[m]$	m_{sup} $[ton]$	m_{MP} $[ton]$	m_{TP} $[ton]$	m_{tow} $[ton]$	t_{MP} $[m]$	t_{TP} $[m]$	t_{tow} $[m]$	L_p $[m]$	f $[Hz]$
70	4.68	3.99	945	565	228	151	0.114	0.108	0.051	27	0.320
70	4.68	4.00	945	565	228	151	0.114	0.108	0.051	27	0.320
80	5.48	4.72	997	570	230	197	0.097	0.089	0.049	28	0.309
80	5.53	4.78	995	570	227	198	0.096	0.087	0.049	28	0.312
80	5.52	4.79	998	575	227	195	0.097	0.087	0.048	28	0.312
90	5.92	5.20	1119	611	256	253	0.094	0.086	0.051	29	0.292
90	6.37	5.58	1120	617	253	250	0.087	0.080	0.047	30	0.309
90	5.69	4.96	1120	614	250	256	0.098	0.092	0.054	29	0.282
100	7.11	6.31	1251	658	280	313	0.082	0.075	0.047	31	0.302
100	6.44	5.71	1259	654	286	318	0.091	0.084	0.053	30	0.280
100	6.45	5.71	1259	655	286	318	0.091	0.084	0.053	30	0.280
110	7.40	6.66	1413	710	313	390	0.083	0.076	0.051	32	0.284
110	7.36	6.66	1414	707	317	390	0.083	0.077	0.051	32	0.284
110	7.51	6.75	1411	711	312	388	0.082	0.075	0.05	32	0.287
120	8.13	7.42	1572	753	347	471	0.079	0.073	0.051	33	0.280
120	8.15	7.41	1572	754	347	471	0.079	0.073	0.051	33	0.280
120	8.26	7.52	1582	767	347	469	0.078	0.072	0.050	34	0.283
130	9.62	8.00	1843	892	384	567	0.078	0.072	0.053	35	0.280

Table H.9: Output Sensitivity Analysis: Effect of hub height on GBS substructure

z_{hub} $[m]$	D_{bs} $[m]$	D_{cyl} $[m]$	m_{sup} $[ton]$	m_{GBS} $[ton]$	m_{bal} $[ton]$	m_{tow} $[ton]$	t_{tow} $[m]$	f $[Hz]$
70	18.38	4.00	4000	1726	2125	150	0.049	0.290
70	18.38	4.00	4000	1726	2125	150	0.049	0.290
70	18.38	4.00	4000	1726	2125	150	0.049	0.290
80	19.38	4.45	4591	1903	2490	199	0.051	0.280
80	19.38	4.45	4591	1903	2490	199	0.051	0.280
80	19.38	4.45	4591	1903	2490	199	0.051	0.280
90	20.54	5.06	5362	2122	2986	254	0.051	0.280
90	20.54	5.06	5362	2122	2986	254	0.051	0.280
90	20.54	5.06	5362	2122	2986	254	0.051	0.280
100	21.72	5.71	6240	2358	3563	319	0.051	0.280
100	21.72	5.71	6240	2358	3563	319	0.051	0.280
100	21.72	5.71	6240	2358	3563	319	0.051	0.280
110	22.94	6.40	7235	2612	4232	392	0.052	0.280
110	22.94	6.40	7235	2612	4232	392	0.052	0.280
110	22.94	6.40	7236	2612	4232	392	0.052	0.280
120	24.20	7.14	8359	2883	5003	474	0.052	0.280
120	24.20	7.14	8360	2883	5003	474	0.052	0.280
120	24.20	7.14	8359	2883	5003	474	0.052	0.280
130	25.48	7.93	9622	3172	5886	564	0.052	0.280
130	25.48	7.93	9621	3172	5885	564	0.052	0.280
130	25.48	7.93	9621	3172	5885	564	0.052	0.280
140	26.80	8.76	11034	3479	6891	664	0.052	0.280
140	26.79	8.76	11033	3479	6890	664	0.052	0.280
140	26.82	8.75	11045	3483	6898	664	0.052	0.280
150	28.14	9.63	12608	3805	8030	773	0.051	0.280
150	28.13	9.63	12606	3805	8029	773	0.051	0.280
150	28.13	9.63	12606	3805	8028	773	0.051	0.280

Table H.10: Output Sensitivity Analysis: Effect of soil friction angle on MP substructure

ϕ [m]	$D_{MP,up}$ [m]	$D_{MP,low}$ [m]	m_{sup} [ton]	m_{MP} [ton]	m_{TP} [ton]	m_{tow} [ton]	t_{MP} [m]	t_{TP} [m]	t_{tow} [m]	L_p [m]	f [Hz]
20	6.89	6.12	1461	862	283	316	0.085	0.078	0.049	47	0.280
20	7.09	6.31	1457	865	280	313	0.082	0.075	0.047	48	0.286
20	7.11	6.33	1460	866	280	313	0.082	0.075	0.047	48	0.286
22	4.00	3.00	2300	1460	427	412	0.268	0.262	0.118	42	0.197
22	7.01	6.23	1450	855	280	315	0.083	0.076	0.048	47	0.283
22	7.10	6.32	1448	855	280	313	0.082	0.075	0.047	47	0.286
24	6.92	6.16	1453	855	281	317	0.084	0.077	0.049	47	0.281
24	7.09	6.31	1446	854	280	313	0.082	0.075	0.047	47	0.286
24	7.10	6.31	1448	855	280	313	0.082	0.075	0.047	47	0.286
26	6.87	6.15	1447	846	284	317	0.085	0.078	0.049	46	0.280
26	7.01	6.23	1435	840	280	315	0.083	0.076	0.048	46	0.283
26	7.02	6.25	1439	842	281	316	0.083	0.076	0.048	46	0.284
28	6.96	6.18	1440	845	282	313	0.084	0.077	0.048	46	0.282
28	7.00	6.23	1435	840	280	315	0.083	0.076	0.048	46	0.283
28	7.11	6.32	1434	841	280	313	0.082	0.075	0.047	46	0.286
30	6.69	5.95	1434	832	283	319	0.087	0.08	0.051	45	0.282
30	6.84	6.09	1427	831	282	314	0.085	0.078	0.049	45	0.287
30	7.12	6.32	1436	842	280	313	0.082	0.075	0.047	46	0.295
32	6.12	5.86	1480	874	286	320	0.099	0.082	0.052	44	0.280
32	6.84	6.09	1427	831	282	314	0.085	0.078	0.049	45	0.291
32	6.93	6.15	1433	831	285	317	0.084	0.078	0.049	45	0.295
33	6.56	5.80	1439	834	287	318	0.090	0.083	0.052	44	0.283
33	6.84	6.08	1426	830	281	314	0.085	0.078	0.049	45	0.292
33	7.01	6.23	1424	829	280	315	0.083	0.076	0.048	45	0.298
33.5	6.56	5.84	1429	825	285	319	0.089	0.082	0.052	44	0.284
33.5	6.92	6.16	1427	829	281	317	0.084	0.077	0.049	45	0.296
33.5	7.01	6.24	1425	829	281	315	0.083	0.076	0.048	45	0.299
34	6.84	6.09	1427	831	282	315	0.085	0.078	0.049	45	0.293
34	6.98	6.25	1434	837	281	316	0.084	0.076	0.048	45	0.299
34	7.00	6.23	1438	840	284	315	0.084	0.077	0.048	45	0.299
34.5	6.61	5.89	1422	822	284	316	0.088	0.081	0.051	44	0.286
34.5	6.85	6.09	1428	832	281	314	0.085	0.078	0.049	45	0.294
34.5	7.00	6.23	1424	829	280	315	0.083	0.076	0.048	45	0.299
35	6.61	5.89	1372	771	284	316	0.088	0.081	0.051	40	0.286
35	6.62	5.90	1372	772	284	317	0.088	0.081	0.051	40	0.286
35	7.12	6.32	1376	783	280	313	0.082	0.075	0.047	41	0.303
36	6.42	5.72	1307	701	287	319	0.091	0.084	0.053	34	0.280
36	7.11	6.32	1303	709	280	313	0.082	0.075	0.047	35	0.303
36	7.11	6.32	1302	709	280	313	0.082	0.075	0.047	35	0.303
38	6.62	5.91	1252	650	285	317	0.088	0.081	0.051	30	0.288
38	7.09	6.31	1238	645	280	313	0.082	0.075	0.047	30	0.302
38	7.10	6.32	1239	646	280	313	0.082	0.075	0.047	30	0.302
40	6.76	6.01	1208	610	282	316	0.086	0.079	0.050	27	0.291
40	6.79	6.08	1210	614	281	314	0.086	0.078	0.049	27	0.293
40	6.85	6.09	1207	611	282	314	0.085	0.078	0.049	27	0.294

Table H.11: Output Sensitivity Analysis: Effect of soil friction angle on GBS substructure

ϕ $[m]$	D_{bs} $[m]$	D_{cyl} $[m]$	m_{sup} $[ton]$	m_{GBS} $[ton]$	m_{bal} $[ton]$	m_{tow} $[ton]$	t_{tow} $[m]$	f $[Hz]$
30	35.57	5.47	12494	4583	7589	321	0.054	0.280
30	35.57	5.47	12494	4583	7589	321	0.054	0.280
30	35.57	5.47	12495	4584	7590	321	0.054	0.280
32	30.99	5.51	10095	3741	6033	321	0.054	0.280
32	30.99	5.51	10095	3741	6033	321	0.054	0.280
32	30.99	5.51	10095	3741	6033	321	0.054	0.280
34	27.15	5.57	8330	3115	4895	320	0.053	0.280
34	27.15	5.57	8330	3115	4895	320	0.053	0.280
34	27.15	5.57	8330	3115	4895	320	0.053	0.280
36	23.88	5.64	7011	2640	4052	319	0.052	0.280
36	23.88	5.64	7011	2640	4052	319	0.052	0.280
36	23.88	5.64	7011	2640	4052	319	0.052	0.280
38	21.05	5.74	6018	2276	3423	318	0.051	0.280
38	21.05	5.74	6018	2276	3423	318	0.051	0.280
38	21.05	5.74	6019	2276	3424	318	0.051	0.280
40	18.59	5.87	5275	1996	2962	317	0.050	0.280
40	18.59	5.87	5275	1996	2962	317	0.050	0.280
40	18.59	5.87	5275	1996	2962	317	0.050	0.280

Appendix I

Sensitivity Analysis Installation Process Model

In this Appendix the rest of the sensitivity analysis perfomed on the installation process model is presented.

Installation strategy and distance to harbor: The distance to port directly influences the amount of traveling time. The two earlier defined installation strategies, Feeding and Traveling method, differ mainly on this aspect. Therefore two scenarios are defined; one based on the Traveling strategy (reference) and one Feeding strategy, see table I.1. The results for TS and WP can be found respectively in figure I.2 and I.3. Here, it can be observed that the distance to harbor has practically no effect on the installation time of the feeding strategy scenario, because it only return trip is required for the entire process.

In theory it should be possible to calculate the installation time of the traveling strategy by using the installation time of the feedings strategy. The extra required traveling and loading at harbor time can simple be added to the total feeding installation time. This is visualized by the black lines in figure I.2 and I.3 labeled "Feeding + Net Difference". Now it is observed that the black lines do not coincide with the graphs for the TS method.

The WP method computes a lower installation time compared to the net difference, see figure I.3. The reason behind this under prediction is that the correlation between the required weather window for traveling and other activities is not taken into account. In reality the time spend traveling cannot be used to perform acclivities.

The TS method computes a higher installation time compared to the net difference, see figure I.2. Once the installation vessel has completed the installation of the last on-board substructure component it needs to travel back to the harbor to reload new components. Moments of good weather conditions often occur in long periods in the order of several days. Therefore, it is often the case that it could have continued installing components it they were available on-board. Hence, traveling occurs more often during good environmental conditions than during bad environmental conditions.

For the Wikinger location the difference between the WP and TS method for the computed and and theoretical case is less pronounced for its milder environmental conditions compared to the Hohe See location.

Property	Traveling	Feeding	Unit
Ship's carrying capacity	5	-	[-]
Vessels traveling speed	12	12	[kts]
Loading at harbour time	4 hours per substructure	1	[h]

Table I.1: Data input of a process, consisting of for activities, for the WP method

Contingency factor and linking of activities: The contingency factor determines the amount of time the model looks ahead for non-allowable environmental conditions. In section 5.2.2 the linking of activities has been explained. The contingency factor influences installation cycles where activities have been linked together more strongly, see figure I.1. Here, three cases have been used; the unlinked, half linked and fully linked case, see table to table I.2.

The total installation time is barely influenced by the contingency factor for the WP method. However, linking activities strongly affects the total average total installation time. Here, the total installation time increases stepwise with each added linked activity as a result of the multiplication of the workability percentages of the linked activities. The workability percentage of each individual activity only slightly decreases as a result of an increasing contingency factor.

For the TS method this is the other way around. Here, a contingency factor of one results in almost the same result for al three cases. Increasing the contingency factor results in an increase of the average total installation time. The highest increment is expected and observed for the fully linked case.

Activity number	1	2	3	4
Unlinked	a	b	c	d
Half linked	a	a	b	b
Fully linked	a	a	a	a

Table I.2: Linking of activities used for figure I.1. Activities with the same letter are linked together.

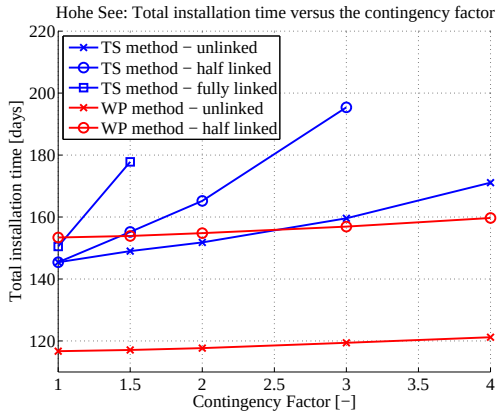

(a) **Note: It was not possible to install all sub-structures for the fully linked case using the WP method*

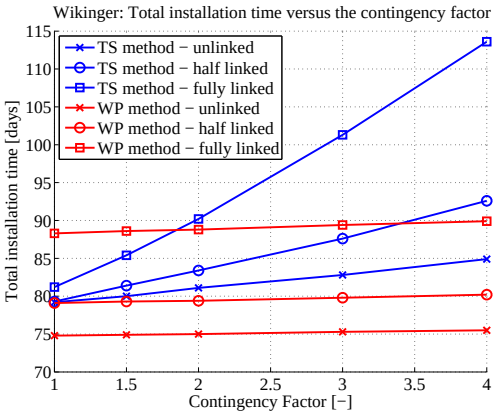

(b)

Figure I.1: Effect of contingency factor and linking of activities on total isntallation time

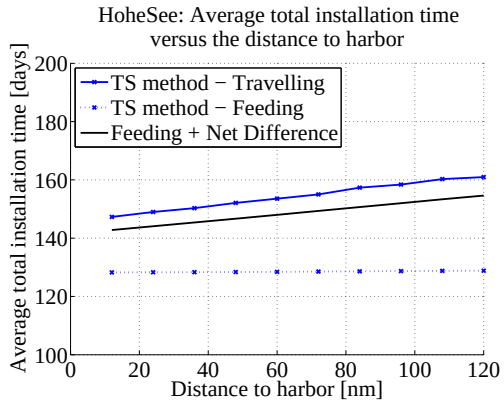

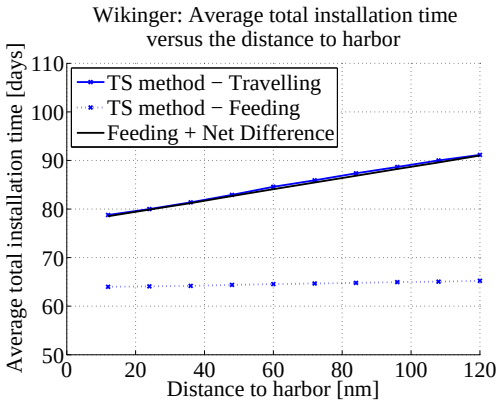

Figure I.2: Effect of distance to harbor and the installation strategy on total installation time for TS method

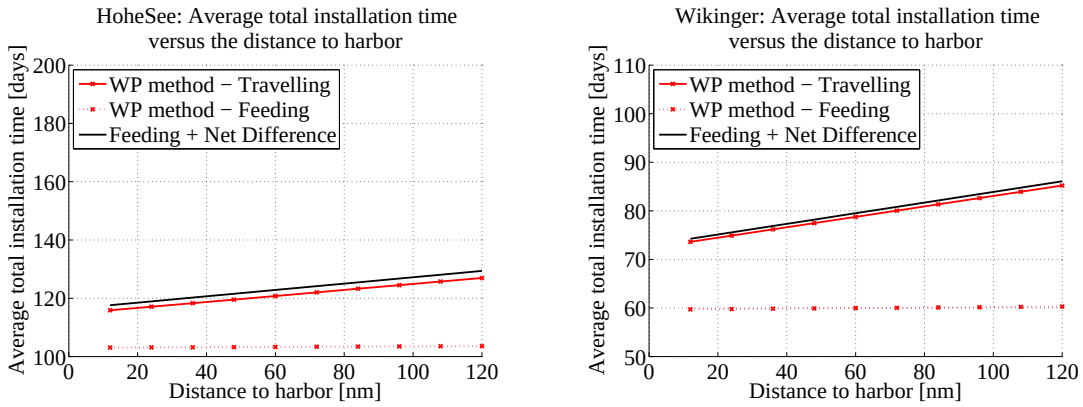

Figure I.3: Effect of distancte to harbor and the installation strategy on total installation time for WP method

Grout curing time: Increasing the grout curing time will result in a higher total installation time. Two main differences are observed between the WP and TS methods.

Firstly, there is the initial step difference between a grout curing time of 0.0 and 1.0 hours, see figure I.4. The WP method always computes an initial increase of the total installation time in this first step, due to the workability of the grouting activity being multiplied with the workability of the grout curing process. In other words the WP method does not account for the correlation of the required environmental conditions for the grouting activity and the grout curing process. Hence, always an initial increase of the total installation time occurs, unless the grouting process has a workability of 100%.The initial step of the TS method depends on the allowable significant wave height for the grouting activity and for the grout curing process. This difference can be observed by looking at the Wikinger graph, figure I.4(b). Here, an allowable significant wave height for grout curing of 0.5 meters does have an initial step, but at a $Hs = 1.0$ meters no initial step can be observed. In table 6.24 an allowable significant wave height for the grouting activity of 1.0 meters has been chosen. As a result it is less likely that a grouting activity weather window will be followed by a grout curing weather window with $Hs = 0.5$, but very likely that it is followed by by a grout curing weather window with $Hs = 1.0$.

Secondly, there is the difference between the WP and TS method for long grout curing times, see figure I.5. The WP method computes a significantly lower installation time than the TP method. The WP method calculates the relative amount of time in a month the grouting curing conditions occur. If a high grout curing time is required and the WP method identifies one single weather window, than still a fairly large workability is obtained. However, only on single moment in that particular months occur for which the grouting activity can be performed and be succeeded by the aforementioned grout curing weather window. The WP method simply calculates the gross grouting activity time. Since the grouting activity time itself is only 2.0 hours it is possible to install multiple substructures even though this would not be possible in practice. The TS method does account for the exact moment a suitable weather window occurs.

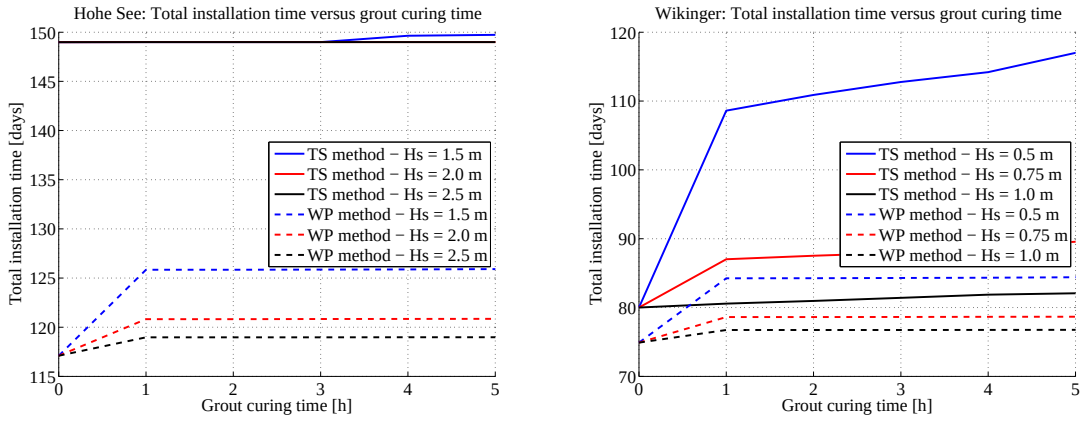

(a) (b)

Figure I.4: Small time scale effect of the grout curing time on the total installation time

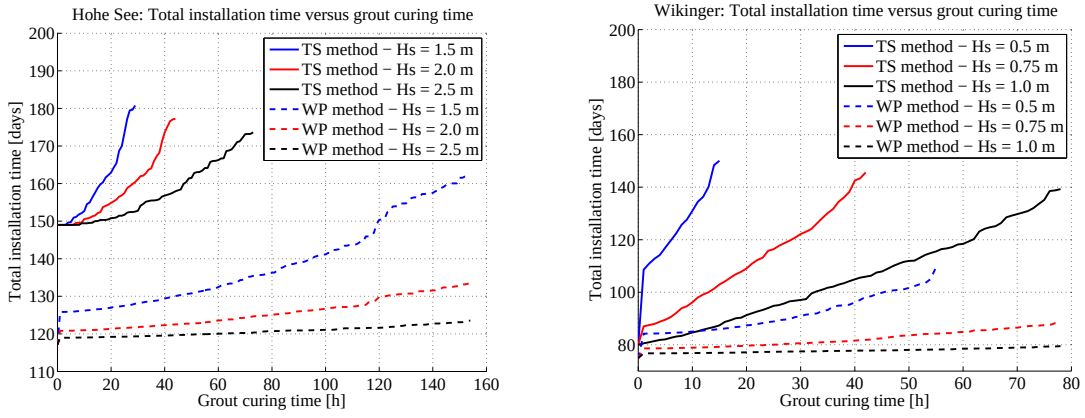

(a) (b)

Figure I.5: Large time scale effect of the grout curing time on the total installation time

Appendix J

Reducing the computation time

In section 7.1.3 it is found that the current model requires to much of computation time for an practical implementation within a micro siting model. In this Appendix a number of measures, that can reduce the computation time, are presented.

J.1 Parallel computation process

Parallel computing is done by dividing the computation process over multiple processors. If this is done efficiently than the computation time can be reduced by approximately the number of processors.

N. Wang states that genetic algorithms have computations independent of the computation sequence in their search procedure and are therefore very suitable for a parallel computation process [79]. An example of the implementation of an parallel computation process within the genetic algorithm optimization process is shown in figure J.1. Due to the current genetic algorithm settings a population size of 29 individuals is generated. It is therefore expected that the computation time of the MP structural optimization process can be reduced by a factor 29 by implementing parallel computing.

The GBS structural optimization process can be performed parallel to the MP optimization process. Since the GBS optimization process requires less computation time than the MP optimization process, the MP optimization process remains the limiting factor. Furthermore, the installation process can also be computed parallel to the structural design process. The installation process itself can also be parallel computed for the same reason as it can be performed for a genetic algorithm. Namely, the performed computations are independent of the computations sequence. An impression of the implementation of a parallel computing process for the installation process is presented in figure J.2. In that case the installation time for all vessels is computed regardless of their crane capacity. Then based on the results of the structural design model a number of vessels can be eliminated for not complying with the crane capacity requirement.

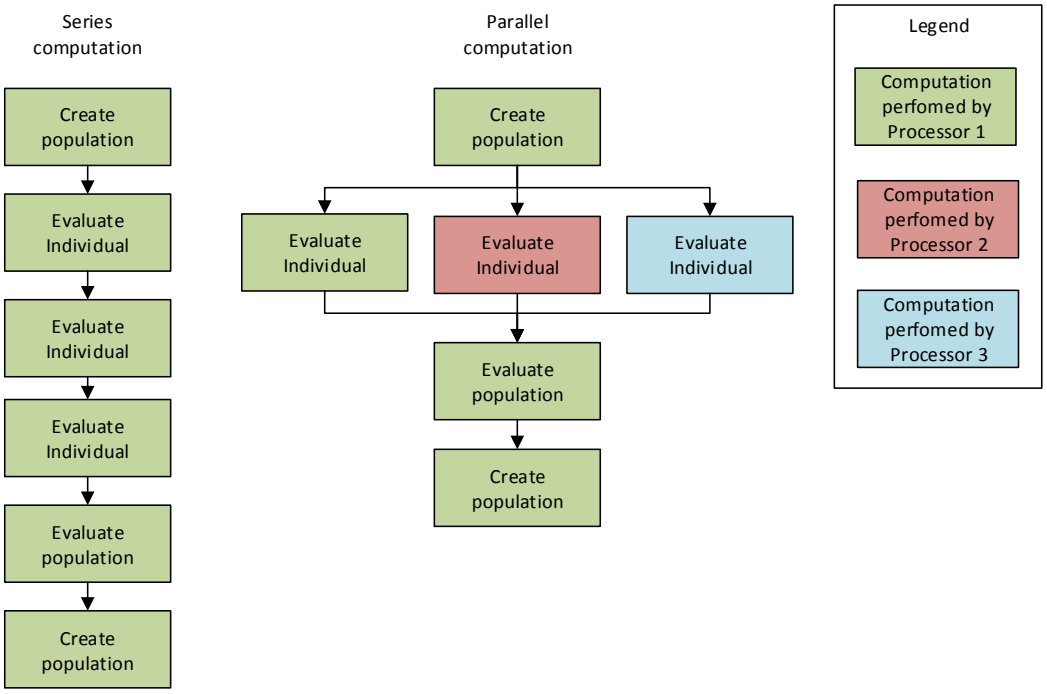

Figure J.1: Impression of potential implementation of parallel computing within genetic algorithm

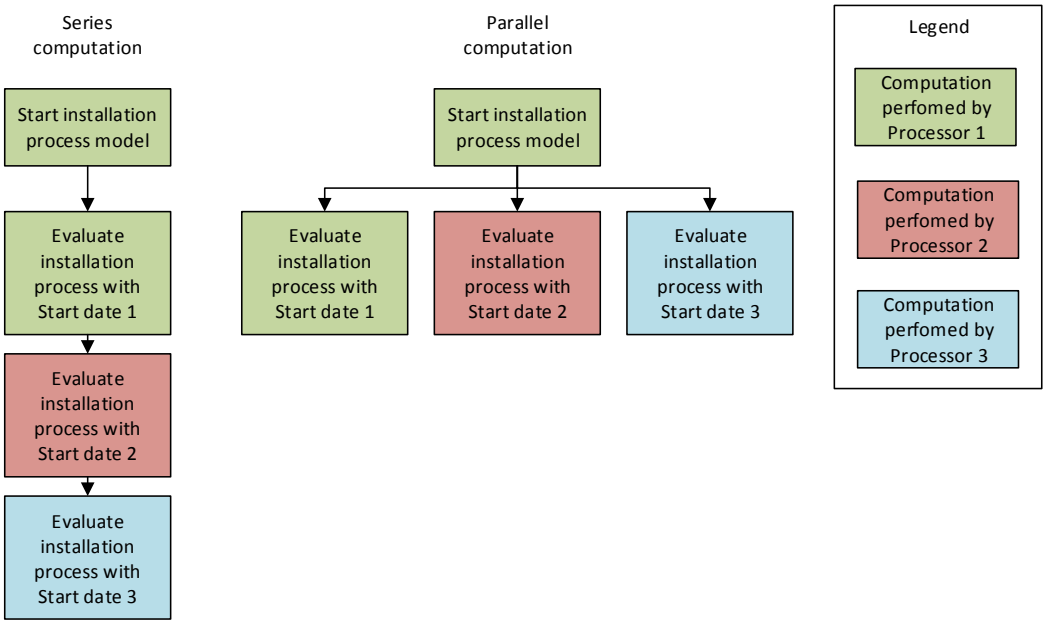

Figure J.2: Impression of potential implementation of parallel computing within the installation process model

In theory the computation time can be reduced to that of only the parallel computing process of the MP structural optimization. The case study of section 7.1 required a computation time of 9 hours and 13 minutes using a series computation process. With parallel processing this could be reduced to $\frac{1}{29}$ of the MP optimization process, which results in a total time of 12 minutes and 21 seconds for two iterations of the micro siting model. Note that a best case scenario is assumed here, where no time is lost in the commutation between different processors. Also the computation time of the master processor is assumed to be negligible. The amount of processors required for this process is estimated to be approximately 70. For two times 29 processors are required by the structural design model and approximately 10 processors for the installation process.

J.2 Monopile support structure evaluation

It has been shown that the evaluation of a single monopile based support structure requires much computation time. The relative amount of computation time per submodel required by the structural design of a MP is presented in table J.1. Most computation time is spent on the lateral soil stability requirement for creating an inverse matrix, according to equation 4.32.

Table J.1: Relative amount of computation time per sub-module

Sub-Module	**Relative amount of computing time**
MP lateral soil stability computations	81.2%
Natural frequency computations	3.5%
Support structure dimensioning	3.5%
Loading of WT and site specific data	2.5%
Wave loads computation	2.3%
Local buckling computations	1.8%
Other load computations	0.6%
Other	4.8%

note: *averaged over the optimization of 24 support structures for 6 locations within OWF Butendiek*

Currently the evaluation of a single MP based support structure requires at least four lateral soil stability computations. At least two to computations are required to set the pile penetration depth, one is required to compute the lateral soil stiffness and one is required to compute the rotational soil stiffness. A possible method to reduce the two (or more) computations required to set the pile penetration depth is to keep track of the pile penetration depth computed by previous MP design option evaluations. If the values of the MP lower diameter and ULS loads acting at the mud line are between the values of two earlier performed design option evaluations which have the same pile penetration depth, then the pile penetration depth will be equals to that of these earlier performed design option evaluations. The probability of such a situation occurring is high, because the design options converges toward an ideal design solution. Consequently, the values of the two optimization variables and corresponding ULS mud-line loads converges

towards an ideal value.

Appendix K

Wind Turbine Properties

The technical specifications of the Vestas V112, Siemens 3.6MW and the Repower 5.0MW offshore wind turbines are presented respectively in tables K.1, K.2 and K.3.

Property	Value	Unit	Source
Rotor radius	56	[m]	[77]
Rater wind speed	12	[m/s]	[77]
Operating range	6.7 - 17.7	[rpm]	[77]
Nacelle mass	119.5	[ton]	[77]
Blade mass	11.9	[ton]	[77]
Hub mass	22	[ton]	[78][a]
Yaw bearing diameter	3.0	[m]	[22]

[a] *unknown hub weight, therefore value taken from Vestas V90*

Table K.1: Properties of the Vestas V112 3.0 MW wind turbine

Property	Value	Unit	Source
Rotor radius	60	[m]	[67]
Rater wind speed	13.5	[m/s]	[67]
Operating range	6.4-16.8	[rpm]	[20]
Nacelle, hub and blade mass	238	[ton]	[67]
Yaw bearing diameter	3.0	[m]	[22]

Table K.2: Properties of the Siemens 3.6 MW wind turbine

Property	Value	Unit	Source
Rotor radius	63	[m]	[62]
Rater wind speed	13.0	[m/s]	[62]
Operating range	6.9-12.1	[rpm]	[62]
Nacelle mass	290	[ton]	[62]
Hub and blade mass	120	[ton]	[62]
Yaw bearing diameter	4.0	[m]	[22]

Table K.3: Properties of the Repower 5.0 MW wind turbine

Appendix L

Supplements to Theoretical Case Study

The main installation vessels and supply vessel properties, used for the theoretical case study of section 7.1, are presented in tables L.1, L.2 and L.3.

Table L.1: Installation vessel properties for MP installation vessels

Property	**Vessel 1**	**Vessel 2**	**Vessel 3**	**Vessel 4**	**Unit**
Earliest date	1 July	1 July	1 July	1 July	[-]
Installation cycle:					
• time	18	16	14	12	[h]
• Hs,max	1.25	1.50	1.75	2.00	[m]
• Vw,max	12.0	12.0	12.0	12.0	[m/s]
• Tp,max	8.0	8.0	8.0	8.0	[s]
Ship's carrying capacity	3.0	4.0	5.0	6.0	[-]
Vessels traveling speed	6.0	8.0	10.0	15.0	[kts]
Costs	100	150	200	250	[k€/day]
Crane capacity	600	800	1000	1200	[ton]
Grout curing time	24.0	24.0	24.0	24.0	[h]
Allowable wave height during grout curing	2.0	2.0	2.0	2.0	[m]
Loading at time per substructure	4.0	4.0	4.0	4.0	[h]
Distance to harbor	60.0	60.0	60.0	60.0	[nm]

Table L.2: Installation vessel properties for GBS installation vessels

Property	**Vessel 5**	**Vessel 6**	**Vessel 7**	**Vessel 8**	**Unit**
Earliest start date	1 April	1 April	1 April	1 April	[-]
Installation cycle:					
• time	18	16	14	12	[h]
• Hs,max	1.25	1.50	1.75	2.00	[m]
• Vw,max	12.0	12.0	12.0	12.0	[m/s]
• Tp,max	8.0	8.0	8.0	8.0	[s]
Ship's carrying capacity	3.0	4.0	5.0	6.0	[-]
Vessels traveling speed	6.0	8.0	10.0	15.0	[kts]
Costs	100	150	200	250	[k€/day]
Crane capacity	3500	4500	5500	6500	[ton]
Distance to harbor	120.0	120.0	120.0	120.0	[nm]

Table L.3: Properties support vessels for transportation of GBS substructures

Property	**Support Vessel**	**Unit**
Ship's carrying capacity	2.0	[-]
Vessels traveling speed	10.0	[kts]
Costs	25	[k€/day]